UNIVERSITY of the WESTERN CAPE

RESEARCH AND DEVELOPMENT

High resolution gamma-spectroscopy of environmental samples

By

Metsi Monnicca Rapetsoa

A dissertation in partial fulfillment of the

requirements for the degree of

MAGISTER SCIENTIAE

AT

UNIVERSITY OF THE WESTERN CAPE

SUPERVISOR: Prof. Dr Arnaud FAANHOF
South African Nuclear Energy Corporation SOC Ltd. (Necsa)
Specialist Scientist / Professional Service Provider: Research & Development

CO-SUPERVISOR: Prof. Robert LINDSAY
University of the Western Cape (UWC)
Department of Physics and Astronomy

2018

DECLARATION

I declare that this research, "**High resolution gamma-spectroscopy of environmental samples.**", carried out in the RadioAnalysis Department of the South African Nuclear Energy Corporation SOC Ltd. (Necsa) in collaboration with the University of the Western Cape between February 2012 and February 2017 has not been submitted for any degree in any other university, and that all the sources of data I have used, have been indicated and fully acknowledged.

Full name: **Metsi Monnicca Rapetsoa** Date: 2018

Signed: .....

ACKNOWLEDGEMENT

I express my deepest appreciation to a number of individuals who contributed on the development and success of this project, without their support, this work could not have been completed.

First, I would like to thank my supervisor, Prof Dr. Arnaud Faanhof, who offered me the opportunity to perform this research, guided and supported me throughout this work. Without his support, advice and encouragement, this work could not have been possible.

I would like to thank my co-supervisor, Prof Robert Lindsay, for his continuous support, believing in me and tireless efforts in constant visits to Necsa for progress monitoring.

I would like to thank my mentor, Deon Kotze, whose doors were open 24 hours to help me from the conception to the completion of this project, without his support, I could not have managed.

I would also like to thank Maxie Willemse for the valuable guidance and support throughout this study. You went beyond your call of duty in assisting me and for that, I thank you.

Special thanks go to the University of the Western Cape and the NRF for funding and giving me the opportunity to pursue my career in the nuclear industry and Necsa for giving the opportunity to do the necessary practical research.

Many thanks to my friends who motivated me to study.

Finally, I would like to express my gratitude to my family for the support and encouragement throughout this journey.

Above all, I would like to thank God for making all this possible, for giving me the strength, the wisdom, and perseverance throughout the journey.

ABSTRACT

In this study, a comparison has been made between the available commercial software package Genie 2000 developed by Canberra and Virtual Gamma Spectroscopy Laboratory (VGSL) developed by the Radionuclide Development Unit of the International Data Centre of the Comprehensive Nuclear Test-Ban Treaty Organization (CTBTO) to provide quality assessment of the data delivered by eighty (80) international monitoring stations distributed around the world to monitor nuclide emissions after an illegal nuclear weapon test, either in the atmosphere, under water or underground.

The lessons learned from the Proficiency Test Exercises (PTEs) will be applied to NORM nuclide analyses of environmental samples. Results provided are based on three (3) IAEA reference materials: stream sediments, milk powder, and soil. These samples contain decay products of uranium and thorium, which produce multiple gamma-rays, and thus a High Purity Germanium detector (HPGe) will be used. The study has been conducted in the South African CTBTO laboratory (ZAL14) situated at the South African Nuclear Energy Corporation SOC Ltd. The laboratory is equipped with two ultra-low background gamma-spectrometry systems accredited according to world-class standards.

The CTBTO PTEs spectra and IAEA certified samples have been analyzed looking at a variety of parameter settings including sum-coincidence and matrix-dependent self-absorption using both software mentioned. Optimization of various parameters has been done by gamma-ray spectra used in the CTBTO proficiency tests over the past decade.

The average activity ratio results for the soil sample of LABSOCs to the certified activity values was 1.04 ± 0.13 and for VGSL was 0.93 ± 0.12. The average activity ratio for the stream sediment sample to the certified activity values was 1.03 ± 0.15 and for VGSL was 0.93 ± 0.15. For the milk powder ~ Cs-137, the LABSOCs ratio to the certified activity values is 0.95 ± 0.03 and for VGSL was 0.82 ± 0.03.

The results of the study indicated that LabSOCS software in general can be considered reliable for gamma-ray efficiency calibration for NORM analysis, while VGSL is a reasonable alternative.

For more accurate results an empirical efficiency calibration is the preferred option, although not for routine analysis of environmental samples as this option is not cost effective.

VGSL and LabSOCS software can be considered reliable for gamma-ray efficiency calibration for CTBTO sample analysis.

Keywords

Gamma Spectrometry instrumentation

Gamma Spectrometry software

Naturally Occurring Radioactive Material

High Resolution Gamma Spectrometry

Ultra-Low Background Gamma Spectrometry

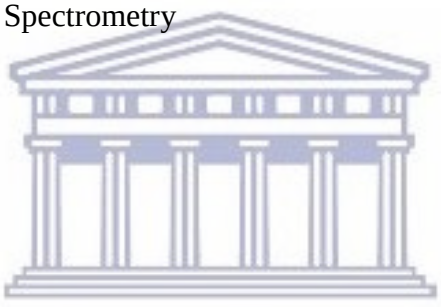

TABLE OF CONTENTS

LIST OF FIGURES

LIST OF TABLES

SYMBOLS AND ABBREVIATIONS

- ANSI — American National Standards Institute
- ARAME — Automatic Radionuclide Air Monitoring Equipment
- BEGe — Broad Energy Germanium Detector
- CAM — Configuration Access Method
- COI — Coincidence correction factor
- CTBT — Comprehensive Nuclear Test-Ban Treaty
- CTBTO — Comprehensive Nuclear Test-Ban Treaty Organization
- CVS — Concurrent Versions System
- DOS — Disc Operating System
- ETNA — Efficiency Transfer for Nuclide Activity Measurement
- FEP — Full Energy Peak
- FWHM — Full Width at Half Maximum
- HPGe — High Purity Germanium Detector
- IAEA — International Atomic Energy Agency
- IDC — International Data Centre of the CTBTO
- IMS — The International Monitoring System of the CTBTO
- IPC — Inter Process Communication
- MCA — Multi-channel Analyzer
- MCNP — Monte Carlo N-Particle
- MDA — Minimum Detectable Activity
- Necsa — The South African Nuclear Energy Corporation SOC Ltd.
- NIST — National Institute of Standards and Technology
- NORM — Naturally Occurring Radioactive Material
- NPL — National Physical Laboratory
- ppm — Parts per million
- PTE — Proficiency Test Exercises
- QA — Quality Assurance
- RASA — Radionuclide Aerosol Sampler Analyzer
- SRM — Standard Reference Material

- UKAS United Kingdom Accreditation Service
- Unc. Uncertainty
- VDM Virtual Data Manager
- Z Atomic number
- α Alpha
- β Beta
- ε Counting efficiency
- γ Gamma

TERMINOLOGY

Activity of a sample:	The rate at which the nuclear decay occurs, i.e. the number of nuclei that decay per second.
Algorithm:	A set of steps that are followed in order to solve a mathematical problem or to complete a computer process.
Background:	A property of any detector, due to radiation in its vicinity, electric noise, the spontaneous emission of electrons from the photocathode etc. The reading obtained during a pre-set counting period, or the observed count rate (cps), when the system is operated normally, but with an empty counting chamber. Background can be reduced by shielding or guard detectors, but hardly eliminated totally. The background is usually subtracted from the sample reading to obtain background corrected values.
Background radiation:	A level of radiation present at the detector due to cosmic radiation, natural radioisotopes that are present in the building material and in the air and radioactive material (e.g. calibration sources and active samples) present in the laboratory where radioactivity is being measured.
Branching ratio:	Ratio for a particular decay mode is the number of atoms decaying by that decay mode to the number decaying in total.
Calibration:	Is a process of evaluating and adjusting the precision and accuracy of measurement equipment.

Canning material:	Material normally made from stainless steel with a carbon-fiber or beryllium entrance window that surrounds the germanium detector material.
Concurrent Version system:	A tool designed to keep track of changes to files made by groups of designers working on the same files, allowing them to stay in synchronization with each other as each individual chooses.
Cosmogenic radiation:	High-energy particles from the galaxy and sun, especially protons (70%) and helium nuclei (20%) but also a very small proportion of gamma radiation, hit the earth atmosphere producing amongst others radionuclides like ^{3}H, ^{14}C and ^{22}Na.
Counts per second (cps):	The number of events registered per second.
Cross-over point:	The point that divides the low and high energy regions of the efficiency curve ($E_{\gamma} \approx 120keV$).
Detector resolution:	The ability of a detector to distinguish between two peaks of equal size that are close together.
Disintegrations per second (dps):	The number of nuclear decays per second.
Efficiency:	The ratio of measured counts to the number of decays that occurred during a measurement.
Energy resolution:	The ability of the detector to distinguish gamma rays that are close in energies.
Gamma ray spectrometry:	Is an analytical method that allows the identification and quantification of gamma emitting radionuclides in a variety of matrices.
Half-life:	The time interval required to reduce the number of radioactive atoms in a sample to half of its original value.

Intrinsic efficiency:	The ratio of the number of pulses recorded by the detector to the number of gamma rays hitting the detector.
Ionizing radiation:	Radiation that carries enough energy to discharge electrons from atoms or molecules, thereby ionizing them.
Measurement uncertainty:	The uncertainty of a measurement is defined as a parameter, associated with the result of a measurement that characterizes the dispersion of values that could reasonably be attributed to the measurand. The uncertainty of a measured value is typically expressed as an estimated standard deviation, called the standard uncertainty.
Multiplets:	A set of closely spaced lines in a spectrum, resulting from small difference between the energy levels of atoms or molecules.
Neutron Activation Analysis:	The analysis technique based on irradiating samples with neutrons and measuring the activity of induced radionuclides in the samples.
Photopeak efficiency:	The efficiency for producing full-energy pulses. It is dependent on the energy of the photon and the shape and material of the detector.
Quantitative Analysis:	The collection, organization, analysis, interpretation, quantification and presentation of data.
Radiation:	The emission or transmission of energy in the form of waves or particles through space or a material.
Radionuclide/Nuclide:	A radionuclide is an element or isotope that is radioactive as a result of the instability of the nucleus of its atom (e.g. uranium or radium).
Radioactive/Nuclear decay:	A spontaneous change within the nucleus of an atom, which results in the emission of particles.

Radioactive equilibrium:	A situation in which the ratio between the activities of the successive members of the decay series remain constant (i.e. in a radioactive decay the parent decays into a daughter nucleus that itself is radioactive).
Standard Solution:	The accurately known concentration of an element or a substance in a solution.
Terrestrial radiation:	Radiation originating from the earth and its atmosphere.
Ultra-low Background:	Strongly reduced background due to shielding.
ZAL14:	One of the sixteen (16) CTBTO laboratories that specializes in measurements of gamma radiation and nuclide identification situated within the RadioAnalysis infrastructure of Necsa.

CHAPTER 1

1. INTRODUCTION

Gamma spectrometry is the widely known method for identifying and quantifying radionuclides by analyzing gamma-ray spectra produced by a gamma spectrometer. It is a useful tool in many fields such as environmental sciences, health physics and industrial process monitoring. Gamma spectrometry using HPGe detectors is widely used due to the excellent energy resolution of this kind of detector. In particular, it can be used for activity determination of gamma-emitting radioactive sources whenever the full-peak detection efficiency calibration curve is known, from which the efficiency value for single gamma ray energies is obtained by interpolation (if needed) [1].

In this study, in order to evaluate the ability to accurately analyze low-level NORM-containing environmental samples, a comparison will be made between a well-known available commercial software package (Genie 2000) and a specific software package, Virtual Gamma Spectroscopy Laboratory (VGSL), developed by the Radionuclide Development Unit of the International Data Center of the Comprehensive nuclear Test-Ban Treaty Organization (CTBTO) [2]. Efficiency calibrations obtained from simulations using Canberra calibration software (LabSOCS), MCNP based Virtual Gamma Spectroscopy Laboratory software (VGSL) and from the real-time measurement of certified radionuclide sources prepared by the National Physical Laboratory in the United Kingdom, will be compared. These efficiency calibrations will be used to analyze the spectra obtained in various Proficiency Testing Exercises (PTEs) issued by the Provisional Technical Secretariat of the CTBTO to the sixteen official Nuclide Laboratories in the world-wide monitoring network. As the results of the PTEs are known, the comparison of the results obtained by the application of the three individual efficiency calibrations with the “true” values should provide insight into which of the three calibrations could be used best, or even if two or more calibrations can be used best in specific energy regions.

According to these “best” findings a quantitative method will be developed for application in NORM and artificial nuclide analysis in stream sediments, soil and milk powder. These samples

normally contain decay products of uranium and thorium, which produce multiple gamma-rays. The study was conducted in the ZAL14 laboratory equipped with ultra-low background gamma-spectrometry systems at the Radioanalytical laboratory of the South African Nuclear Energy Corporation SOC Ltd. (Necsa).

The samples will be analyzed looking at a variety of parameter settings, sum-coincidence effects and matrix-dependent self-absorption using the software mentioned. Optimization of parameters will be done using known calibrated reference sample spectra obtained from the CTBTO laboratory Proficiency Test Exercises (PTE) performed over the past decade. The results of the study will show if the empirically generated efficiency calibration by the Genie 2000 Canberra software currently used at the Radioanalytical laboratories of Necsa will be adequate or may be complemented by the efficiency calibrations obtained from the LabSOCS and/or VGSL software, with regard to their user friendliness, accuracy, precision and consistency in spectral analysis.

1.1. Aims and Objectives of the study

In the daily routine of the Radioanalytical Laboratory at Necsa the commercial software Genie 2000, which is one of the frequently used programs worldwide, is generally used for gammy spectrometric analysis.

The aim of this study is to evaluate software packages (LabSOCS and VGSL) that were specifically developed to calculate, geometry and energy dependent absolute efficiency, on their applicability and accuracy in analyses of environmental samples of NORM-nuclides.

The objectives of the study are:

- to critically compare several commercial software Packages including Genie 2000,
- to compare efficiency calibration curves obtained from simulations using LabSOCS and VGSL with empirical calibration curves derived from certified reference sources,
- to test the ability of both the software over the empirical efficiency calibrations to identify the nuclides present in the reference sources available from a number of the PTEs organized by the CTBTO during the last decade (From this the “best” approach for sample analysis will be defined); and

- to determine which programs can be used best for NORM sample analysis with regard to their accuracy and consistency after samples of certified reference materials of stream sediment, soil and milk powder containing NORM-nuclides and ^{137}Cs are prepared and analyzed using the "best" analysis approach.

1.2. Overview of the study

1.2.1. Importance of the Comprehensive Nuclear Test-Ban Treaty

The Comprehensive Nuclear Test-Ban Treaty (CTBT) inhibits countries from performing nuclear weapon test. The main significance of the Treaty is to prohibit the five nuclear power states (The United States of America, United Kingdom, France, the Russian Federation and China) from manufacturing more nuclear explosives and to make it difficult for others to make nuclear explosives [3]. The Treaty intends to protect living organisms from radiological disasters, which may be caused by nuclear explosives.

Between 1994 and 1996 some efforts were made to negotiate the Treaty in Geneva. Out of 196 countries, 183 countries signed the Treaty, but only 161 countries have ratified it. These includes France, the Russian Federation and the United Kingdom. There are 44 countries regarded to be specific nuclear technology holders (that are regarded to have the potential to develop nuclear explosives), that must sign and ratify the treaty before the CTBT can enter into force. Of the 44 countries, 8 are still missing; they are China, Egypt, India, Iran, Israel, North Korea, Pakistan and the USA. Of the 8 countries India, North Korea and Pakistan have not yet signed the CTBT [3].

Since the CTBT is not yet in force, the organization is called the Preparatory Commission (PrepCom) for the Comprehensive Nuclear Test Ban Treaty Organization, which was founded in 1996. It has over 260 staff from over 70 countries, and is based in Vienna, Austria.

1.2.2. CTBTO Task

The Treaty has a comprehensive verification regime to make sure that no nuclear explosion goes undetected. It bans all nuclear explosions whether for war or peaceful purposes. The International Monitoring System (IMS) consists of 337 facilities for

monitoring signs of nuclear explosives worldwide and 85% of the facilities are already in use. The IMS uses four state-of-the-art technologies, which are seismic, hydro-acoustic, infrasound and radionuclide technology.

This study will focus on radionuclide state-of-the-art technology. Under this technology, there are 80 stations that perform radioactive particle measurements in the atmosphere. Forty (40) out of the eighty (80) also detect radioactive noble gases, which is the most reliable technique to give an indication if the detected explosion is nuclear or not. The eighty stations are supported by 16 radionuclide laboratories, one of them located at the Radioanalytical Laboratories of the South African Nuclear Energy Corporation SOC Ltd. [3].

1.2.3. Radionuclide Monitoring

The main objective of radionuclide monitoring is to detect residual radioactivity in the form of radioactive particles or noble gasses. North and South America, Europe and Eurasia, Asia and Oceania, and the Mediterranean and Africa are the four regions over which a network of 80 radionuclide monitoring stations are more or less equally spread. Each one of the four regions is supported by four radionuclide laboratories. The function of the laboratories is to analyze particulate samples independently, to validate the data from the 80 stations and to ensure quality control and quality assurance through routine station sample analysis and Proficiency Test Exercises.

This study will be conducted in one of the radionuclide laboratories in the African region, known as ZAL14, situated within the RadioAnalysis infrastructure of Necsa. The radio-analytical laboratory specializes in measurements of nuclear radiation in all its forms and assesses radiological risk to workers and the public. Routine analyses are carried out for NORMs and anthropogenic radioactivity in various sample matrices including bottled water, agricultural products, biological samples, geological materials and liquid and solid waste generated by the nuclear and related industries.

1.2.4. Commercial Software

There are many computer software packages that perform gamma-spectra deconvolution and peak content analysis. Potential advantages and flaws in the available worldwide commercially available software are evaluated in this chapter. The Packages include [5]

Hyperlab,

Hypermet (version 4.00),

GANAAS (version 3.3),

SAMPO 90(version 3.6),

UniSampo,

PC-SPAN (version 3.1),

VISPECT,

SAANI,

Gamma Vision (version-32),

Gamma Plus (version 1.02.0),

ActAn (version 2.5),

Gamma Track (version 1.3),

Winner Gamma (version 3.42),

Genie 2000, and

VGSL.

Non-commercial systems used mainly in research environments such as ROOT and Radware will not be discussed since the main interest in this work is systems that do not require much user input.

The **Hyperlab** software was found to be the most sophisticated and reliable, for gamma spectrum analysis that is used mostly by research and industrial laboratories [4]. The popular spectrum file formats in the software are CNF, Ortec's SPC and MCA Accuspec.

The measurement data can be recovered and processed easily. In terms of non-linearity and efficiency corrections, it has exact peak location and peak areas for further processing such as identification and activity calculations.

Hypermet uses sophisticated peak shapes and most multichannel spectrum formats such as CVS (keeps track of all work and changes in a set of files) and SAMPO are supported for data processing. The program has a code that is simple and user friendly for adding and deleting peaks. When using the default parameters, the code requires only information for two peaks that are well resolved to carry out energy and automatic shape calibration. Flaws with the program are; the 511 keV peak is not automatically recognized, but can only be fitted manually. [5].

GANAAS is actually neutron activation analysis software operated under DOS [5]. Its installation is quite simple and effective. Results of efficiency calculation are very convenient since the calculations require only one experimental point and the detector's characteristics.

SAMPO 90 is a well-known gamma analysis program, which has an energy plot with unique and colorful features that indicate high uncertainty in energy while extrapolating outside the range of the calibration points. SAMPO's interface is reasonably friendly and fast. The program can automatically find and fit suitable peaks for the shape and energy calibration. For the 511 keV peak, a separate peak shape can be used. The drawback about the program is that it has no mouse support, but provides a user's operation through the keystrokes and it does not support all valid DOS files [5].

UniSampo is a member of the SAMPO family for gamma spectrum analysis. It consists of features, which earlier versions of SAMPO do not have. The program provides users with QA- reports to make sure that the measurement system is working correctly and can analyze a lot of spectra due to its scripting ability. To allow visibility, the peaks are color coded. A re-analysis of the full spectrum can be performed within a very short period of time and the program has a powerful tool for unattended analysis, where email is used to send the spectrum to the computer running UniSampo and the analysis results are returned automatically by email. UniSampo is a program that runs under Linux. It can analyze about 32K spectra with up to 2500 peaks and 32 peaks in a single multiple

extending over a fitting interval of 1024 channels. Other SAMPO versions analyze fewer spectra than UniSampo [6].

PC-SPAN is also used for neutron activation analysis and is operated by the DOS system. The popular spectrum file formats accommodated by the software are Canberra, Ortec or Silena data acquisition systems. The latest version (v5.1) supports the new XML-based SPAN and position file formats. The program is easier to use and has the capability to re-calibrate the energy automatically. The disc protection scheme used by the code makes the installation quite difficult [5]. The 511 keV peak is not properly handled, the code usually combines the total peak method for singlets with a non-linear least squares fit to calculate the peak area and uncertainties for multiplets.

VISPECT is also neutron activation analysis software that aims at assisting the nuclear analytical laboratories. Linux, Windows NT/2000 and Window XP operating systems are used by the program. It is able to record spectra in a short period of time while used by a new trainee. The data analysis results in VISPECT are presented only in printed report form and cannot be presented on screen. Concentration calculations can be obtained by entering the printed data manually, which is a drawback to users [7].

SAANI software was developed and used for gamma ray spectra analysis in the Neutron Activation Laboratory (LAN) of the Nuclear and Energetic Research Institute (IPEN-CNEN/sp) and replaced the old software VISPECT. The software runs under Windows, Linux and other operating programs. SAANI allows better visualization and greater flexibility in the inspection of the spectrum. The graphic routines implemented in the software facilitate the identification and enlargement of the peaks in the spectrum in a fast, simple and easy way. SAANI has no limitations and the data analysis results can be presented in both screen and in a printed form. The SAANI interface is able to offer superior capabilities to the user when using all the resources of the QT (by Trolltech) graphics library and modern operating systems [7].

Gamma Vision has a powerful graphic user interface that is easy to use and operates under MS Windows with multiple detectors. The program consists of automatic peak detection for calibrations (efficiency and energy), which is implemented easily and efficiently, together with a variety of mathematical function selections for efficiency

calibration. After performing the energy calibration, radionuclides can be identified and activities reported. The program can connect up to 250 detectors and offer true coincidence summing corrections [5]. A new Winplots feature can create a report for a specified spectrum region. In the interactive mode the peak position and the region to fit is suggested, but during the fitting process peaks may be dropped by the program.

Gamma Plus, operated under DOS, only works with Silena type of MCA acquisition add-on cards as a data acquisition device. The interface implementation is fast for users and the installation is quite simple [5]. Energy calibration is done automatically. The 511 keV peak is detected and skipped from calibration procedures.

ActAn is a multipurpose software package, which is also used for neutron activation analysis. The program has mouse support and its job records are well kept by listing all the files that were used for calibration [5].

Gamma Track is a DOS operated program developed on the basis of MCA emulation software. Works only with Oxford Nucleus cards as the data acquisition device. The installation is quite simple, with a very easy and convenient way to operate energy calibration procedures [5]. The software finds uncertain standard energies automatically from the ROIs in the spectra. The 511 keV is not properly treated, if the peak is marked for calibration, the FWHM will be erroneous and this can be corrected by removing the 511 keV peak from the list.

Winner Gamma is a MS Windows-based program that controls and operates most of commercially available MCA cards as a data acquisition device. The program is easily installable with energy and resolution calibration provided in automatic mode. It sports a nice and effective interface, making use of all provisions of the Windows operating system. One flaw about the program is that the different spectrum formats cannot be converted and the x-axis cannot be viewed in channel number [5]. Residuals of the fitting procedure are not displayed. There is no online help provided.

Genie 2000, which will also be discussed in 1.3 below, is the newest member of the Canberra Gamma-spectrometry analysis software, which includes a set of algorithms for further processing of gamma spectra acquired. The program is easily used and simply

installable. It detects and analyzes doublets and is capable of dealing with interfering peaks during nuclide identification. A special feature in the program treats the 511 keV line separately. Procedures for energy calibration are simple, effective and powerful. The full multitasking architecture of Genie 2000 allows the software to run multiple independent count procedures for several detectors simultaneously. When the default fit is not satisfactory, the fit is modified either by adding peaks to the multiplets or changing the fitting region. The report generated by the program is flexible and has user defined content.

The automatic gamma spectrometry software, Genie 2000 delivers good reliable results. It performs very well in nuclide identification, fitting peaks and activity determination. Zahn et al. [8] stated that it is convenient to use the software for daily routine work due to the good reliability of results.

VGSL (version 1.2) or the Virtual Gamma Spectroscopy Laboratory is a software package designed to generate gamma spectra through simulation for HPGe detectors, particularly in such systems normally encountered in low-level (environmental) gamma spectrometry laboratories [11]**.**

1.3. Short review on Genie 2000

Genie 2000 is capable of acquiring and analyzing spectra with a variety of functions such as MCA control, spectral display and basic spectrum analysis and reporting. Genie 2000 can also perform alpha spectra analysis, as one of its optional capabilities [9].

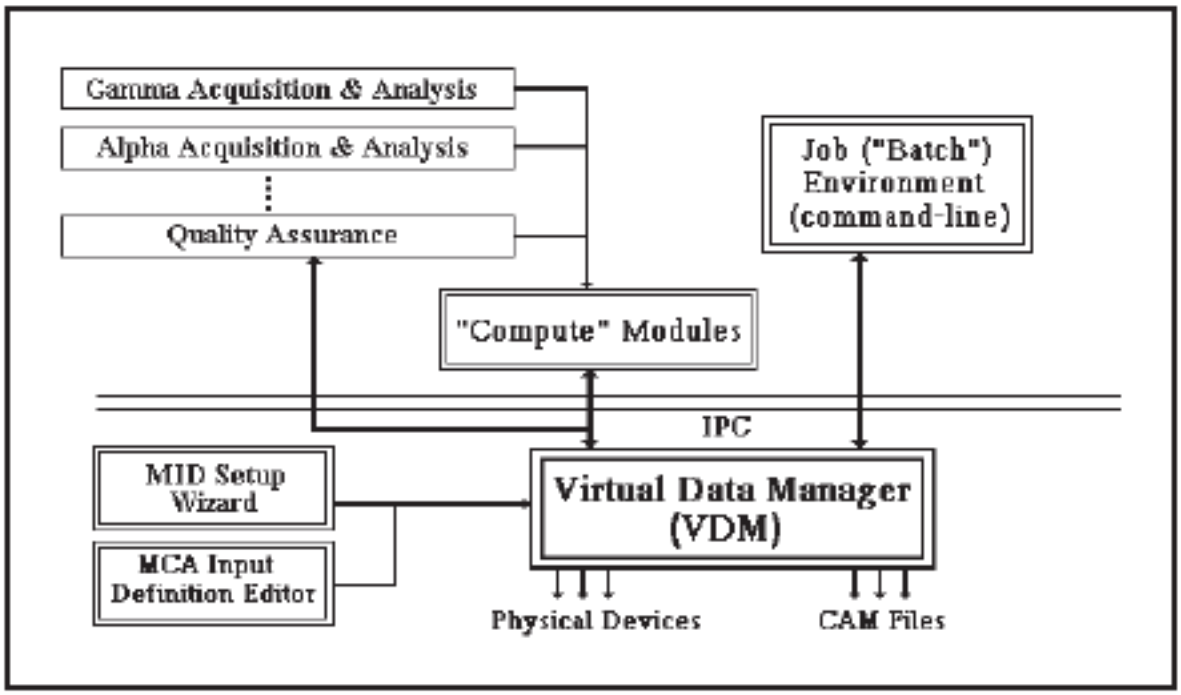

Figure 1.1: Genie 2000 architecture [9]

The Virtual Data Manager (VDM) illustrated in Figure 1.1 is the heart of the software that manages the flow of information in the system. The user can operate on all spectra, regardless of the location with consistent features made possible by the VDM. The VDM is designed to communicate to subsequent layers of software via Inter Process Communication (IPC). The IPC is designed to function both within a single computer and over a network. Thus an MCA hardware device connected to one computer's VDM can be accessed for control, display and analysis over a network from another computer.

Compute modules in Figure 1.1 are modular programs that perform basic functions such as starting or stopping the acquisition. These individual modules can operate together for a certain application requirement [9].

The software has a special feature; the batch environment that allows new users, who are trained to count samples, to easily use the software. It provides an explicit guide on some of the operations and it forbids the new user to access important files, which can only be accessed by qualified operators. Genie 2000 addresses specific applications such as gamma and alpha sample counting, waste assay, whole body counting, safeguard confirmatory measurements and others in the batch environment.

The Genie 2000 spectrometry software manual can be found in softcopies, computer readable format (PDF) following an installation path, or as a folder on the disk.

1.4. Short review on the Virtual Gamma Spectroscopy Laboratory (VGSL) Software

In order to carry out a quantitative analysis, gamma-ray spectrometry requires standard reference samples to establish an experimental efficiency calibration, which is so far the most accurate way to do this. Nevertheless, it can be laborious if numerous sample geometries and various gamma-ray detectors are available [10]. Standard samples are expensive and at times unreliable due to the complexity of some configurations. Due to the short half-life of some radionuclides, standard samples need also to be renewed periodically. The density and chemical composition of the standard sources must be known in order to consider the self-absorption (absorption of gamma-rays in the sample material), especially in the case of large samples, and accordingly it is difficult to establish an efficiency calibration using standard radionuclide sources [10].

To overcome the above mentioned downside, some efficiency calibration calculation codes are available,

- The Canberra calibration software (LabSOCS), and
- The MCNP based Virtual Gamma Spectroscopy Laboratory Software (VGSL).

The VGSL software uses Window 98, 2000, NT, XP or Unix Solaris operating systems. It is a Monte Carlo-based software with a modified version 2.5.e of MCNPX as the transport simulation engine still being developed at the Los Alamos National Laboratory [11]. It provides ten menu options as shown in Figure 1.2 on the opening desktop display, namely Acquisition, Source, Set-up, Detector, Shielding, Source Geometry, Material, Resolution, Refresh time and Settings.

VGSL has a program layer, which builds the input file for the simulation and also displays and interprets the results. This layer is written in MATLAB. Without such an input/output interface MCNP simulations can be tedious and are not suited for users unfamiliar with the program. The user needs no knowledge about the VGSL interface.

Figure 1.2: The initial display of VGSL software

1.4.1. The main features of the VGSL Software

The VGSL software has several important features.

- Performs efficiency calibration calculation for different detector systems.
- It simulates true coincidence summing phenomena.
- Downloads nuclear data from the Evaluated Nuclear Structure Data File (ENSDF) and follows any nuclide decay scheme. The nuclear data are interpreted by the code to model a decay scheme, which includes all possible routes from the initial decay of the parent to the ground state of the daughter. At each nuclear state where there are multiple decay options, one is selected randomly according to the probabilities extracted from data in the ENSDF databases.
- Produces nine kinds of spectra, one natural and eight with combination of natural/sharp resolution, coincidence on/off and peaks only / background only.

1.4.2. Advantages of the VGSL Software

The VGSL software has several advantages.

- A larger and more typical International Monitoring System (IMS) detector with more true coincidence summation effects can be used during spectra simulation.
- Through its simple and complete graphical user interface, any non-Monte Carlo user can easily acquire a gamma spectrum as in a normal lab.

- The spectrum needs not to be stretched to 8192 channels and to change the calibration from originally 2ch/keV to International Monitoring System (IMS) practice of 3ch/keV is easily done [12].

1.5. Short Review on the Laboratory Sourceless Calibration software (LabSOCS)

Geometry Composer is a tool that is used to model complex counting geometries, and combined with Canberra's In Situ Object Counting Systems (ISOCS) and Laboratory Sourceless Calibration software (LabSOCS) products it allows the user to generate a custom efficiency calibration without the need for calibration sources [13].

The LabSOCS is a Monte Carlo-based code integrated in the Genie 2000 gamma-ray spectrometry system of Canberra, which runs on Windows-based PCs. Before using the code, the considered germanium detector must undergo a so called 'characterization' which is carried out by the LabSOCS manufacturer. This characterization is a procedure to obtain the response of the detector for specified sources located within a 500 m radius from the detector, and over a photon energy range of 45 keV to 7 MeV [10].

LabSOCS enables users to create laboratory quality efficiency calibrations while eliminating the need for purchasing and tracking of radioactive calibration sources and standards. By combining a detector characterization produced with the MCNP modeling code, geometry templates, and a few physical sample parameters the LabSOCS calibration software has the ability to quickly produce quantitative gamma assays of almost any sample type and size [13].

1.5.1. Main features of LabSOCS

LabSOCS has several important features.

- No radioactive sources needed for efficiency calibration in the laboratory.
- Calibration is valid from 10 keV to 7000 keV.
- 3D visualization speeds geometry creation and error identification.
- There is no need for source-based peak-to-total calibration for sourceless cascade summing corrections.
- Consists of uncertainty estimator and assay planning tool.

- Includes library of common absorber materials and tools to create new material types [14].

1.5.2. Advantages of LabSOCS

LabSOCS has several important advantages.

- A full factory characterization is performed on the detector. The process uses NIST–traceable sources and the well-known MCNP Monte Carlo modeling code.
- In the software, the characterized detector is incorporated into the model and can be selected from a list of available detectors.
- The software does not require any additional information relating to the detector itself as this information is automatically extracted from a detector characterization file that is generated through the characterization process and is shipped with the detector on CD [15].
- The difference between the intrinsic detection efficiency calculated from the manufacturer's dimensional information and the actual intrinsic detection efficiency can cause significant measurement bias. LabSOCS eliminates this bias since the actual detector crystal is accurately characterized [15].

1.6. Differences and Similarities between VGSL and LabSOCS

There are many similarities but also some important differences between VGSL and LabSOCS.

- VGSL is designed to simulate gamma spectra acquired using HPGe detectors and to perform efficiency calibration calculations for different detector systems. LabSOCS performs efficiency calibration calculations for a wide variety of sources. Both eliminating the need for purchasing radioactive standards.
- VGSL and LabSOCS are MCNP-based software programs. VGSL consists of a simulation engine that uses an MCNP code that was developed, and is still being further developed at the Los Alamos National Laboratory. LabSOCS also uses MCNP Monte Carlo modeling during the calibration process [11].

- LABSOCS software requires no additional information relating to the detector itself, this information is automatically extracted from the detector characterization file while VGSL requires the additional information relating to the detector.
- LabSOCS program has several geometry templates for creating a particular source geometry. VGSL consists of four basic source geometry options offered through the menu by the software.
- VGSL offers a shielding definition option with different layers, types and thickness of the shielding materials, while LabSOCS does not offer any shielding definition option.
- VGSL determines the cascade summing correction factors independently. Genie 2000 software uses LabSOCS computational DLLs to help determine the cascade summing correction factors for measured spectra, including NORM spectra.

1.7. The choice of software for the aim of this study

This study will mainly focus on one of the available commercial software packages, Genie 2000, with its specifically developed software programs for use in high resolution gamma-spectrometry. The focus will be especially on the applicability and accuracy in NORM analysis of environmental samples, which includes optimization of spectrum analysis parameter settings and sum-coincidence and self-absorption corrections. Two additional efficiency calibration software packages, LabSOCS and VGSL will be evaluated as to their applicability in NORM-analysis.

1.8. Dissertation outline

The thesis consists of six chapters. The next chapter will discuss the theory on gamma spectrometry and present the literature review focusing on coincidence summing. Chapter 3 will be on the methodology used in conducting the experimental work. The results obtained for the efficiency calibrations will be presented and discussed in Chapter 4. Chapter 5 will focus on the applicability of the applied software for NORM-nuclide analysis in environmental samples and Chapter 6 will summarize the findings and present the conclusions of the study.

CHAPTER 2

2. BACKGROUND THEORY

2.1. Introduction

The interpretation of features or phenomena of a gamma-ray spectrum requires an understanding of the interaction of gamma-rays with matter, which plays an important role in gamma spectrometry. Other important theoretical topics include coincidence summing.

Coincidence summing in gamma-ray spectra has been a well-known phenomenon for more than 30 years. The initial observation was the change of the relative peak intensities when changing the source-to-detector distances. It was established that this effect increases with the complexity of the decay scheme and with the detection solid angle. This phenomenon is referred to as 'true coincidence 'or 'cascade summing'. Coincidence summing corrections are required for accurate measurements of radionuclides and their activity [16].

2.2. Interaction of gamma-rays with matter

Ionizing radiation interacts with matter and this interaction is, however, very subtle and the direct effect cannot be detected by human senses. A gamma-ray must interact with a detector material in order to be 'seen' [17]. Many radionuclides emit gamma-rays at fixed energies and the gamma ray intensity measured outside a sample is always attenuated because of gamma-ray interactions within the sample. This attenuation must always be considered when using gamma-ray instruments.

When gamma radiation of intensity I_0 is incident on an absorber x, the emerging intensity I transmitted by the absorber is given by the exponential expression

$$I = I_0 e^{-\mu_L x} \tag{2.1}$$

where μ_L is the linear attenuation coefficient. The ratio I/I_0 is called the gamma-ray transmission Figure 2.1 illustrates exponential attenuation for three different gamma-ray interaction processes and shows that the transmission increases with increasing gamma-ray energy. Measurements with different sources and absorbers show that the attenuation coefficient μdepends on the gamma-ray energy and the atomic number (Z) and density (ρ) of the absorber.

For example, lead has a high density and atomic number and transmits a much lower fraction of incident gamma radiation than does a similar thickness of aluminum or steel. The attenuation coefficient in Equation 2.1 is called the linear attenuation coefficient. Figure 2.1 shows the linear attenuation of germanium, a common material used in gamma-ray detectors. The reciprocal of the attenuation coefficient $1/\mu$ has units of length and is often called the mean free path. The mean free path is the average distance a gamma ray travels in the absorber before interacting; it is also the absorber thickness that produces a transmission of $1/e$, or 0.37.

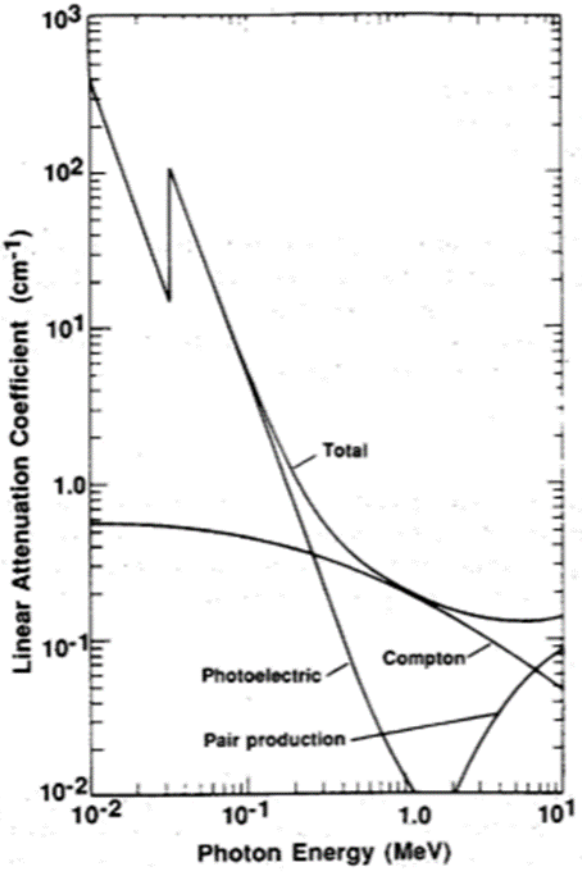

Figure 2.1: Linear attenuation coefficient of germanium showing contributions from photoelectric absorption, Compton scattering and pair production. [18]

2.2.1. Photoelectric Effect

The photoelectric process arises by interaction of a photon with one of the bound electrons in an atom [18]. This electron is ejected from that atom, as shown in Figure 2.2, with a kinetic energy, E_e of

$$E_e = E_\gamma - E_b \tag{2.2}$$

where E_γ is the gamma-ray energy and E_b is the energy binding the electron in its atom.

The atom is left in an excited state with an excess energy of E_b and recovers its equilibrium in one of two ways,

- the atom may de-excite by redistribution of the excitation energy between the remaining electrons in the atom, which can result in the release of further electrons from the atom which transfers a further fraction of the total gamma-ray energy to the detector [18].
- alternatively, the vacancy left by the ejection of the photoelectron may be filled by a higher energy electron falling into its 'orbit' with the emission of a characteristic X-ray, which is called X-ray fluorescence. This X-ray may then undergo photoelectric absorption, emitting further X-rays, which are absorbed until ultimately all the energy of the gamma-ray is absorbed [18].

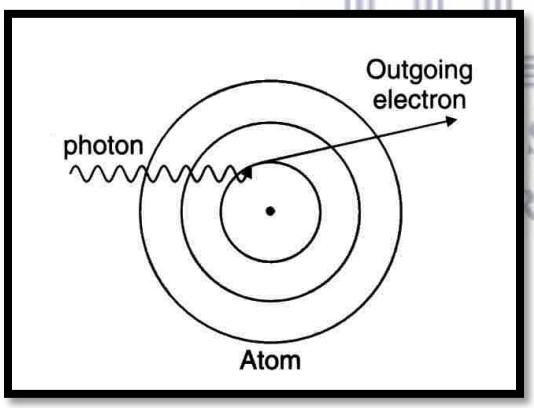

Figure 2.2: Schematic representation of the photoelectric effect [19].

The photoelectric effect probability is determined by the energy of the incident photon and the atomic number of the absorbing material as illustrated in Equation 2.3. The higher the energy of the incident photon, the smaller the chance for the effect to occur and the higher the atomic number of the absorbing material, the larger the chance for the effect [20].

$$Probability\ of\ the\ effect: P_{PE} \propto \frac{Z^5}{E_\gamma{}^{3.5}} \quad (2.3)$$

where, Z is the atomic number of the absorbing material and E_γ is the energy of the photon.

2.2.2. Compton Effect

Compton scattering as depicted in Figure 2.3 is a direct interaction of a photon with an electron, transferring part of the gamma-ray energy to the electron where only free electrons in the outer orbitals are involved in the process. The energy imparted to the recoil electron is given by the following equation:

$$E_e = E_\gamma - E_{\gamma'} \quad (2.4)$$

where E_γ is the gamma-ray energy and $E_{\gamma'}$ is the energy of the scattered gamma-ray.

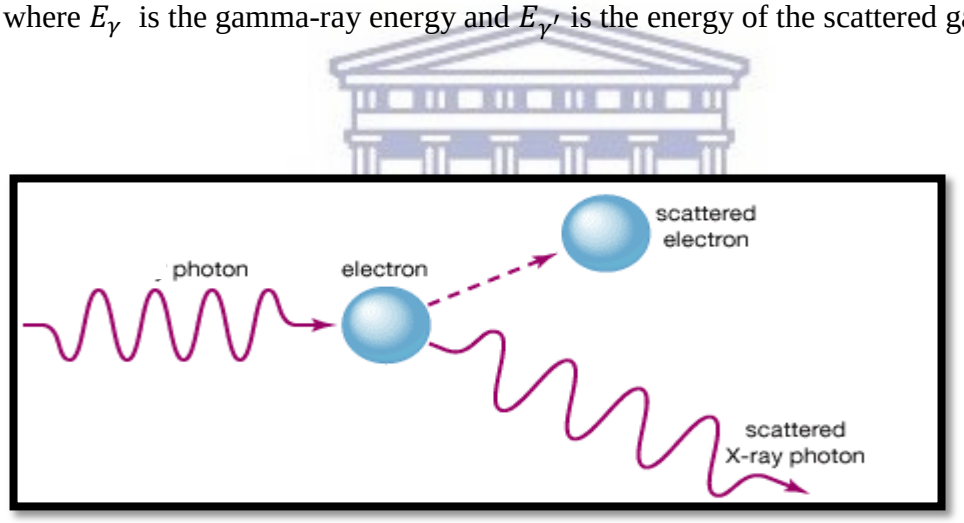

Figure 2.3: Schematic representation of Compton scattering [21].

The angle at which the electron is moving, including the ratio in which the available energy of the incident photon is divided between the electron and the scattered photon can be calculated if the angle θ is known as given by Equation 2.5. When the photon is scattered directly backwards and the electron moves in the direction of the incident photon, the photon will transfer a maximum energy at $\theta = 180^\circ$. This energy transfer is always less than the total energy that can be transferred by the same photon in a

photoelectric interaction. The angle of scatter is any value between 0°and 180°, and the amount of energy is related to the scattering angle.

$$E_e = E_\gamma \left\{ 1 - \frac{1}{1 + \frac{E_\gamma [1 - cos\theta]}{m_0 c^2}} \right\} \tag{2.5}$$

The probability for Compton interaction increases approximately with the atomic number of the absorber, and decreases with the energy of the incident photon [20]. This can be summarized by:

$$Probability\ of\ the\ effect : P_{COM} \propto \frac{Z}{E_\gamma} \tag{2.6}$$

2.2.3. Pair Production

Pair production results from the interaction of the gamma-ray with the atom as a whole. The process takes place within the Coulomb field of the nucleus resulting in the conversion of a gamma-ray into two particles with the same mass but opposing electrical charges as shown in Figure 2.4.

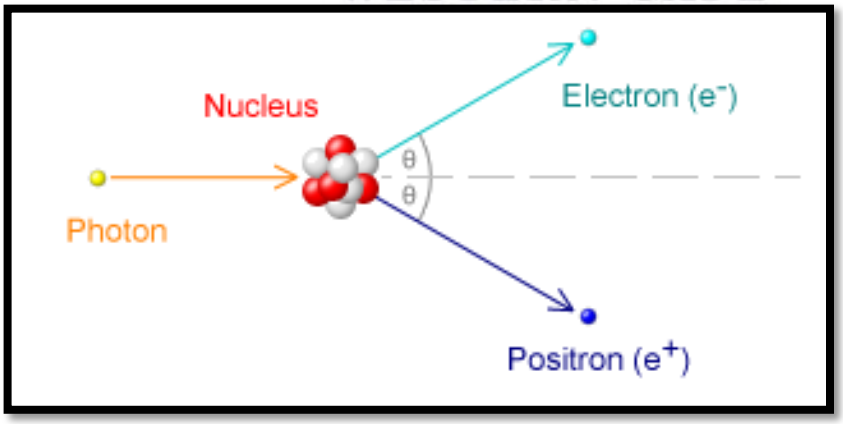

Figure 2.4: Schematic representation of the pair production process [22].

The electron and the positron are particles involved in the process. The excess energy is shared by the electron and the positron in the form of kinetic energy:

$$E_\gamma = 1022 + \left({}^1/_2\, mv^2\right)_+ + \left({}^1/_2\, mv^2\right)_- \quad (2.7)$$

The + and – signs indicate the kinetic energy for the positron and electron respectively. In principle, pair production can also occur under the influence of the field of an electron but the probability is much lower and the energy threshold is four electron rest masses, and the pair production cross-section is about two orders of magnitude lower than for direct interaction with the nucleus, making it negligible as a consideration in gamma spectrometry [18]. Pair production can only occur if the energy of the gamma ray is equivalent or larger than the combined rest mass of an electron and a positron, which is 511 keV each, thus 1022 keV in total.

Once a positron has been produced by pair production, the positron will lose its kinetic energy by interaction with electrons in the absorbing material [20]. Then it will undergo annihilation. In this process the positron and an electron pair destroy or annihilate each other with the production of two photons with an energy of 511 keV each. The two photons involved conserve momentum and can be represented by

$$\beta^+ + \beta^- \Rightarrow \gamma_1 + \gamma_2 \quad (2.8)$$

and

$$E_{\gamma_1} = E_{\gamma_2} = 511\ keV \quad (2.9)$$

2.3. Attenuation coefficients

Gamma rays interact primarily with atomic electrons; therefore, the attenuation coefficient must be proportional to the electron density, which is proportional to the bulk density of the absorbing material. However, for a given material the ratio of the electron density to the bulk density is a constant, Z/A independent of bulk density. The ratio Z/A is nearly constant for all except the heaviest elements and hydrogen [65].

$$P \propto Z\rho/A \quad (2.10)$$

where P = electron density, Z = atomic number, ρ = mass density and A = atomic mass.

The ratio of the linear attenuation coefficient to the density (μ_L/ρ) is called the mass attenuation coefficient μ. The units of this coefficient hint that one may think of it as the effective cross-sectional area of electrons per unit mass of absorber. The mass attenuation coefficient can be written in terms of a reaction cross section, σ

$$\mu = \frac{N_0 \sigma}{A} \tag{2.11}$$

Where N_0 is Avogadro's number (6.02×10^{23}) and A is the atomic mass of the absorber. The cross section is the probability of a gamma ray interacting with a single atom. Equation 2.1 can be rewritten as

$$I = I_0 e^{-\mu_L x} = I_0 e^{-\mu \rho x} \tag{2.12}$$

Where $\mu_L = \rho\mu$

The mass attenuation coefficient is independent of density. Equation 2.13 is used to calculate the mass attenuation coefficient for compound materials:

$$\mu = \sum \mu_i w_i \tag{2.13}$$

where μ_i is the mass attenuation coefficient of i^{th} element and w_i is the weight fraction of i^{th} element.

The attenuation coefficient is dependent upon the type of material and the energy of the radiation. Generally, for electromagnetic radiation, the higher the energy of the incident photons and the less dense the material in question, the lower the corresponding attenuation coefficient will be. Gamma-ray shielding materials should be of high density and high atomic number for a high total linear attenuation coefficient and a high photoelectric absorption probability. In this study, shielding is required to limit the detector's response to background gamma rays and to shield the operator from strong sources such as activation sources. The shielding and detector materials used for this study will be discussed in section 3.1 and 4.2.

2.4. Coincidence summing

Coincidence summing of gamma-radiation occurs when two or more gamma-rays are emitted during the same decay event of the nucleus, and are recorded as one pulse within the resolving time of a detector. There are three types of phenomena that result from the coincidence summing. The first phenomenon is referred to as 'summing out'. This occurs when two gamma rays sum; the apparent efficiency for each gamma ray is less than a gamma ray of the same energy with no coincidence summing. The second phenomenon, known as 'summing in', occurs when two gamma rays in coincidence sum to give a photo peak with the same energy as one that occurs from a single transition. Thirdly, if one of the gamma-rays undergoes Compton scattering, the absorbed energy does not correspond to a peak in the spectrum and the event only contributes to the background [23].

There are a number of nuclides which emit multiple gamma-rays though for which summing of the specified gamma-rays, are usually negligible (e.g. ^{113}Sn and ^{131}Am). Other gamma-rays are emitted with such a low abundance that summing, although possible, can be ignored [66]. If both gamma-rays arriving at the detector within the resolving time of the amplifier were fully absorbed and contribute to their respective full-energy peaks, the coincidence will result in the loss of one count from each peak and the appearance of a count somewhere else in the spectrum. This will create many difficulties in achieving a valid efficiency calibration for close geometry measurements.

This study shows the need for coincidence summing correction factors for the gamma lines in the ^{232}Th series for determining accurate activity concentrations in environmental samples. For the PTE samples, gamma lines such as, 898.0 keV and 1836.1 keV of the ^{88}Y, 898.0 keV and 165.85 keV of the ^{139}Ce together with the 1173.2 keV and 1332.5 keV gamma lines of the ^{60}Co, are particularly prone to coincidence summing.

A simplified decay scheme for ^{88}Y, ^{139}Ce and ^{60}Co are depicted in Appendix C.

The likelihood that two gamma rays will be detected together, decreases with increasing distance between source and detector [66]. It should be noted that at any source-to-detector distance, there will be some degree of summing. But in practice, depending on the detector size, coincidence summing losses beyond a certain distance are negligible. It should be noted that for a given solid

angle, the number of true coincidence summing events per second is proportional to the sample activity. In this study the source is placed directly on the detector.

There are several ways of computing coincidence summing corrections, each method having its advantages and drawbacks. Coincidence summing is at present one of the main sources of systematic error in gamma-ray spectrometry. The errors made in neglecting coincidence summing effects are frequently larger than the accuracy required by the measurement procedure.

2.4.1. Development of computer programs for coincidence summing corrections

The original formulae were given by Andreev D.S. et al. [27, 28] and were further rewritten by Coote G.E. and McCallum G.K. [25] who developed a computer program to calculate integrated effects of all coincidence summing in a complex spectrum, which incorporates a general method for calculating full-energy efficiencies at any distance between the source and the detector.

A few years later, Debertin K. and Schotzig U. [26] developed a computer program KORSUM to calculate the correction for nuclides with arbitrary decay schemes. The contribution of gamma-ray emission following internal conversion or electron capture was incorporated in the program. Other effects such as coincidence with beta-rays or bremsstrahlung and angular correlations were not regarded as being worthwhile to consider as their contribution to the total summing correction usually is low and smaller than the uncertainty of the correction. The best solution to the problem of coincidence summing corrections was to calibrate the detector with an equally sized standard source of the nuclide of interest. In that case, the coincidence summing effects need not be considered. They concluded that for all other close geometry measurements, coincidence summing corrections have to be calculated or at least estimated.

Morel J. [29] also developed a computer program CORCO. The importance of coincidence summing for some commonly used radionuclides for calibration purposes was evaluated. Since these innovative works, new developments were carried out about twenty years later. A new technique to calculate coincidence-summing corrections in gamma-ray spectrometry was developed by Semkow T. M. et al. [24]. They developed a method to determine the peak-to-total ratio for a germanium detector in the presence of an interfering gamma-ray. The general coincidence-summing equations were derived in

matrix notation so as to be used for decay schemes of any complexity, whether from radioactive decay or in-beam experiments.

Korun M. and Martini R. [30] incorporated coincidence-summing effects due to X-rays from the technique developed by Semkow T. M. et al. [24]. They showed how the technique can be applied for calculation of the full energy peak and detection efficiencies. The study revealed that if the measurements are performed with low-energy detectors, the additional coincidence summing effects due to X-rays must not be ignored. The technique can be applied to assess the ratios of probabilities for emission of X-rays and for parameter optimization in peak-evaluating procedures.

New developments were made with Monte Carlo simulation for computing efficiencies and numerical computation of the correction factors. Haase, G. et al. [31], developed a Monte Carlo simulation technique for gamma-spectrometric measurement systems, which allowed calculation of the fraction of photons of a given energy in the detector from the photon path lengths along with the calculation of the efficiency, which can be calculated from the known number of photons generated. From the mentioned parameters, correction factors for self-attenuation and coincidence summing could be estimated. The method provided accurate estimations of the total efficiency and correction factors for both summation effects and self–attenuation for a wide range of sources and detectors. Calculations required only readily obtainable data and were rapidly carried out with commercially available personal computers.

A different method was developed by Wang, T.K. et al. [32] to estimate the gamma-gamma true coincidence correction factor (COI) for extended cylinders and Marinelli-beakers. The validity of using the developed method was successfully demonstrated by comparing the predicted COI values with the experimentally determined values for several radionuclides, i.e. the estimated COI factors were in good agreement with the measured COI values.

De Felice et al. [33] developed a different approach by investigating simplified and fast procedures for coincidence summing correction in gamma-ray spectrometry. These procedures were based on the usual theoretical expression of the correction factors, but

differ in the determination of the efficiency curve, and are particularly important for applications where extreme accuracy is not required and where time and costs are important factors to consider.

Dias M.S et al. [1] developed a code named COINCIG that calculates the cascade summing correction using efficiencies, calculated by the Monte Carlo method or obtained experimentally. The main objective of the study was to develop a code that can estimate the parameters (value of peak detection efficiencies) for point and cylindrical sources. The cascade summing correction requires total and peak efficiencies, so an additional Monte Carlo code, MCEFFIC, has been developed for estimating these parameters. For testing this procedure the radionuclides ^{60}Co, ^{133}Ba and ^{131}I were used. The peak and total efficiencies have been numerically calculated by the Monte Carlo method and compared with the experimental results used for both point and cylindrical sources. The cascade summing correction involves the decay scheme characteristics and detection efficiencies. In this work a second Monte Carlo algorithm was developed, which follows each path in the decay scheme, from the beginning state of the precursor radionuclide decay level, down to the ground state of the daughter radionuclide. With this procedure it was possible to calculate the cascade summing correction for all of the gamma-ray transitions present in the decay scheme. The obtained results showed that the calculated peak detection efficiency was higher than the experimental efficiency by 10% at 50 keV and by 40% at 3000 keV. However, the probability of simultaneous total absorption of two gamma rays at high energies is very low. Therefore, the contribution of the peak efficiency error to the cascade summing uncertainty is usually small. The preliminary version of COINCIG does not take into account coincidence with X-rays. Therefore, it can be used when the X-ray detection efficiency is low. Improvements in the code are planned to include this feature. Experimental peak efficiencies can be easily obtained from the code COINCIG to yield accurate cascade summing corrections. The uncertainties in the summing correction do not include the uncertainty in the efficiency. It was concluded that a complete description of the total uncertainties must take into account the covariance analysis, which was planned for a future version of the COINCIG code.

A great deal of effort has gone into the coincidence summing corrections in gamma-ray spectrometry. Thus today, there are several ways of computing the coincidence corrections and each method has advantages and drawbacks [16].

2.4.2. Intercomparison of methods for coincidence summing corrections

Nielsen S.P. and Palsson S.E. [34] made an intercomparison study of software used for the analysis of gamma-ray spectra obtained by germanium detectors, by testing the quality of calculated areas and associated uncertainties of well-isolated single peaks in IAEA test spectra. Fifteen sets of data were submitted for the intercomparison with ten different software packages. The intercomparison comprised tests of precision and accuracy. The method used for peak-area calculation by the different software packages were classified into simple summation, fitting techniques and other categories. The fitting technique was known to be a more sophisticated method, according to which an analytical representation of the peak is fitted to the data, using a least-squares technique [34], and the peak is determined from the fitted parameters.

The results of the intercomparison showed that the quality of results from gamma-spectrometric analysis of radionuclides providing well isolated single peaks (e.g. ^{137}Cs) varied significantly between software packages. The intercomparison encompassed tests of precision and accuracy, and only four of the fifteen data sets showed both acceptable precision and accuracy. The data sets based on sophisticated methods for calculating peak areas did not show higher accuracy compared to those based on more simple methods. The tests for precision have shown that only eight of the fifteen data sets showed agreement between the calculated and observed variability of the peak areas. Accuracy tests have shown that only six data sets demonstrate agreement between calculated peak-area ratios and true values from the IAEA spectra considering the calculated uncertainties. The overall ranking of the Genie 2000 package in terms of accuracy of peak-area ratios was average to high accuracy. The rankings for the various software packages are shown in Table 2.1.

Arnold D. et al. [35] carried out a study on the intercomparison of widely available software packages, Agnes 1.0, Gamma Vision 5.3, Gamma W 1.68, Ganaas 3.11, Genie 2000 2.1, Hyperlab 2002 3.2.18, Inter-winner 5.0 and UniSampo 1.97 used in low-level

gamma-ray spectrometry. The objective of the study was to compare the obtained activities with the certified activities; results were presented and suggestions were made for further improvements. The software packages were compared on peak determination, activity determination and library comparison. The reported peak areas were compared with the reference peak areas in terms of z-scores and χ^2 reduced values. Findings showed that some programs came with multiple libraries, which were considered separately. The Gamma Vision and Genie 2000 packages claimed to have coincidence summing correction abilities. Genie 2000's default threshold setting of its peak search algorithm apparently was high compared to the others, but it failed completely for 'sum peaks' since it reports nothing for any pure sum peak. It performed no correction for any of the natural radioactivity nuclides, since these are missing from its database of decay schemes. This database cannot be edited or supplemented by the user. The best statistical control was exhibited by Gamma-W; the best activities were reported by Gamma-W and Genie 2000. None of the programs dealt with the 1459-1460 keV doublets of ^{228}Ac and ^{40}K. All programs tested in this intercomparison were efficiency-curve based, and all failed in some respect to accomplish their task.

Karhu P. [36] did a survey to determine if a simulated spectrum would also be effective for proficiency testing, realistic enough to achieve correct results and challenging enough to test the analysis process. The gamma spectrum with the characteristics of an atmospheric nuclear test was used as reference material produced by the MCNP-based VGSL software package. A Monte Carlo simulation spectrum was used instead of a measured spectrum. VGSL reference values were considered true values without uncertainties. These values were used as input to the simulation. All spectra and the total efficiency calibration corresponded to the same detector system and sample set-up. The spectra were provided in IMS 2.0, Canberra Genie 2000, Ortec Gamma Vision and Ortec InterWinner formats. At the end of the test analysis, the results were deemed to agree with the VGSL reference values. The comparison of the PTS test analysis results and participants' mean results against VGSL reference values indicated that the simulated reference spectrum was realistic enough to be used in proficiency tests.

Table 2.1: Overall ranking of data sets according to the accuracy of peak-area ratios. Repetition of codes refers to different users using the same code – see Ref [34] for detail.

Data No.	Software	Accuracy
1	CompAct/NTS Ltd., v. 2.1	High accuracy
2	GammaVision/EG&G Ortec	Low accuracy
3	GammaVision/EG&G Ortec	Low accuracy
4	GammaVision/EG&G Ortec v. 2.3	High accuracy
5	Genie-PC/Canberra	Average accuracy
6	Genie-PC/Canberra	Average accuracy
7	C-BASE	Average accuracy
8	Genie-PC/Canberra	High accuracy
9	GAMANAL	Average accuracy
10	GRILS	Low accuracy
11	EMCAPLUS/Silena	High accuracy
12	ANSP	High accuracy
13	GammaTrac/Oxford, v. 1.21	High accuracy
14	GammaTrac/Oxford	Average accuracy
15	GAMMA-96	High accuracy

Pibida L. [37], made a comparison of software packages for germanium detectors. Several gamma-ray data analysis software packages were compared to one another in order to determine their accuracy and consistency in the determination of the gamma-ray full energy peak efficiency as a function of photon-energy. Four generally available software packages for HPGe detector gamma-ray spectrum analysis including the one currently used at the South African Nuclear Energy Corporation SOC Ltd. (Genie 2000) were tested for efficiency on spectra collected from two HPGe detectors at different source-to-detector distances and two kinds of geometries. The two geometries involving NIST standard reference material (SRM) were prepared and counted three times with each detector for one-day each to ensure a statistical uncertainty in the peaks of less than

0.5%. The application of Efficiency Transfer for Nuclide Activity Measurement (ETNA) [37] is limited to those cases where specific geometries must be described and for which measured efficiency values are not available, and where uncertainties of the order of ~5% to 15% are acceptable for activity or impurity determinations. It was concluded that all available software packages should be modified and refined to meet the American National Standard Institute (ANSI) N42.14-1999 standard (American National Standard for Calibration and Use of Germanium Spectrometers for the Measurement of Gamma-Ray Emission Rates of Radionuclides). This will contribute to better characterization and calibration procedures to obtain greater confidence in reported results on activity and/or impurity measurements.

2.5. Naturally Occurring Radioactive Material (NORM)

In this study gamma spectrometry was used to identify artificial and NORM nuclides in stream sediment (IAEA-314) collected from the Kalan area in Indonesia, milk powder (IAEA-152) obtained from cows that grazed on contaminated land with radioactive fallout resulting from the Chernobyl incident in 1986 and the soil (IAEA-375) collected from 'Staryi Viskov' collective farm in Novozybkov, Brjansk, Russia. All three are certified IAEA Reference Materials.

Gamma spectrometry is one of the techniques used to measure the natural radioactivity content of different environmental materials. It has many advantages such as high accuracy, a wide energy range, able to handle different types of samples, does not need a chemical method in sample preparation and is non-destructive. However, gamma spectrometry of NORM-nuclides is still difficult for a number of reasons. Firstly the activity levels of environmental samples are normally low and if statistically significant results are to be obtained long counting periods are required. Secondly, ideally one needs a gamma spectrometer whose construction materials and physical location are optimized for low activity measurements, ensuring as-low-as possible background spectra. Lastly the accuracy of the analyses is influenced by the fact that there are a large number of mutual spectral interferences between a large number of nuclides in the natural decay series of uranium, actinium and thorium, as well as potassium.

2.5.1. Origin of NORMs

The world is naturally radioactive and about 90% of human radiation exposure is from natural sources such as cosmic radiation, exposure to radon gas, and terrestrial radiation

[37]. Radioactivity of the soil environment (terrestrial radiation) is one of the major sources of exposure to human. The ^{238}U, ^{235}U, ^{232}Th series and natural ^{40}K are the main source of natural radioactivity in soil. Since these have very long half-lives of up to 10^{10} years, their presence in soils and rock can simply be considered as permanent [39].

NORM levels are typically expressed in one of two ways;

- becquerel per kilogram or gram, which indicates the level of radioactivity in general or due to a particular radionuclide (e.g. ^{226}Ra), or
- parts per million (ppm), indicating the concentration of a specific element (uranium, thorium or potassium) in the material [40].

2.5.1.1. Terrestrial NORMs

This is the natural radioactive material that is contained in the earth's crust and mantle. Human activity like mining and mineral processing may result in increased concentrations at the surface and potentially lead to additional radiological exposure. The materials may be minerals containing uranium and thorium or the decay products thereof, or potassium-40. The long half-lives ranging between ~ 1.3 and 14 billion years means that they still exist in measurable quantities today. Potassium, containing 0, 0117% ^{40}K, is one of the more abundant elements in the earth's crust, and is found in many foodstuffs and fulfills important dietary requirements [40].

2.5.1.2. Cosmogenic NORMs

Cosmogenic NORMs (e.g. ^{7}Be) are formed as a result of interaction between certain gases in the earth's atmosphere and cosmic rays. Since most cosmic radiation is deflected by the earth's magnetic field or absorbed by the atmosphere very little reaches the earth's surface. Cosmogenic radionuclides contribute more to the dose received at low altitude than cosmic rays as such. At higher altitudes the dose due to both increases.

2.5.2. NORM decay series

Uranium and thorium nuclides are unstable and decay mainly by alpha-particle emission to nuclides that themselves are radioactive. Natural uranium is composed of three long-lived isotopes: ^{238}U, a smaller portion of ^{235}U and an even smaller portion of ^{234}U, which is the decay series daughter of ^{238}U. Natural thorium has one single isotope,

^{232}Th. Each of these nuclides decays to an unstable daughter leading in turn to a whole series of nuclides that terminate in one of the stable isotopes of lead. Under normal circumstances, in a natural material, the ^{235}U to ^{238}U ratio will be fixed and all nuclides in each of the series will be in equilibrium. Gamma spectrometry of materials containing these nuclides can only be effectively done with a detailed understanding of the decay chains of the nuclides involved.

2.5.2.1. Uranium series

The radionuclide ^{238}U has a very long half-life of 4,468 x 10^9 years [39]. The decay chain of this radionuclide is shown in Figure 2.4. The radionuclide ^{238}U decays into ^{234}Th emitting an alpha-particle. The newly formed nuclide is also unstable and decays further. Finally after a total of fourteen such steps, emitting eight alpha particles and six beta-particles, accompanied by gamma radiation, stable lead-206 is formed. Five nuclides can be measured by gamma spectrometry, ^{234m}Pa, ^{226}Ra, ^{214}Pb, ^{214}Bi and ^{210}Pb. In natural rock this series is said to be in secular equilibrium because all the daughters following ^{238}U have a shorter half-life than the parent nuclide [39]. This decay series includes ^{222}Rn which is an inert noble gas that will not form any chemical bonds with other substances and can escape into the atmosphere where it adsorbs rapidly to aerosols and dust particles deposited in air.

2.5.2.2. Actinium series

The nuclide ^{235}U is the parent of the actinium series. The radionuclide ^{235}U decays into ^{231}Th emitting an alpha-particle, but the newly formed nuclide is unstable and decays further till the stable isotope ^{207}Pb is formed as shown in Figure 2.4. Six nuclides from the series can in principle be measured by gamma spectrometry, ^{231}Pa, ^{227}Th, ^{223}Ra, ^{219}Rn, ^{211}Pb, and ^{211}Bi, although their line intensities are low and spectral interferences from other NORM nuclides are found.

2.5.2.3. Thorium series

Natural thorium is 100% ^{232}Th. The decay series shown in Figure 2.5, illustrates that six alpha and five beta particles are emitted during the decay stages. Four nuclides can be measured by gamma spectrometry, ^{228}Ac, ^{212}Pb, ^{212}Bi and ^{208}Tl. The decay of ^{212}Bi is branched; 35.94% [64] of the decays produce ^{208}Tl by alpha decay, while the rest goes

through the beta decay branch to produce ^{212}Po. If a ^{208}Tl measurement is used to estimate the thorium activity, the measured activity must be divided by the branching ratio to correct for the branching.

2.5.2.4. Potassium

In 1905, J.J Thompson discovered the natural radioactivity in potassium due to ^{40}K. This nuclide is part of the natural potassium in the human body, which is present in the body at a level of about 4.0 gram per kg body weight (≈ 0.45 mg ^{40}K per kg) and accordingly makes everybody radioactive. This radionuclide can decay through three general modes: positron emission, K-electron capture and by beta emission. In the first mode, ^{40}K disintegrates directly into the ground state of ^{40}Ca by the emission of a beta-particle with an energy of 1321 keV and a probability of 89.28% of the decays, and no gamma emission is associated with this type of transformation [39]. Through the second mode, the ^{40}K nuclide can be transformed into the stable state (ground state) of ^{40}Ar by two ways. In the first one, ^{40}K disintegrates directly into the ground state of ^{40}Ar by electron capture with a probability of 0.048%. In the second mode, ^{40}K decays by positron emission to ^{40}Ar , first to an excited state and then to the ground state, through emission of a gamma ray of 1460 keV with a probability of 10,67%[39].

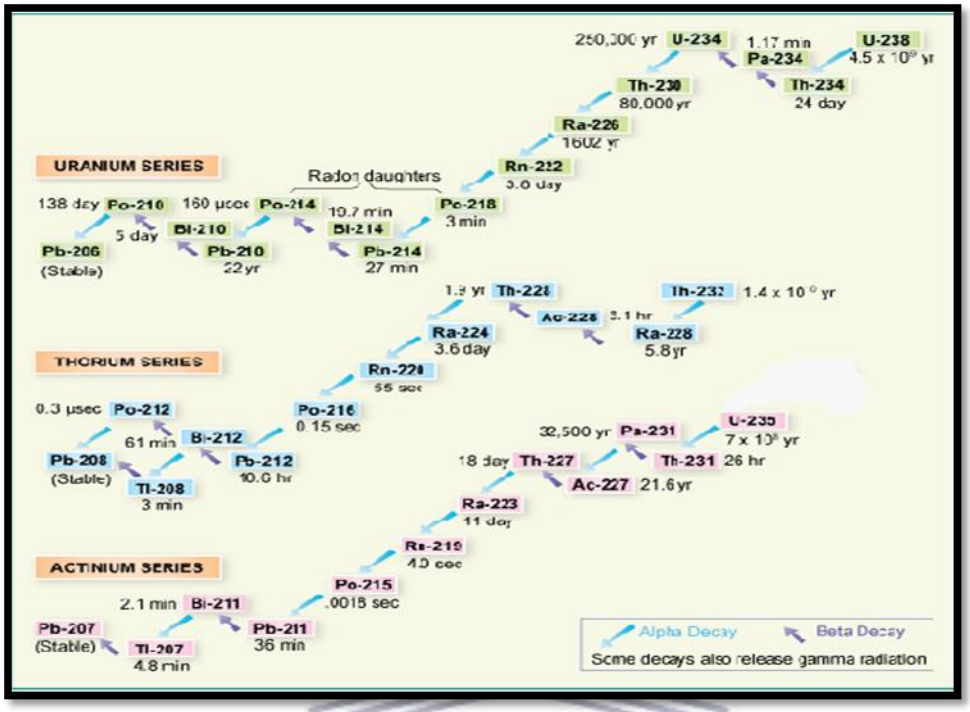

Figure 2.5: Radioactive decay series of Uranium, Thorium and Actinium [40].

2.6. Spectrum Analysis Algorithms in Genie 2000

Canberra offers a variety of nuclear measurement systems, which perform data acquisition as well as data analysis, usually using its Genie spectroscopy software. The systems range from small stand-alone instruments to more sophisticated configurations involving a variety of computer platforms; typical applications include environmental monitoring, body burden analysis, nuclear waste assay, safeguards and other applications [41].

2.6.1. Peak locate and area

The Genie 2000 architecture provides five algorithms for locating peaks of interest in a spectrum. The chosen algorithm for this study is the 'Second Difference Method', which can then be used by peak analysis algorithms for peak area calculations. The peak search method used by Genie can be understood by looking at Figure 2.6. A model peak with the expected FWHM is moved across the channels and the Chi-square calculated for the model peak and the measured spectrum as shown in the insert on the figure. This will lead to a Chi-square vs channel plot that will give a minimum when the model peak coincides with a peak in the spectrum. The fitted minimum is then used as the peak

position. Appendix D gives the mathematical formulae that give the peak position as well as the uncertainty as given by Canberra.

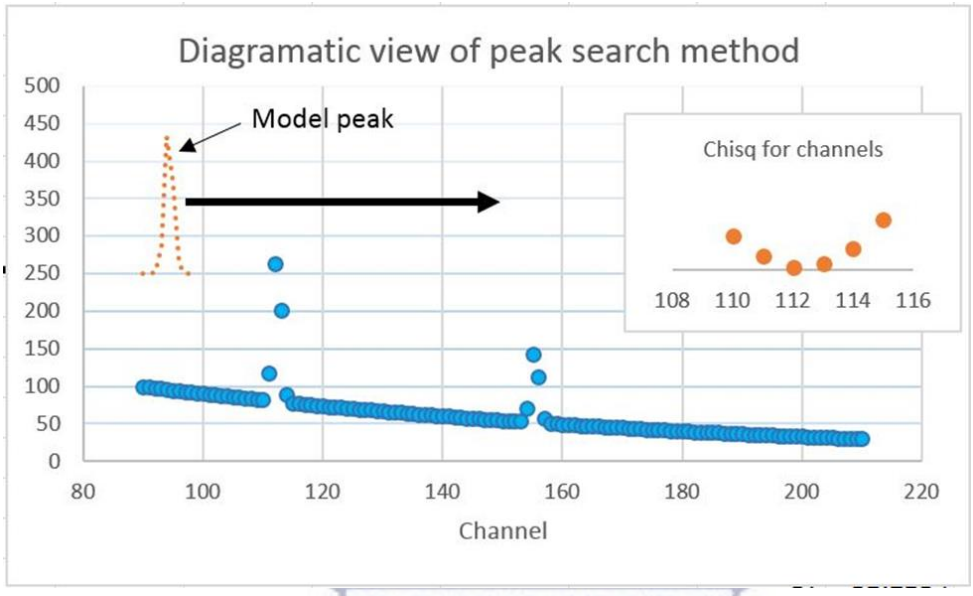

Figure 2.6: Diagrammatic view of the peak search method used

Background subtraction

The background subtraction allows the subtraction of the environmental background which is emitted from the walls of the laboratory. The study is conducted in an ultra-low background laboratory. A background spectrum is periodically obtained for the laboratory routine work; the spectrum must be analysed separately for its peak locations and associated areas.

2.6.2. Efficiency correction

The value for efficiency is dependent on the geometry of the sample, the size, density, and distance from the detector. For the detectors used in gamma analysis the efficiency varies significantly with energy. Therefore, each counting geometry requires a separate efficiency calibration, using a known standard in the same geometry, which has multiple energies. A series of data pairs of efficiency vs. energy are generated from the relationship:

$$Efficiency = \frac{Net\ Area}{(Live\ time)(Activity)(Yield)} \tag{2.14}$$

where,

(Activity) is the strength (in Bq) of the standard source (at collection time) at the given energy,

(Yield) is the branching ratio fraction, and

(Live time) is the actual ADC live time.

In the Genie software system, the calibration data from the standard are entered into a "Certificate File", with these data being used for subsequent efficiency calibrations. The software will automatically correct for source decay between the calibration date and the measurement date.

Two methods are included in the correction phase, the standard and the ISOCS efficiency correction. The standard efficiency correction uses the actual established efficiency calibration for its calculation and the ISOCS efficiency correction uses a mathematical calibration that directly calculates the efficiencies.

The standard efficiency correction phase was chosen for the spectra analysis in this study. The phase consists of four correction modes; the dual, linear, empirical and interpolated mode. Figure 2.7 and Figure 2.8 are graphical displays of the dual efficiency calibration curves on a linear and dual scale that allows adjusting of the order of the polynomial of the curve in order to obtain the best fit. The dual mode calculates the efficiency at each peak-energy using the dual efficiency curve. The dual mode was used for this study because it supports two separate models, the “two curves” with the low energy region and the high energy and the “single curve” model where the cross-over is zero. For the “two curves” model, a cross over point is defined typically between 120 and 150 keV.

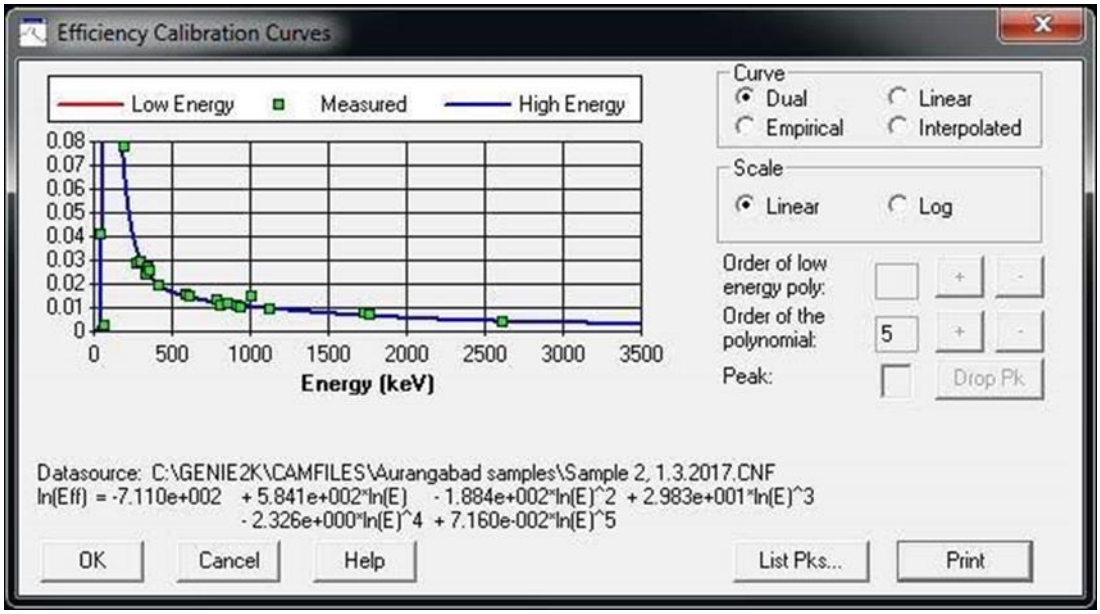

Figure 2.7: Efficiency calibration curve on a linear scale.

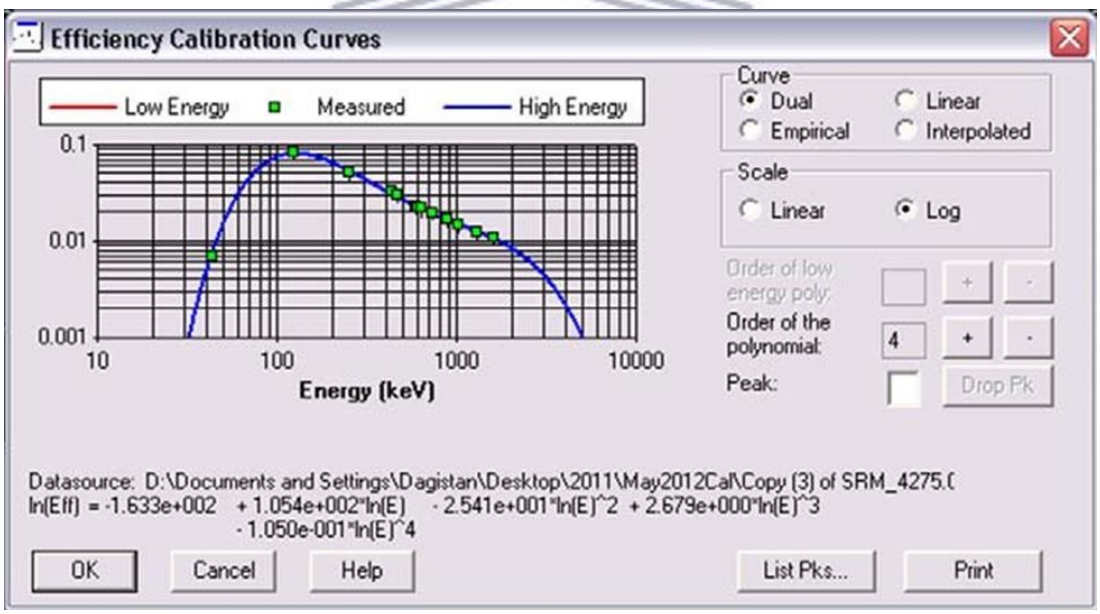

Figure 2.8: Efficiency calibration curve on a dual scale.

2.6.3. Nuclide Identification

Many applications with high purity germanium (HPGe) detector spectra involve identifying particular gamma rays and allocating them to specific nuclides. A radionuclide can be identified by its mode of decay, its half-life, and the energies of its nuclear emissions [46]. The sharp peaks in the HPGe spectra, coupled with an accurate

energy calibration, can be used for unique determinations of the nuclides in a sample. If an automatic peak search capability is provided then a complete sample analysis can be accomplished without operator intervention, which is ideal for analyzing large numbers of samples. A sample printout of a Genie 2000 nuclide identification report is shown in Figure 2.7. In the Genie software platforms, the peak search locates peak centroids and then enters a region of interest about each peak. This is especially useful for observing the quality of data obtained.

Nuclide Identification Report   2014/04/15 11:30:39 AM   Page 1

****
***** N U C L I D E   I D E N T I F I C A T I O N   R E P O R T *****
****

Sample Title: GENIE-PC Spectrum No. 2
Nuclide Library Used: C:\GENIE2K\CAMFILES\STDLIB.NLB

.... IDENTIFIED NUCLIDES ....

Nuclide Name	Id Confidence	Energy (keV)	Yield (%)	Activity (uCi/Unit)	Activity Uncertainty
K-40	0.999	1460.81*	10.67	8.091E-002	7.547E-003
CO-60	1.000	1173.22*	100.00	9.924E-002	2.257E-003
		1332.49*	100.00	1.030E-001	2.329E-003
KR-85	0.999	513.99*	0.43	6.980E+000	2.284E-001
SR-85	0.989	513.99*	99.27	8.041E-002	2.631E-003
Y-88	0.996	898.02*	93.40	1.942E-001	5.523E-003
		1836.01*	99.38	1.962E-001	7.103E-003
SN-113	0.940	255.12	1.93		
		391.69*	64.90	3.819E-002	1.838E-003
CS-137	1.000	661.65*	85.12	8.220E-002	2.522E-003
BI-214	0.358	609.31*	46.30	2.920E-003	1.218E-003
		768.36	5.04		
		806.17	1.23		
		934.06	3.21		
		1120.29	15.10		
		1155.19	1.69		

Figure 2.9: Nuclide Identification Report

The final step in nuclide analysis is to determine the intensity of the radioactivity corresponding to each isotope. The net area of the peak is directly related to the intensity, but it is also necessary to correct for the efficiency of the detector, the branching ratio of the nuclides in the sample source, and the half-life (if it is desired to relate the activity to an earlier or later time). The branching ratio (or yield) is used to correct the number of gamma rays observed to obtain the number of disintegrations of the nuclide in the sample source. The activity of a particular nuclide is:

$$A(Bq) = \frac{Net\ Area}{(Live\ time)(Efficiency)(Yield)} \quad (2.15)$$

where,

(Yield) is the branching ratio fraction and

(Live time) is the actual ADC live time in seconds.

If the original activity is required, half-life corrections are made by multiplying the activity by an exponential factor

$$A_0 = A_t e^{+kt} \quad (2.16)$$

where,

A_0 is the activity at time zero which is required.

A_t is the activity at time t that was measured.

t is the elapsed time

k is the decay constant equivalent to:

$$k = \frac{ln2}{T_{1/2}} \quad (2.17)$$

where $T_{1/2}$ is the half-life.

The decay time and half-life must be in the same units (seconds, minutes, hours, or years). Specific data analysis is highly dependent upon the application, detector and electronics configuration. Further corrections are needed if the nuclide activity changes substantially during the measurement period.

2.6.4. Reporting

This is the final phase of the spectral data analysis. Choosing the sequence allows the output of analysis results and the information in the data source by selecting the template name, section name, activity units preferred etc. Executing the selections made, the analysis results will be displayed.

2.7. Scope of the present study

Intercomparison of software used for the analysis of gamma-ray spectra obtained by germanium detectors has been done intensively over the last few decades. In the present study, the PTE samples will be studied to investigate the "best" efficiency curves, the significant threshold parameters and the importance of coincidence summing corrections. Secondly, Genie 2000 together with specifically developed efficiency calibration software (LabSOCS and VGSL) will be evaluated for their applicability to the analysis of NORM nuclides in environmental samples in Chapter 5. The results will indicate if the empirically generated efficiency calibration through the Genie 2000 software will be adequate to perform NORM-analyses or whether these calibrations should be complemented by the efficiency calibration obtained from the LabSOCS and /or VGSL software.

CHAPTER 3

3. METHODOLOGY

3.1. Germanium detectors

High purity germanium detectors (HPGe) are well known for their high energy resolution capabilities and for easy maintenance. Germanium detectors are semiconductor diodes having a p-i-n structure in which the intrinsic region is sensitive to ionizing radiation, particularly X-rays and gamma rays. An electric field extends across the intrinsic region under the reverse bias. When photons interact with the material within the depleted volume of the detector, charge carriers are produced and are swept by the electric field to the p and n electrodes [47]. The charge generated by the photon is transformed into a voltage pulse by an integral charge sensitive preamplifier. Germanium detectors have a small band gap, and such detectors need to be cooled to maintain the high resolution, which may be destroyed by leakage-current induced noise. Liquid nitrogen with a temperature of 77 K is used for cooling this type of detector.

In this study a Broad Energy Germanium detector (BEGe) model BE5030 manufactured by CANBERRA is used.

3.1.1. Broad Energy Germanium detector

A BEGe detector has a cylindrical shape and moderate thickness; typically 80 mm in diameter and 30 mm high. It has a large detection area with an entrance window that is made of a composite carbon. Its efficiency is high in the low energy region and relatively low in the high energy region. The energy range of a BEGe detector typically ranges from 3 keV to 3 MeV. The BEGe detector can specifically be applied for samples containing NORM-nuclides, as most of the gamma-rays emitted are below 1.5 MeV. The use of a BEGe detector and sufficient amount of sample material (≥ 100 gram), together with its high resolving power of complex gamma spectra, will be a good choice for a first order dose rate estimation of environmental samples. Especially if nuclides emitting low-energy gamma rays should be measured simultaneously with nuclides emitting high energy gamma rays, where the amount of sample is restricted, the choice of this type of detector will have some merits [48].

The detector employed in this study is a p-type BEGe detector with a rated relative efficiency of 50%. The dimensions as quoted by the supplier are given in Table 3.1. This BEGe detector as shown in Figure 3.1 is housed in a lead castle with sliding doors as shown in Figure 3.2 in order to shield the detector from external gamma-rays to provide a low background. The interior dimensions of the castle are 40×40×40 cm, with an outer layer of ~13 cm thick lead with an activity of less than 50 Bq/kg, and an inner layer of ~2 cm thick lead with an activity of less than 10 Bq/kg. Photons, both from the sample and background radiation are interacting with the shield. If this happens through the photoelectric effect, the X-rays of lead will be emitted, and can be detected by the detector. To reduce this effect a ~1 mm cadmium layer is placed inside the shield to absorb the lead X-rays, and a ~2 mm copper layer is added on the inside to absorb the cadmium X-rays as well as a ~4 mm Perspex layer to further reduce the X-rays to energies beyond the "useful" part of the spectrum to measure the NORM-nuclides.

A gas-port is provided to flush the interior with nitrogen gas to eliminate the presence of radon and its progeny inside the shield.

Table 3.1: BEGe detector dimensions from the Canberra for Model BE5030

Detector dimensions	
crystal diameter	80.5 mm
crystal length	32.5 mm
dead layer top	0.0003 µm
dead layer outside	0.5 µm
dead layer inside/bottom	0.5 µm
crystal holder thickness (copper)	0.8 mm
end cap outer diameter	102 mm
end cap thickness	1.5 mm
end cap window thickness	0.6 mm
end cap window diameter	81 mm
end cap distance to crystal	6.61 mm

Figure 3.1: Lead castle with sliding doors.

Figure 3.2: BEGe detector in a lead castle.

3.1.2. Advantages of the BEGe detector

A BEGe is known for its high energy resolution and a relatively wide energy range from 3 keV to 3 MeV (although beyond ~1 MeV the efficiency loses out on "thicker" crystals). For the specific application of NORM-nuclide analyses the region where most gamma peaks of interest are situated is 40 – 1500 keV; hence the detection efficiencies and energy resolution are optimized. Some higher energy peaks in the ^{238}U and ^{232}Th decay series are eliminated by this choice, but they are in the region where the efficiency of the detector is relatively low. The BEGe detector consists of a flat entrance window, which allows optimum efficiency for samples that are counted close to the detector and accordingly reducing solid angle calculation errors [49].

The detector has very low electronic noise and a low background compared to the coaxial detectors because of their transparency to high energy cosmogenic background radiation (i.e. low efficiency for high-energy gammas and accordingly a low Compton continuum). All BEGe detectors are basically the same; this is more advantageous for calibration and computer modeling purposes, as this can be done only once for all detectors.

3.1.3. Crystal thickness

The BEGe detector's counting efficiency is governed by three major considerations,

- the detector size,
- the photon energy, and
- the canning material.

The detector crystal (germanium) is housed in a small vacuum container to enable it to be kept at low temperature. The canning is normally made from stainless steel to obtain a rigid container. This material will absorb some of the (low energy) photons before they reach the germanium material. However, the materials that are used for the entrance Windows (facing the sample to be measured) are either carbon, beryllium or aluminum. The BEGe detectors use carbon windows that provide good transmission for gamma-energies up-to below 10 keV. Aluminium is used when energies below 30 keV are not of interest.

3.2. Proficiency Test Exercises

Since the year 2000, PTEs have been organized by the International Monitoring System (IMS) for radionuclide laboratories, which support the network of radionuclide stations for verification of the Comprehensive Nuclear-Test-Ban Treaty (CTBT), as indicated in Chapter 1, section 1.2. The PTEs are a means to ensure that the radionuclide laboratories are capable of achieving and do achieve, on an ongoing basis, the level of accuracy of nuclide identification and measurement required in order to reliably confirm or verify spectral data and/or samples from radionuclide monitoring stations. They are organized annually [50].

Three samples, the blank sample, the calibration sample and the reference sample, are provided to each participating laboratory for every PTE. The blank filter samples provided

should be counted for seven days or more to check for the presence of any radioactive contamination of the counting equipment and/or the blank filter material. Calibration samples are spiked with solutions containing certain radionuclides of which the activity is provided to the laboratories, while the reference samples are prepared in the similar way as the calibration sample, but with activities not known to the laboratories.

3.2.1. PTE Objectives

The PTEs organized by the IMS for radionuclide laboratories started in the year 2000 and are still continuing annually. The primary objective for the PTEs is to assess how capable the laboratories are in identifying the radionuclides in the reference samples. In addition to this, the ability to measure the radioactivity levels of radionuclides in the filter samples is evaluated [50].

The 2011 PTE was altered from other exercises because two samples were involved in the analysis. The samples contained radionuclides from the Fukushima-Daiichi nuclear power plant accident, which occurred in March 2011 [51]. The other exercise involved reference material "spiked" with known amounts of selected radionuclides.

3.2.2. Sampling systems

There are three major types of systems used in the radionuclide particulate monitoring network, all designed to detect fission products in the form of particulate debris from atmospheric nuclear explosions [53].

The MANUAL3M filter sample is the most common type of air-particulate sampling method among the three major types of systems as depicted in Figures 3.3 and 3.4. The MANUAL3M can be split into two as shown in the Figure 3.5, which is commonly known as the 'HALF-MOON' geometry.

Another type of filter sample is the ARAME (Automatic Radionuclide Air Monitoring Equipment) also known as the CINDERELLA geometry as shown in Figures 3.6 and 3.7.

RASA (Radionuclide Aerosol Sampler and Analyzer) is another type of sampling method with sample geometry of a cylindrical filter draped around the detector as shown in Figure 3.8.

Figure 3.3: MANUAL3M sample [50].

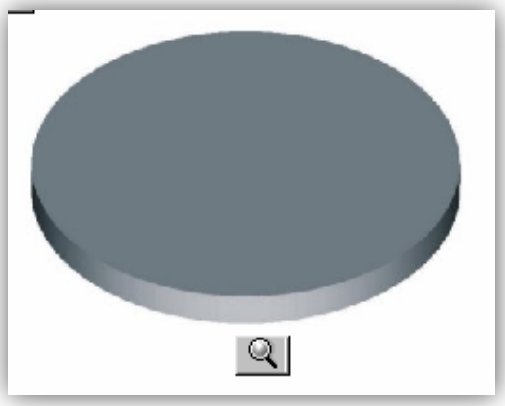

Figure 3.4: MANUAL3M sample as depicted by VGSL.

Figure 3.5: Half-Moon sample [51].

Figure 3.6: ARAME sample [52].

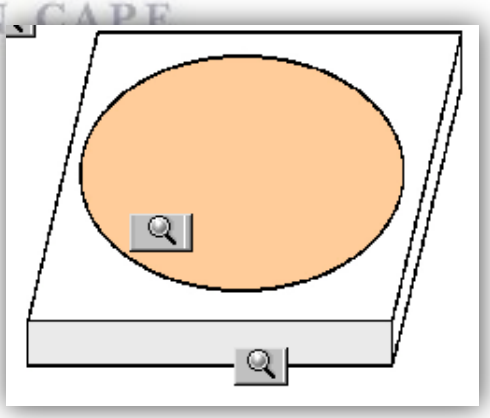

Figure 3.7: ARAME sample as depicted by VGSL.

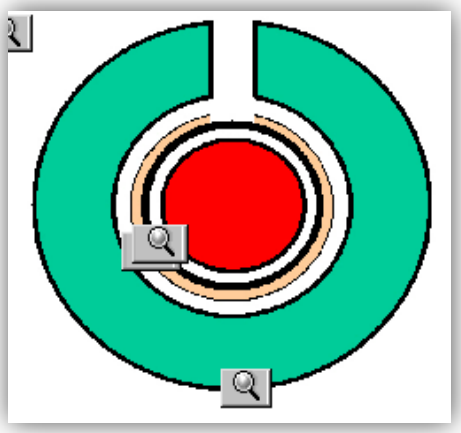

Figure 3.8: RASA sample as depicted by VGSL.

The filter sample used in the year 2007 and 2008 was a MANUAL3M. The split sample known as HALF-MOON was selected for 2009, 2010 and for 2011. The ARAME filter sample was selected for the year 2012. These sample geometries were used in the study because they are the common types of air-particulate sampling used in the radionuclide particulate monitoring network.

3.2.3. Preparation and measurements

In the year 2007, the calibration sample was firstly prepared by adding a standardized solution of ^{210}Pb and secondly a standardized mixed radionuclide solution that contained the following radionuclides: ^{241}Am, ^{109}Cd, ^{57}Co, ^{139}Ce, ^{51}Cr, ^{113}Sn, ^{85}Sr, ^{137}Cs, ^{54}Mn, ^{88}Y, ^{65}Zn and ^{60}Co. The solutions were added drop-wise to a polypropylene filter sheet of 57cm × 46 cm [50]. The filter was dried and then compressed to a 50 mm × 5 mm disc. The calibration sample used for the year 2007 was the same as for the year 2008 and 2009.

In the year 2010 the sample was prepared by adding a solution that contained a mixture of fission products, to a 460 mm × 285 mm filter sheet. The filter sheet was dried, folded and compressed to a semicircular disc with a diameter of 50 mm [54].

For the year 2011 the “spiked” filter sheet was compressed to a cylindrical disc (MANUAL3M), which was then split into two.

In the year 2012 the sample was prepared by adding a standardized solution of ^{210}Pb and a mixed radionuclide solution that contained the same radionuclides from the year 2007 to an 82 cm × 8.4cm fifteen-layer filter sheet. The filters were dried, compressed and placed in a plastic container.

3.2.4. ZAL14 Participation

The Radioanalytical Laboratory of the South African Nuclear Energy Corporation SOC Ltd. also known as ZAL14 participated in the PTEs from the year 2007. All the 16 radionuclide laboratories listed in the Treaty participated in the exercise, but only the results of 14 laboratories were included in the 2007 PTE annual report. ZAL14 was one of the two laboratories that were not included in the report due to the low grading of the results obtained. For the following four years, ZAL14 performed well in the PTEs and was outstanding in the year 2012[52]. The Laboratory is still participating and performing well in the PTEs.

3.3. Sample Preparation

Three samples with certified radionuclide content were used in this study to evaluate the lessons learned from the CTBTO Proficiency Test Exercise reference sample analysis. These samples are certified reference materials from the IAEA, i.e. stream sediment, soil and milk.

- The IAEA-314 stream sediment sample was collected from the Kalan area of the west Kalimantan, Borneo, Indonesia, and donated to the IAEA by the Indonesian Atomic Energy Commission. This material was gamma-sterilized to ensure long term stability of the material by inhibiting microbial action [55].

- The IAEA-375 material (top soil to a depth of 20 cm) was obtained from the Staryi Viskov collective farm in Novozybkov, Brjansk, Russia in July 1990. The material was air dried and milled to give a grain size less than 0.3 mm by the Brjansk Centre for Agricultural Radiology and Chemistry and dispatched for further processing to the IAEA laboratories, Seibersdorf, in November 1990. This material was also gamma-sterilized [56].

- The IAEA-152 material was produced from cow's milk obtained from animals that had grazed on land contaminated with radioactive fallout resulting from the Chernobyl incident in 1986. A bulk sample of approximately 500 kg (in 25 kg sacks) of milk powder prepared in a single batch was received by the Agency's Laboratories at Seibersdorf. After a preliminary homogeneity test, the material was bottled into plastic bottles in 250 g units without any further processing. Subsequently, the samples were irradiated to a dose of 2.5×10^4 Gy using a ^{60}Co source to ensure long-term stability of the material by inhibiting microbial action [57].

The three samples were regarded as potentially radioactive and therefore the normal precautionary measures for handling radioactive materials were adhered to.

The shape of the source or the source container is one factor that influences the full energy peak detection efficiency. There are special containers used by the Radioanalytical laboratory of the South African Nuclear Energy Corporation SOC Ltd. (Necsa) for various techniques currently employed for gamma-spectrometric analysis. The use of these containers depends on the amount of sample material and the nature of the sample. For dry and soft samples, disc containers with a variety of dimensions are used, some of which are shown in Figure 3.9. In this study the three sample materials were prepared; two in a 7.0×1.5 cm and one in a 5.0×1.5 cm disc container.

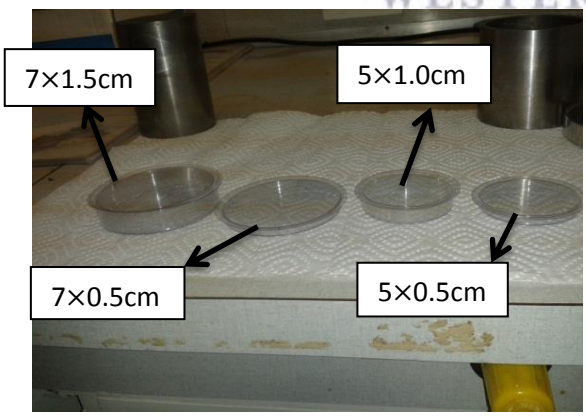

Figure 3.9: Disc containers used for sample preparation.

In preparation of the samples to be counted and analyzed, a variety of equipment and materials were used. Some of these items are depicted in Figure 3.10.

- an analytical balance,
- a spatula,
- a manual press,
- a vacuum sealer,
- a holder that holds the base of the sample container,
- a marking pen,
- a paper towel,
- disposable gloves,
- a wash bottle filled with ethanol, and
- aluminum or polyethylene laminated foil.

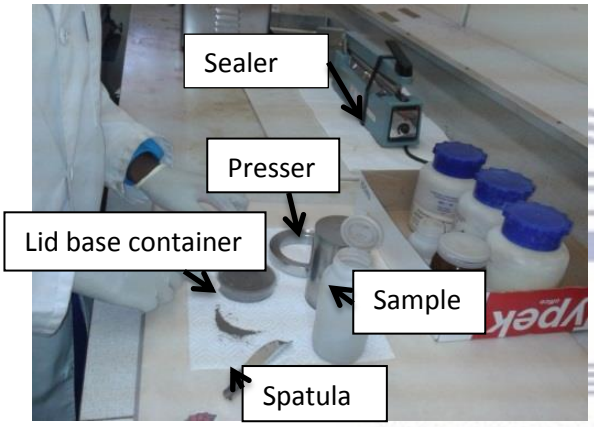

Figure 3.10: Equipment and materials used for sample preparation.

3.3.1. Pressing and weighing

The preparation bench was covered with a clean paper towel for each of the three samples. An empty disc container was weighed on the analytical balance and then fitted into the holder as shown in Figure 3.11.

Figure 3.11: Empty container fitted into the holder.

A spatula was used to fill the empty plastic container and the sample was then manually pressed as depicted in Figure 3.12 and Figure 3.13 until the container was filled to its maximum level. Different samples usually have different densities and thus the mass of the material will vary and accordingly the sensitivity of the measurement of various samples upon equal counting times.

The spatula was wiped with ethanol-drenched tissue after every sample was prepared to prevent cross contamination. The sample was then weighed. The mass of the sample (corrected for the mass of the empty container) was recorded and the container was capped with a lid as shown in Figure 3.14. A marker was used to write the sample code on the base of the container.

Figure 3.12: The sample being filled into the container.

Figure 3.13: Sample pressing.

Figure 3.14: Filled and marked sample container.

3.3.2. Sealing

^{226}Ra is commonly determined in soil samples by measuring the decay products ^{214}Pb and ^{214}Bi, both high energy gamma emitters. A prerequisite for this methodology is that radioactive equilibrium must be established between ^{226}Ra and its direct daughter ^{222}Rn, which is a noble-gas and accordingly may escape through the wall of the plastic sample container. A sealing method was developed to seal the sample radon tight with applicable aluminium foil, in a way that will not cause significant attenuation of low energy gamma-rays [58]. All samples are sealed gas tight to ensure equilibrium and allowed to stay for three weeks, which is about 5.5 half-lives of ^{222}Rn, and accordingly ^{222}Rn and its short-lived progeny has grown in to approximately 97.8% of the activity of the parent ^{226}Ra.

The aluminium foil sheet was cut with a ‘cutting supplier’ on a reel dispenser as depicted in Figure 3.15, and folded into a rectangular envelope as shown in Figure 3.16 and sealed with an impulse sealer for five seconds, such that the sample can fit in the envelope with only one side open. The sample was then placed onto the vacuum packaging machine that seals the sample gas tight as depicted in Figure 3.17 and Figure 3.18 with the time set to thirty seconds and a heating voltage of 1 V. The vacuum packing machine automatically completes the whole process and the samples are left as shown in Figure 3.19. The sealed samples were left in the preparation room for three weeks for equilibrium to be reached before counting commenced.

After three weeks the samples were counted for twenty four hours on the BEGe detector. All relevant parameters like the detector dimensions (see Table 3.1), the detector shield,

the distance between the sample and the detector's entrance window, the dimensions of the samples and their specific mass were used to simulate/determine the efficiency calibration through the LabSOCS and VGSL software.

Figure 3.15: Reel dispenser.

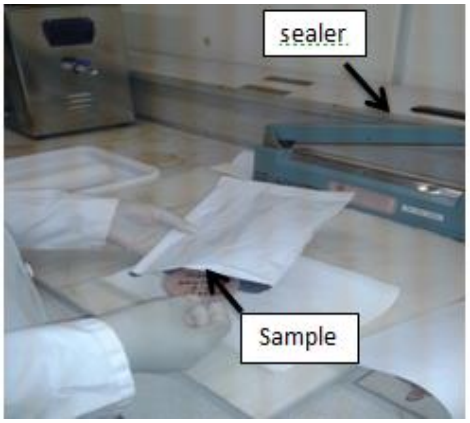

Figure 3.16: Rectangular enveloped foil sheet.

Figure 3.17: Vacuum packaging machine.

Figure 3.18: Sample on the vacuum machine.

Figure 3.19: Completely sealed NORM sample.

CHAPTER 4

EFFICIENCY CALIBRATIONS

4. The VGSL and LabSOCS calibration efficiencies and activities with the PTEs

Gamma-ray spectrometry is the most accurate for quantitative analysis and requires standard samples to establish an experimental efficiency calibration [59]. Such reference standards are generally expensive and have limited shelf-life due to the decay of some of the nuclides of interest. The density and composition of the standard must always be known for the efficiency calibration, which is not always possible. Efficiency calibration codes are now commercially available to overcome this downside.

This chapter reports the results obtained using the efficiency calculation codes LabSOCS and VGSL. The reported uncertainties are based on standard uncertainties multiplied by a coverage $k = 2$ factor, providing a level of confidence of approximately 95%. These calculation codes predict efficiency calibration curves for a number of germanium detectors. The energy ranged from 46.54 keV (^{210}Pb) to 1836.01 keV (^{88}Y) for the simulated efficiency curves, which were then compared with the experimental or empirical efficiencies obtained from certified reference sources used in the PTEs.

4.1. Efficiency Calibration

For Proficiency Test Exercises, three samples are usually provided. The blank, the calibration and the reference sample, also known as the 'unknown' sample. The Radioanalytical laboratory of Necsa has an ultra-low background gamma-spectrometry system. The blank, calibration and reference samples were counted for seven days each. The unknown nuclides were identified by nuclide identification analysis as discussed in Chapter 2, section 2.5.4. The calibration certificates were provided with the known number of nuclides, the nuclide's half-life, the gamma energy, the activity and the gamma emission rate. The calibration certificate for the year 2009 was also used for the 2010 PTE.

From the year 2008 to the year 2012, three types of geometries, MANUAL3M, Half-Moon and ARAME were used. The study focuses on these geometries. The Half-Moon geometry was modeled as a MANUAL3M because the software packages used can only model simple

cylinders or disk-shaped containers. Efficiency curves were generated from the different software in the study. The empirical efficiency calibration was performed using the PTE calibration samples using Genie 2000 for the empirical curves. LabSOCS and VGSL software were used to simulate the efficiency curves for the three sample geometries.

4.2. MANUAL3M Sample Geometry

The acquisition of the gamma-ray calibration spectra for a MANUAL3M geometry were carried out in the year 2008 with sufficient counting statistics for the gamma-energy lines of interest as shown in Figure 4.1. Figure 4.2 shows the nuclides of interest in the low energy region. The calibration spectrum was acquired with an average dead time below 2%.

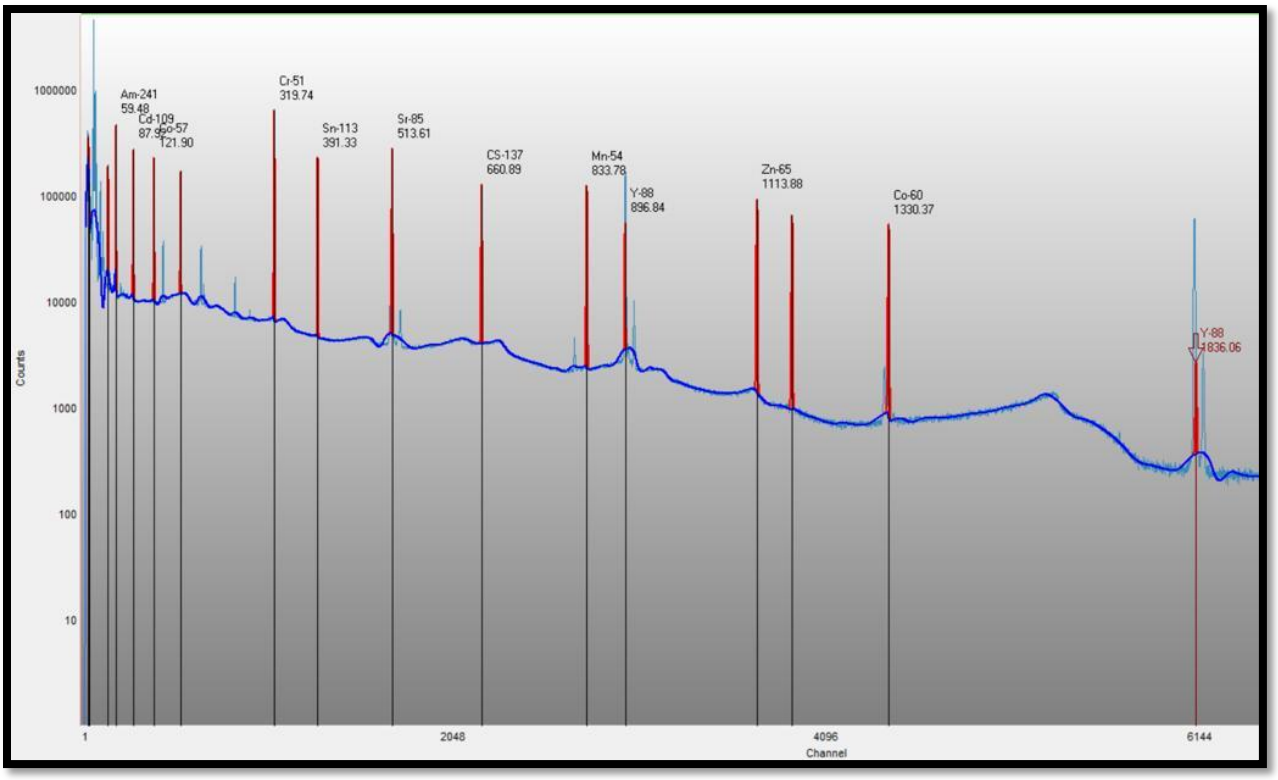

Figure 4.1: Full energy region of the calibration spectrum for a MANUAL3M filter sample.

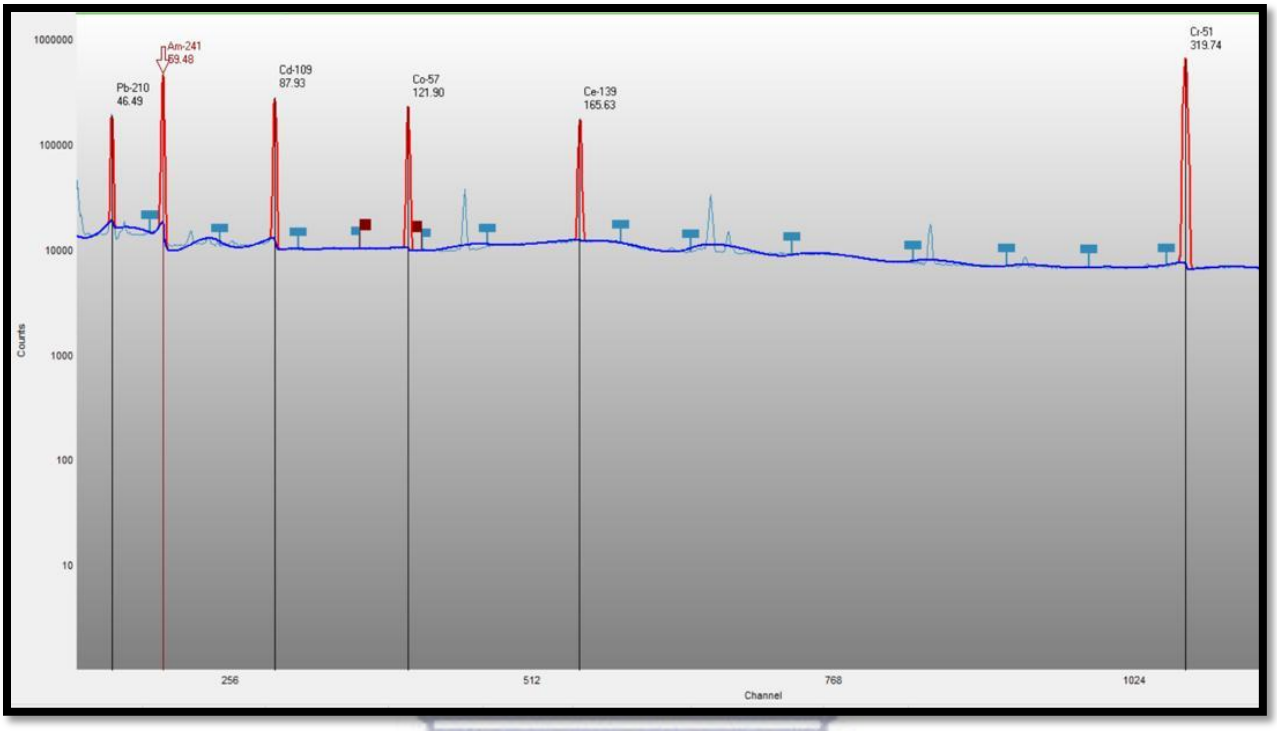

Figure 4.2: Low-energy region of the calibration spectrum for a MANUAL3M filter sample.

4.2.1. Empirical Calibration

The empirical efficiency calibration was performed using the Genie 2000 software. A certificate file was used for entering the energies of the nuclides concerned, the nuclide's assay date and time and the activity of each nuclide. Calibration points and curves were then generated as shown in Figure 4.3. Genie 2000 supports the Dual, the Empirical, the Linear and the Interpolated curve for the efficiency. The linear efficiency curve uses no logarithms on the number side and the default degree of the polynomial depends on the number of calibration points available. The Empirical and the Interpolated curve are also dependent on the number of calibration points. The Dual curve supports two models, the 'two curves' and a 'single curve'. The two curves consist of both the low and high energy region with a single crossover point while a single curve consists of a crossover point at zero. The dual curve was chosen for this study because 'the order of the low polynomial' can only be enabled if the Dual curve has been chosen. By specifying the crossover point, the low energy curve can be adjusted up to a fifth order polynomial and the high energy curve up to a ninth order polynomial.

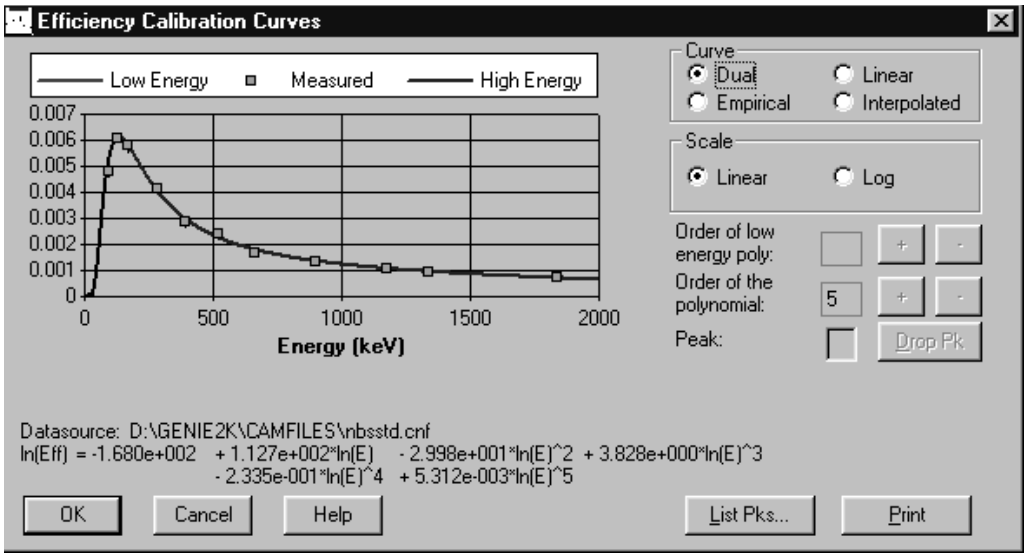

Figure 4.3: Genie 2000 Dual efficiency calibration curve for a MANUAL3M sample. The nuclides and gamma-rays in this sample can be found in Table 4.1.

4.2.1.1. Characterized detector

For the empirically fitted efficiency curve, the efficiency values were calculated from measuring the calibration source from PTE using Genie 2000 software package. Genie 2000 computes true coincidence summing with the aid of LabSOCS using the most appropriate detector characterized by CANBERRA and the sample geometric model (chapter 7 in ref 13).

4.2.1.2. Parameter variations

The significance threshold is one of the parameters in the Genie 2000 software that can be chosen by the operator. The significance threshold regulates how resolved a peak must be to be recognized as a peak. The larger the peak, with respect to the continuum that it is superimposed on, the larger the significance of that peak. Only peaks that exceed the significance threshold will be accepted as valid. Table 4.1 and Table 4.2 respectively show the activities and ratios of the measured value of a PTE calibration sample over the reference value obtained at various threshold values. The results do not deviate much from the certified values, which shows that the choice of the threshold significance level is not really important as one can expect from a spectrum with well-defined peaks with little uncertainty due to counting statistics.

Note that the standard deviations given in Tables 4.1 to 4. 6 are 1σ values. The nuclear data used in the analyses, such as the branching ratios, are from reference [65].

4.2.1.3. Polynomial order variation

The main objective in this section is to determine the "best" empirical efficiency curve for the MANUAL3M geometry used in the 2008 PTE by varying the polynomial order. This was done because during efficiency calibration the user has to select the order of the polynomial. Table 4.3 and Table 4.4 -show the activity values and ratios obtained from varying the order of the polynomial with a significance threshold of 1.25 (standard setting for CTBTO PTEs) after correcting for coincidence summing. Table 4.5 and Table 4.6 respectively represent the activity values and ratios obtained from varying the order of the polynomial with a significance threshold of 3.00 after correcting for coincidence summing. Figures 4.4 to 4.7 illustrate the ratios of the 2^{nd}-, 3^{rd}-, 4^{th}- and 5^{th}-order polynomials, at the two threshold significance settings (1.25 and 3.00), over the certified activity values.

From this it can be seen that the higher order polynomials and threshold significance settings, in general, provide better results.

Table 4.1: Empirical activity values obtained from varying the threshold from 1.00 to 4.00 compared to the certified activity values.

Nuclide	Energy (keV)	Activity(Bq)													
		Certified		Threshold 1.00		Threshold 1.25		Threshold 1.50		Threshold 2.00		Threshold 3.00		Threshold 4.00	
		Value	Unc.	Value	Unc.	Value	Unc.	Value	Unc.	Value	Unc.	Value	Unc.	Value	Unc.
^{210}Pb	46.54	583.0	12.0	584.4	66.4	584.4	66.4	584.1	66.4	584.1	66.4	583.9	66.4	584.2	66.2
^{241}Am	59.54	169.4	1.8	169.4	3.1	169.4	3.1	169.4	3.0	169.4	3.0	169.4	3.0	169.4	3.0
^{109}Cd	88.03	939.0	18.0	948.9	66.8	948.9	66.8	946.5	66.6	946.5	66.6	945.1	66.6	947.9	66.7
^{57}Co	122.06	34.9	0.6	34.9	0.2	34.9	0.2	34.9	0.2	34.9	0.2	34.9	0.2	34.9	0.2
^{139}Ce	165.85	37.9	0.8	38.0	0.4	37.9	0.4	38.0	0.4	38.0	0.4	38.0	0.4	38.0	0.4
^{51}Cr	320.08	666.0	12.0	680.4	20.2	678.6	14.1	676.2	20.1	676.1	20.1	675.9	20.1	675.9	20.1
^{113}Sn	391.69	137.2	2.4	139.3	3.3	139.3	2.7	138.7	3.3	138.7	3.3	138.6	3.3	138.6	3.3
^{85}Sr	513.99	127.7	2.2	126.1	1.8	127.4	1.8	126.8	1.8	126.8	1.8	126.8	1.8	126.8	1.8
^{137}Cs	661.65	157.2	2.6	158.0	2.4	157.7	1.9	158.5	2.4	158.5	2.4	158.4	2.4	158.4	2.4
^{54}Mn	834.83	167.4	2.2	170.1	2.5	167.6	2.0	168.1	2.5	168.2	2.5	168.2	2.5	168.2	2.5
^{88}Y	898.02	271.4	3.8	266.9	4.0	269.2	3.6	270.5	4.1	270.7	4.1	270.8	4.1	270.8	4.1
^{65}Zn	1115.5	353.0	6.0	355.6	4.9	353.0	4.7	357.0	4.9	357.2	4.9	356.9	4.9	356.9	4.9
^{60}Co	1173.2	193.5	2.2	191.9	2.7	190.3	2.5	192.9	2.8	192.8	2.8	192.8	2.8	192.8	2.8
^{60}Co	1332.5	193.5	2.2	194.2	3.3	198.1	2.8	193.6	3.3	193.7	3.3	193.6	3.3	193.6	3.3
^{88}Y	1836.0	271.4	3.8	272.3	10.4	268.3	9.6	272.4	10.4	272.4	10.4	272.4	10.4	272.4	10.4

Table 4.2: Ratio of the empirical activity values to the reference activity value obtained from varying the threshold of 1.00 to 4.00.

Nuclide	Energy (keV)	Ratio													
		Certified		Threshold 1.00		Threshold 1.25		Threshold 1.50		Threshold 2.00		Threshold 3.00		Threshold 4.00	
		Value	Unc.	Value	Unc.	Value	Unc.	Value	Unc.	Value	Unc.	Value	Unc.	Value	Unc.
^{210}Pb	46.54	1.000	0.029	1.002	0.116	1.002	0.116	1.002	0.116	1.002	0.116	1.001	0.116	1.002	0.115
^{241}Am	59.54	1.000	0.015	1.000	0.021	1.000	0.021	1.000	0.021	1.000	0.021	1.000	0.021	1.000	0.021
^{109}Cd	88.03	1.000	0.027	1.011	0.074	1.011	0.074	1.008	0.074	1.008	0.074	1.007	0.073	1.009	0.074
^{57}Co	122.06	1.000	0.024	1.001	0.019	1.001	0.019	1.001	0.019	1.001	0.019	1.001	0.019	1.001	0.019
^{139}Ce	165.85	1.000	0.030	1.001	0.023	1.001	0.023	1.002	0.023	1.002	0.023	1.002	0.023	1.002	0.023
^{51}Cr	320.08	1.000	0.025	1.022	0.036	1.019	0.028	1.015	0.035	1.015	0.035	1.015	0.035	1.015	0.035
^{113}Sn	391.69	1.000	0.025	1.015	0.030	1.015	0.026	1.011	0.030	1.011	0.030	1.011	0.030	1.011	0.030
^{85}Sr	513.99	1.000	0.024	0.988	0.022	0.997	0.022	0.993	0.022	0.993	0.022	0.993	0.022	0.993	0.022
^{137}Cs	661.65	1.000	0.023	1.005	0.023	1.003	0.021	1.008	0.023	1.008	0.023	1.008	0.023	1.008	0.023
^{54}Mn	834.83	1.000	0.019	1.016	0.020	1.001	0.018	1.004	0.020	1.005	0.020	1.005	0.020	1.005	0.020
^{88}Y	898.02	1.000	0.020	0.983	0.020	0.992	0.019	0.997	0.020	0.998	0.020	0.998	0.020	0.998	0.020
^{65}Zn	1115.5	1.000	0.024	1.007	0.022	1.000	0.022	1.011	0.022	1.012	0.022	1.011	0.022	1.011	0.022
^{60}Co	1173.2	1.000	0.016	0.991	0.018	0.983	0.017	0.997	0.018	0.996	0.018	0.996	0.018	0.996	0.018
^{60}Co	1332.5	1.000	0.016	1.003	0.020	1.024	0.018	1.001	0.020	1.001	0.020	1.001	0.020	1.001	0.020
^{88}Y	1836.0	1.000	0.020	1.003	0.041	0.989	0.038	1.004	0.041	1.004	0.041	1.004	0.041	1.004	0.041
Average		**1.000**		**1.003**		**1.003**		**1.004**		**1.004**		**1.003**		**1.004**	
Standard deviation		**0.000**		**0.010**		**0.011**		**0.006**		**0.006**		**0.006**		**0.006**	

Table 4.3: Empirical activity values obtained from varying the polynomial orders compared to the certified activity values (threshold significance: 1.25).

Nuclide	Energy (keV)	Certified Activity(Bq)		Activity (Bq)							
				order 2		order 3		order 4		order 5	
		Value	Unc.	Value	Unc.	Value	Unc.	Value	Unc.	Value	Unc.
^{210}Pb	46.54	583.0	12.0	584.4	66.4	584.4	66.4	584.4	66.4	584.4	66.4
^{241}Am	59.54	169.4	1.8	169.4	3.1	169.4	3.1	169.4	3.1	169.4	3.1
^{109}Cd	88.03	939.0	18.0	948.9	66.8	948.9	66.8	948.9	66.8	948.9	66.8
^{57}Co	122.06	34.9	0.6	34.9	0.2	34.9	0.2	34.9	0.2	34.9	0.2
^{139}Ce	165.85	37.9	0.8	39.4	0.3	38.3	0.3	37.9	0.4	38.0	0.4
^{51}Cr	320.08	666.0	12.0	679.0	12.3	664.4	12.4	678.6	14.1	668.7	19.9
^{113}Sn	391.69	137.2	2.4	136.8	2.2	135.9	2.2	139.3	2.7	137.9	3.3
^{85}Sr	513.99	127.7	2.2	123.1	1.4	124.8	1.4	127.4	1.8	127.3	1.8
^{137}Cs	661.65	157.2	2.6	152.3	1.6	156.6	1.9	157.7	1.9	158.6	2.4
^{54}Mn	834.83	167.4	2.2	163.8	1.5	168.9	1.9	167.6	2.0	168.6	2.5
^{88}Y	898.02	271.4	3.8	264.4	2.8	272.3	3.4	269.2	3.6	270.3	4.1
^{65}Zn	1115.5	353.0	6.0	353.9	3.8	359.1	4.0	353.0	4.7	352.3	4.8
^{60}Co	1173.2	193.5	2.2	191.7	2.1	193.5	2.2	190.3	2.5	189.6	2.7
^{60}Co	1332.5	193.5	2.2	202.2	2.7	200.2	2.7	198.1	2.8	196.8	3.3
^{88}Y	1836.0	271.4	3.8	279.3	5.9	255.3	7.3	268.3	9.6	270.7	10.3

Table 4.4: Empirical activity ratios obtained from varying the polynomial orders compared to the certified activity values (threshold significance: 1.25).

Nuclide	Energy (keV)	Certified Activity(Bq)		Ratio							
				order 2		order 3		order 4		order 5	
		Value	Unc.	Value	Unc.	Value	Unc.	Value	Unc.	Value	Unc.
^{210}Pb	46.54	583.0	12.0	1.002	0.116	1.002	0.116	1.002	0.116	1.002	0.116
^{241}Am	59.54	169.4	1.8	1.000	0.021	1.000	0.021	1.000	0.021	1.000	0.021
^{109}Cd	88.03	939.0	18.0	1.011	0.074	1.011	0.074	1.011	0.074	1.011	0.074
^{57}Co	122.06	34.9	0.6	1.001	0.019	1.001	0.019	1.001	0.019	1.001	0.019
^{139}Ce	165.85	37.9	0.8	1.039	0.023	1.010	0.023	1.001	0.023	1.002	0.023
^{51}Cr	320.08	666.0	12.0	1.020	0.026	0.998	0.026	1.019	0.028	1.004	0.035
^{113}Sn	391.69	137.2	2.4	0.997	0.024	0.990	0.023	1.015	0.026	1.005	0.030
^{85}Sr	513.99	127.7	2.2	0.964	0.020	0.978	0.020	0.997	0.022	0.997	0.022
^{137}Cs	661.65	157.2	2.6	0.969	0.019	0.996	0.020	1.003	0.021	1.009	0.023
^{54}Mn	834.83	167.4	2.2	0.978	0.016	1.009	0.018	1.001	0.018	1.007	0.020
^{88}Y	898.02	271.4	3.8	0.974	0.017	1.003	0.019	0.992	0.019	0.996	0.020
^{65}Zn	1115.5	353.0	6.0	1.003	0.020	1.017	0.021	1.000	0.022	0.998	0.022
^{60}Co	1173.2	193.5	2.2	0.991	0.016	1.000	0.016	0.983	0.017	0.980	0.018
^{60}Co	1332.5	193.5	2.2	1.045	0.018	1.035	0.018	1.024	0.018	1.017	0.021
^{88}Y	1836.0	271.4	3.8	1.029	0.026	0.941	0.030	0.989	0.038	0.997	0.040
Average				**1.002**		**0.999**		**1.003**		**1.002**	
Standard deviation				**0.024**		**0.021**		**0.011**		**0.008**	

Table 4.5: Empirical activity values obtained from varying the polynomial orders compared to the certified activity values (threshold significance: 3.00).

Nuclide	Energy (keV)	Certified Activity(Bq)		Activity (Bq)							
				order 2		order 3		order 4		order 5	
		Value	Unc.	Value	Unc.	Value	Unc.	Value	Unc.	Value	Unc.
^{210}Pb	46.54	583.0	12.0	583.9	66.4	583.9	66.4	583.9	66.4	583.9	66.4
^{241}Am	59.54	169.4	1.8	169.4	3.0	169.4	3.0	169.4	3.0	169.4	3.0
^{109}Cd	88.03	939.0	18.0	945.1	66.6	945.1	66.6	945.1	66.6	945.1	66.6
^{57}Co	122.06	34.9	0.6	34.9	0.2	34.9	0.2	34.9	0.2	34.9	0.2
^{139}Ce	165.85	37.9	0.8	39.3	0.3	38.2	0.3	38.0	0.4	38.0	0.4
^{51}Cr	320.08	666.0	12.0	677.4	12.3	663.3	12.4	675.9	20.1	674.9	14.0
^{113}Sn	391.69	137.2	2.4	136.6	2.2	135.7	2.2	138.6	3.3	138.5	2.7
^{85}Sr	513.99	127.7	2.2	123.2	1.4	124.8	1.4	126.8	1.8	126.8	1.8
^{137}Cs	661.65	157.2	2.6	153.6	1.6	157.6	1.9	158.4	2.4	158.5	2.0
^{54}Mn	834.83	167.4	2.2	164.5	1.5	169.3	1.9	168.2	2.5	168.3	2.0
^{88}Y	898.02	271.4	3.8	266.1	2.9	273.5	3.4	270.8	4.1	271.0	3.6
^{65}Zn	1115.5	353.0	6.0	356.9	3.8	361.9	4.1	356.9	4.9	356.8	4.8
^{60}Co	1173.2	193.5	2.2	193.8	2.2	195.4	2.2	192.8	2.8	192.8	2.6
^{60}Co	1332.5	193.5	2.2	197.0	2.6	195.2	2.6	193.6	3.3	193.5	2.7
^{88}Y	1836.0	271.4	3.8	284.8	6.0	261.8	7.5	272.4	10.4	272.6	9.7

Table 4.6: Empirical activity ratios obtained from varying the polynomial orders compared to the certified activity values (threshold significance: 3.00).

Nuclide	Energy (keV)	Certified Activity(Bq)		Ratio							
				order 2		order 3		order 4		order 5	
		Value	Unc.	Value	Unc.	Value	Unc.	Value	Unc.	Value	Unc.
^{210}Pb	46.54	583.0	12.0	1.001	0.116	1.001	0.116	1.001	0.116	1.001	0.116
^{241}Am	59.54	169.4	1.8	1.000	0.021	1.000	0.021	1.000	0.021	1.000	0.021
^{109}Cd	88.03	939.0	18.0	1.007	0.073	1.007	0.073	1.007	0.073	1.007	0.073
^{57}Co	122.06	34.9	0.6	1.001	0.019	1.001	0.019	1.001	0.019	1.001	0.019
^{139}Ce	165.85	37.9	0.8	1.037	0.023	1.009	0.023	1.002	0.023	1.002	0.023
^{51}Cr	320.08	666.0	12.0	1.017	0.026	0.996	0.026	1.015	0.035	1.013	0.028
^{113}Sn	391.69	137.2	2.4	0.996	0.024	0.989	0.023	1.011	0.030	1.010	0.026
^{85}Sr	513.99	127.7	2.2	0.964	0.020	0.977	0.020	0.993	0.022	0.993	0.022
^{137}Cs	661.65	157.2	2.6	0.977	0.019	1.003	0.020	1.008	0.023	1.008	0.021
^{54}Mn	834.83	167.4	2.2	0.983	0.016	1.012	0.018	1.005	0.020	1.005	0.018
^{88}Y	898.02	271.4	3.8	0.981	0.017	1.008	0.019	0.998	0.020	0.998	0.019
^{65}Zn	1115.5	353.0	6.0	1.011	0.020	1.025	0.021	1.011	0.022	1.011	0.022
^{60}Co	1173.2	193.5	2.2	1.001	0.016	1.010	0.016	0.996	0.018	0.996	0.018
^{60}Co	1332.5	193.5	2.2	1.018	0.018	1.009	0.018	1.001	0.020	1.000	0.018
^{88}Y	1836.0	271.4	3.8	1.049	0.027	0.964	0.031	1.004	0.041	1.005	0.038
Average				**1.003**		**1.001**		**1.003**		**1.003**	
Standard deviation				**0.022**		**0.015**		**0.006**		**0.006**	

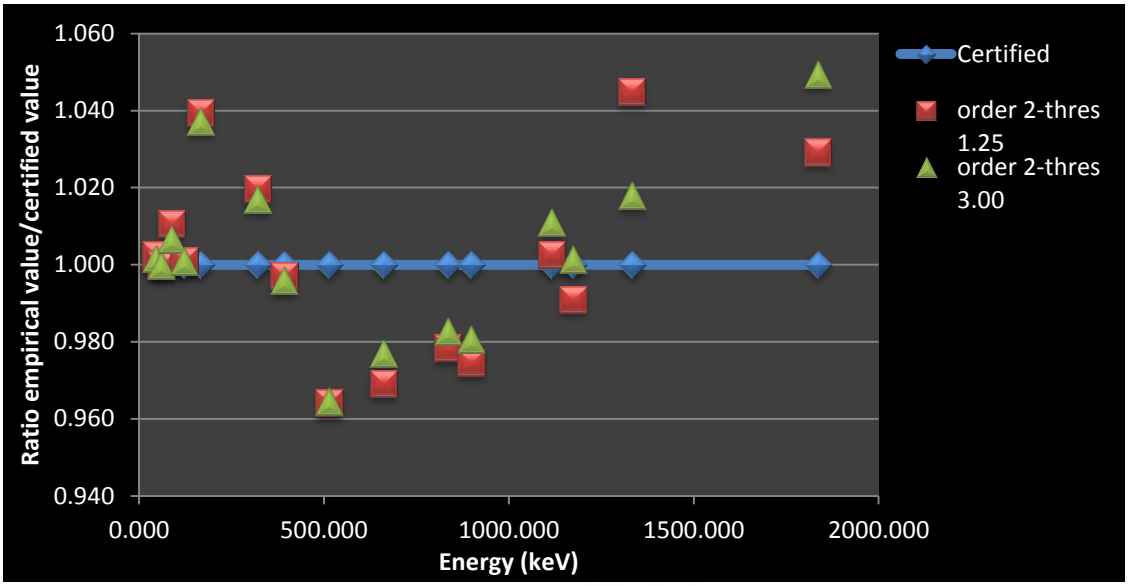

Figure 4.4: Ratio of the empirical values to the reference value obtained from the 2nd order polynomial.

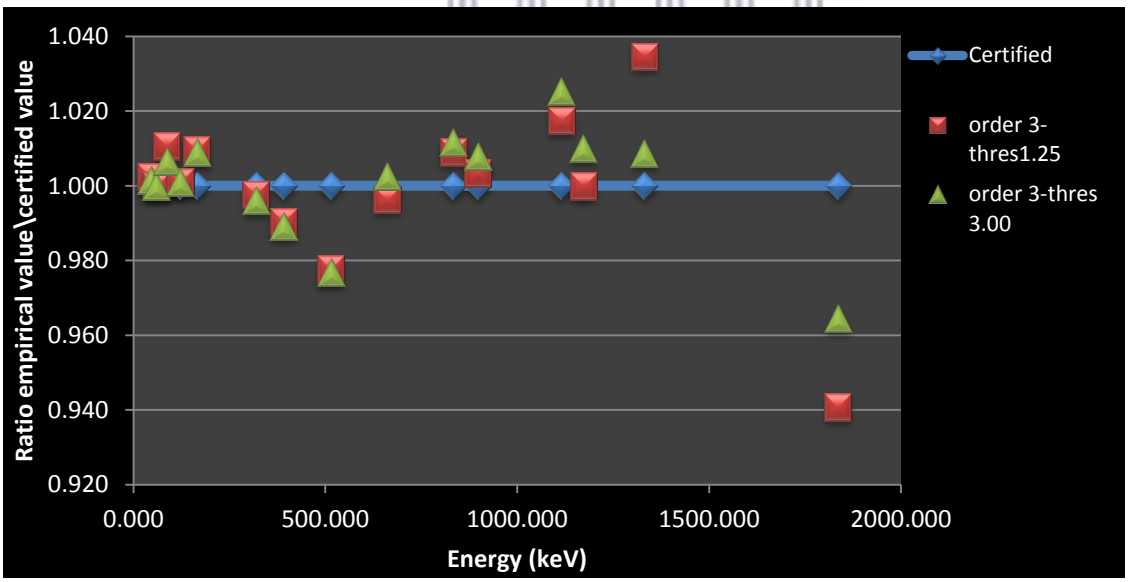

Figure 4.5: Ratio of the empirical values to the reference value obtained from the 3rd order polynomial.

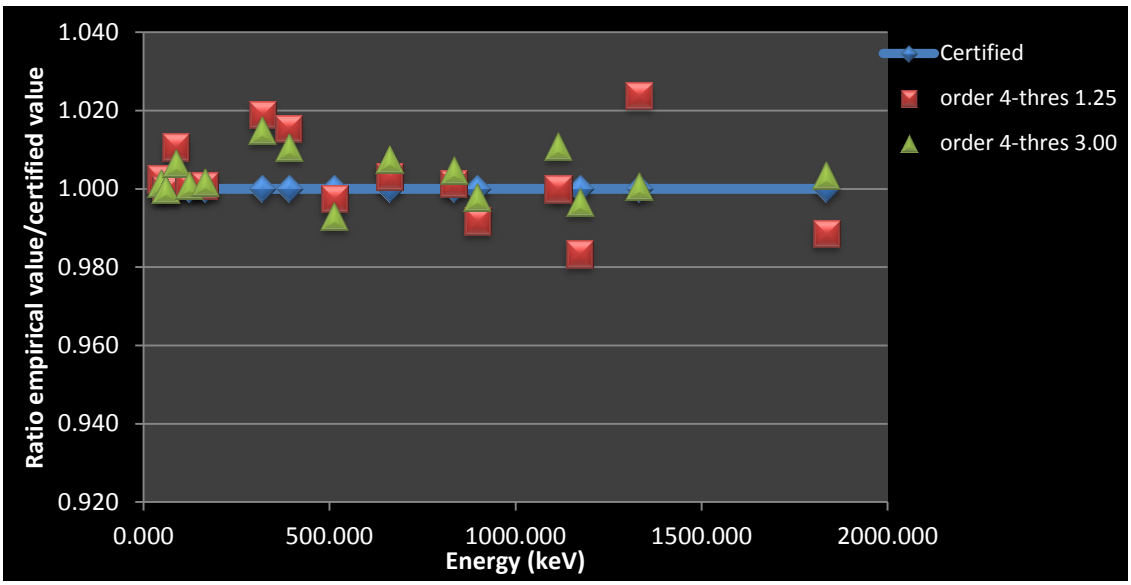

Figure 4.6: Ratio of the empirical values to the reference value obtained from the 4th order polynomial.

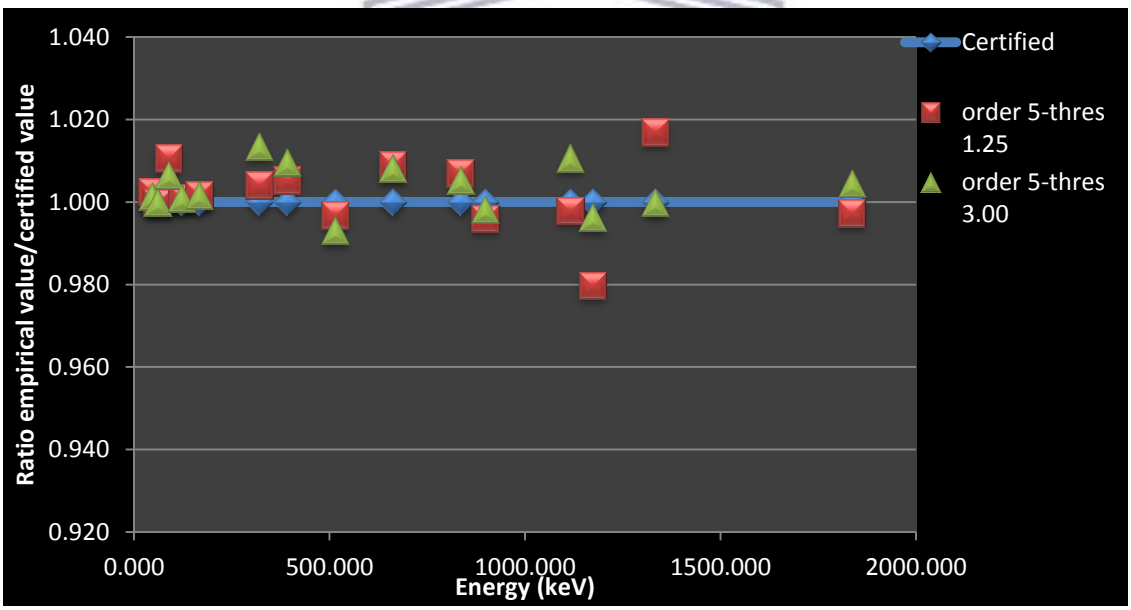

Figure 4.7: Ratio of the empirical values to the reference value obtained from the 5th order polynomial.

4.2.1.4. Mathematical representation of the polynomials

Genie 2000 uses the efficiency values from the fitted efficiency curves to calculate the activity. These curves are established using algorithms entrenched in the software and the efficiency values at the respective nuclide energies provided by the user. For the empirically fitted efficiency curve, the efficiency values were calculated from measuring the calibration source. In all cases Genie 2000 was used to create a fitted

dual efficiency curve comprised of two polynomials. The first polynomial is for the low energy region and the second is for the high energy region with a common crossover point at 122 keV. Tables 4.7 and 4.8 show empirical efficiency values before and after coincidence summing correction at a threshold significance of 1.25. The latter was chosen since it is the standard setting and the earlier results indicate that the exact value is not very important. Figures 4.8, 4.9, 4.10 and 4.11 are graphical representations of the efficiency curves generated by Genie 2000 for the 2^{nd}-, 3^{rd}-, 4^{th}- and 5^{th}- order polynomials respectively. The efficiency curves are represented mathematically by the following equations, of which Equation 4.1 is the low energy polynomial that is the same for all other high energy fitted curves with 2^{nd}-, 3^{rd}-, 4^{th}- and 5^{th}- order polynomials respectively; where ε is the peak efficiency and E is the peak-energy.

$$Ln\,(\varepsilon) = -4.293 + 1.467 \times ln\,(E) - 0.173 \times ln\,(E)^2 \quad (4.1)$$

$$Ln\,(\varepsilon) = 0.8779 - 0.1514 \times ln\,(E) - 0.05971 \times ln\,(E)^2 \quad (4.2)$$

$$Ln\,(\varepsilon) = -11.89 + 6.371 \times ln\,(E) - 1.157 \times ln\,(E)^2 + 0.06077 \times ln\,(E)^3 \quad (4.3)$$

$$Ln\,(\varepsilon) = -63.23 + 41.44 \times ln\,(E) - 10.06 \times ln\,(E)^2 + 1.056 \times ln\,(E)^3 - 0.04137 \times ln\,(E)^4 \quad (4.4)$$

$$Ln\,(\varepsilon) = 135.4 - 125.6 \times ln(E) + 45.71 \times ln(E)^2 8.188 \times ln(E)^3 + 0.7193 \times ln(E)^4 - 0.02486 \times ln(E)^5 \quad (4.5)$$

Table 4.9 and Table 4.10 represent empirical efficiency values before and after coincidence summing correction at a threshold significance of 3.00. Figures 4.12, 4.13, 4.14 and 4.15 are graphical representations of the efficiency curves generated by Genie 2000 for the 2^{nd}-, 3^{rd}-, 4^{th}- and 5^{th}- order polynomials respectively. The efficiency curves are represented mathematically by the following equations, of which Equation 4.6 is the low energy polynomial that is the same for all other high energy fitted curves with 2^{nd}-, 3^{rd}-, 4^{th}- and 5^{th}- order polynomials respectively.

$$Ln\,(\varepsilon) = -4.791 + 1.698 \times ln\,(E) - 0.1997 \times ln\,(E)^2 \quad (4.6)$$

$$Ln\,(\varepsilon) = 0.6907 - 0.08403 \times ln\,(E) - 0.06571 \times ln\,(E)^2 \quad (4.7)$$

$$Ln\,(\varepsilon) = -11.39 + 6.085 \times ln\,(E) - 1.103 \times ln\,(E)^2 + 0.05744 \times ln\,E^3 \quad (4.8)$$

$$Ln\,(\varepsilon) = -53.74 + 35.01 \times ln\,(E) - 8.444 \times Ln(E)^2 + 0.8781 \times ln\,(E)^3 - 0.0341 \times ln\,(E)^4 \quad (4.9)$$

$$Ln\,(\varepsilon) = -74.27 + 52.27 * \ln(E) - 14.21 * \ln(E)^2 + 1.834 \times \ln(E)^3 - 0.1127 \times ln\,(E)^4 + 0.00257 \times ln\,(E)^5 \quad (4.10)$$

For the improvement of the results, coincidence summing corrections were applied during the establishment of the calibration curve with the dual polynomial option in Genie 2000 where the spectrum of a given calibration source was acquired and a certificate file was set up for the calibration. Coincidence summing correction was also applied during complete analysis of the calibration spectra. Nuclides corrected for coincidence summing are ^{60}Co, ^{139}Ce and ^{88}Y as shown in Table 4.11. Appendix C depicts decay schemes for ^{60}Co, ^{139}Ce and ^{88}Y. True coincidence summing can cause systematic peak area errors of 30% or more with certain nuclides and geometries. The Genie 2000 cascade summing correction method uses LabSOCS technology to describe the sample/detector geometry without the need for expensive and time consuming calibrations using certified radioactive standards. From the observed results, the empirical efficiency calibration curve of the 5th order or the 4th order polynomial depending on the visual inspection of the user* with the threshold of 3.00 will be used to calibrate the reference/unknown reference spectra for the PTEs selected for the study and the IAEA reference samples.

* By visual inspection one can select an option of listing peaks. The list comprises of five columns, the X-value (nuclide energy), calculated efficiency, measured efficiency, measured efficiency error and the deviation. From the high energy polynomial, the 5th and 4th order polynomial can be compared by looking at the measured efficiency error and the deviation. The one with less deviation or error can be considered. In this study the 5th order polynomial

was chosen for the MANUAL3M and the HALFMOON while the 4th order polynomial was chosen for the ARAME geometry sample.

Table 4.7: Empirical efficiency values obtained from varying the polynomial order (1.25 threshold significance).

Nuclide	Energy (keV)	Efficiency before cascade correction							
		order 2		order 3		order 4		order 5	
		Value	Unc.	Value	Unc.	Value	Unc.	Value	Unc.
^{210}Pb	46.54	0.297	0.034	0.297	0.034	0.297	0.034	0.297	0.034
^{241}Am	59.54	0.306	0.005	0.306	0.005	0.306	0.005	0.306	0.005
^{109}Cd	88.03	0.303	0.019	0.303	0.019	0.303	0.019	0.303	0.019
^{57}Co	122.06	0.286	0.002	0.286	0.002	0.286	0.002	0.286	0.002
^{139}Ce	165.85	0.213	0.001	0.198	0.002	0.194	0.002	0.194	0.002
^{51}Cr	320.08	0.121	0.001	0.115	0.001	0.124	0.002	0.127	0.003
^{113}Sn	391.69	0.101	0.001	0.100	0.001	0.109	0.002	0.111	0.002
^{85}Sr	513.99	0.079	0.001	0.083	0.001	0.088	0.001	0.089	0.001
^{137}Cs	661.65	0.062	0.001	0.068	0.001	0.069	0.001	0.069	0.001
^{54}Mn	834.83	0.050	0.000	0.055	0.001	0.053	0.001	0.053	0.001
^{88}Y	898.02	0.047	0.000	0.051	0.001	0.049	0.001	0.049	0.001
^{65}Zn	1115.5	0.038	0.000	0.039	0.000	0.037	0.000	0.037	0.000
^{60}Co	1173.2	0.036	0.000	0.037	0.000	0.035	0.000	0.035	0.000
^{60}Co	1332.5	0.032	0.000	0.031	0.000	0.030	0.000	0.030	0.000
^{88}Y	1836.0	0.023	0.000	0.018	0.000	0.021	0.001	0.021	0.001

Table 4.8: Sum-coincidence corrected efficiency values obtained from varying the polynomial order (1.25 threshold significance).

Nuclide	Energy (keV)	Efficiency after sum-coincidence corrections							
		order 2		order 3		order 4		order 5	
		Value	Unc.	Value	Unc.	Value	Unc.	Value	Unc.
^{210}Pb	46.54	0.298	0.034	0.298	0.034	0.298	0.034	0.298	0.034
^{241}Am	59.54	0.305	0.005	0.305	0.005	0.305	0.005	0.305	0.005
^{109}Cd	88.03	0.303	0.019	0.303	0.019	0.303	0.019	0.303	0.019
^{57}Co	122.06	0.289	0.002	0.289	0.002	0.289	0.002	0.289	0.002
^{139}Ce	165.85	0.233	0.001	0.240	0.002	0.242	0.002	0.242	0.002
^{51}Cr	320.08	0.138	0.002	0.141	0.002	0.138	0.002	0.140	0.004
^{113}Sn	391.69	0.116	0.001	0.117	0.001	0.114	0.002	0.115	0.002
^{85}Sr	513.99	0.091	0.001	0.090	0.001	0.088	0.001	0.088	0.001
^{137}Cs	661.65	0.073	0.001	0.071	0.001	0.070	0.001	0.070	0.001
^{54}Mn	834.83	0.058	0.001	0.057	0.001	0.057	0.001	0.057	0.001
^{88}Y	898.02	0.054	0.000	0.053	0.001	0.053	0.001	0.053	0.001
^{65}Zn	1115.5	0.044	0.000	0.043	0.000	0.044	0.001	0.044	0.001
^{60}Co	1173.2	0.042	0.000	0.041	0.000	0.042	0.001	0.042	0.001
^{60}Co	1332.5	0.037	0.000	0.037	0.000	0.038	0.001	0.038	0.001
^{88}Y	1836.0	0.026	0.001	0.029	0.001	0.028	0.001	0.027	0.001

Table 4.9: Empirical efficiency values obtained from varying the polynomial order (3.00 threshold significance).

Nuclide	Energy (keV)	Efficiency before sum-coincidence correction							
		order 2		order 3		order 4		order 5	
		Value	Unc.	Value	Unc.	Value	Unc.	Value	Unc.
^{210}Pb	46.54	0.297	0.034	0.297	0.034	0.297	0.034	0.297	0.034
^{241}Am	59.54	0.306	0.005	0.306	0.005	0.306	0.005	0.306	0.005
^{109}Cd	88.03	0.303	0.019	0.303	0.019	0.303	0.019	0.303	0.019
^{57}Co	122.06	0.286	0.002	0.286	0.002	0.286	0.002	0.286	0.002
^{139}Ce	165.85	0.213	0.001	0.198	0.002	0.194	0.002	0.194	0.002
^{51}Cr	320.08	0.121	0.001	0.115	0.001	0.124	0.002	0.127	0.003
^{113}Sn	391.69	0.101	0.001	0.100	0.001	0.109	0.002	0.111	0.002
^{85}Sr	513.99	0.079	0.001	0.083	0.001	0.088	0.001	0.089	0.001
^{137}Cs	661.65	0.062	0.001	0.068	0.001	0.069	0.001	0.069	0.001
^{54}Mn	834.83	0.050	0.000	0.055	0.001	0.053	0.001	0.053	0.001
^{88}Y	898.02	0.047	0.000	0.051	0.001	0.049	0.001	0.049	0.001
^{65}Zn	1115.5	0.038	0.000	0.039	0.000	0.037	0.000	0.037	0.000
^{60}Co	1173.2	0.036	0.000	0.037	0.000	0.035	0.000	0.035	0.000
^{60}Co	1332.5	0.032	0.000	0.031	0.000	0.030	0.000	0.030	0.000
^{88}Y	1836.0	0.023	0.000	0.018	0.000	0.021	0.001	0.021	0.001

Table 4.10: Sum-coincidence corrected efficiency values obtained from varying the polynomial order (3.00 threshold significance).

Nuclide	Energy (keV)	Efficiency after sum-coincidence correction							
		order 2		order 3		order 4		order 5	
		Value	Unc.	Value	Unc.	Value	Unc.	Value	Unc.
^{210}Pb	46.54	0.297	0.034	0.297	0.034	0.297	0.034	0.297	0.034
^{241}Am	59.54	0.306	0.005	0.306	0.005	0.306	0.005	0.306	0.005
^{109}Cd	88.03	0.304	0.019	0.304	0.019	0.304	0.019	0.304	0.019
^{57}Co	122.06	0.289	0.002	0.289	0.002	0.289	0.002	0.289	0.002
^{139}Ce	165.85	0.233	0.001	0.240	0.002	0.242	0.002	0.242	0.002
^{51}Cr	320.08	0.138	0.002	0.141	0.002	0.138	0.002	0.138	0.004
^{113}Sn	391.69	0.116	0.001	0.117	0.001	0.114	0.002	0.114	0.002
^{85}Sr	513.99	0.091	0.001	0.090	0.001	0.089	0.001	0.089	0.001
^{137}Cs	661.65	0.072	0.001	0.070	0.001	0.070	0.001	0.070	0.001
^{54}Mn	834.83	0.058	0.001	0.056	0.001	0.057	0.001	0.057	0.001
^{88}Y	898.02	0.054	0.000	0.053	0.001	0.053	0.001	0.053	0.001
^{65}Zn	1115.5	0.044	0.000	0.043	0.000	0.044	0.001	0.044	0.001
^{60}Co	1173.2	0.041	0.000	0.041	0.000	0.042	0.001	0.042	0.001
^{60}Co	1332.5	0.036	0.000	0.037	0.000	0.037	0.001	0.037	0.001
^{88}Y	1836.0	0.026	0.001	0.028	0.001	0.027	0.001	0.027	0.001

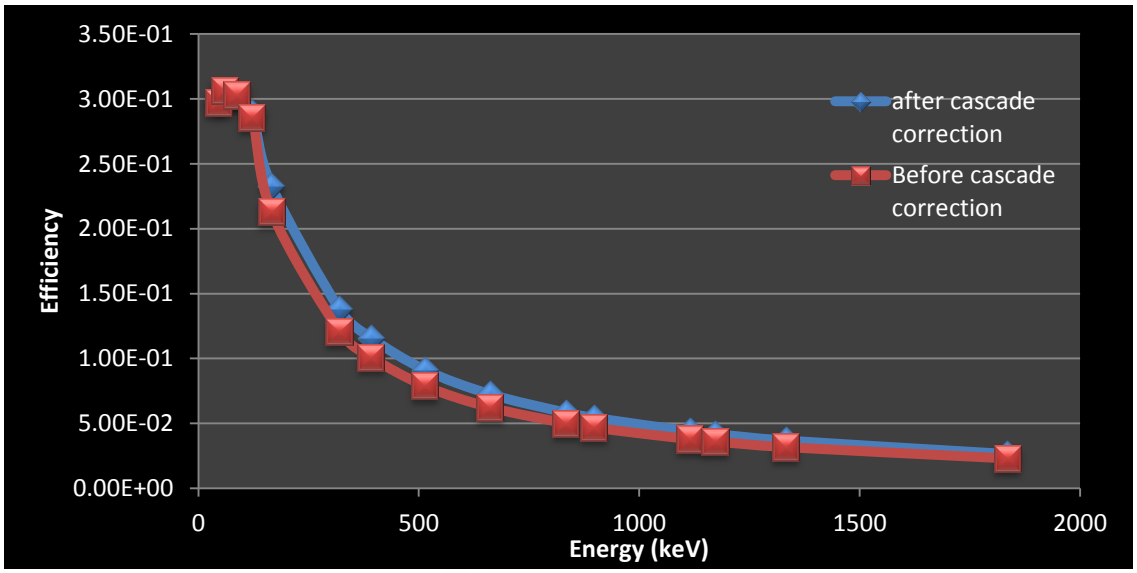

Figure 4.8: Empirical efficiency curves (2nd order polynomial) before and after cascade correction (threshold significance: 1.25).

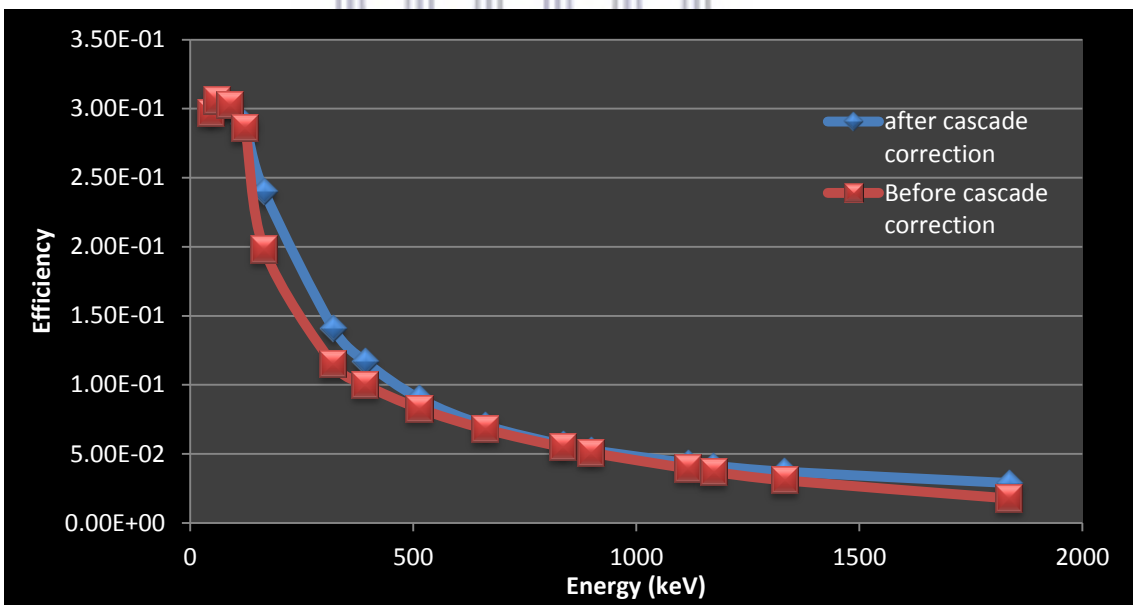

Figure 4.9: Empirical efficiency curves (3rd order polynomial) before and after cascade correction (threshold significance: 1.25).

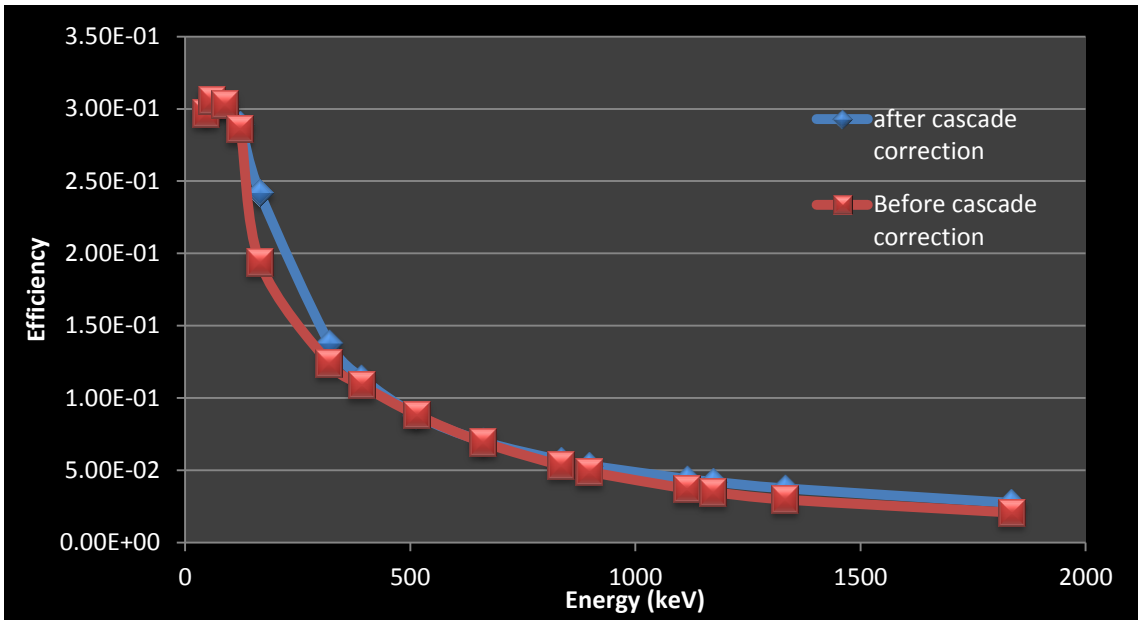

Figure 4.10: Empirical efficiency curves (4th order polynomial) before and after cascade correction (threshold significance: 1.25).

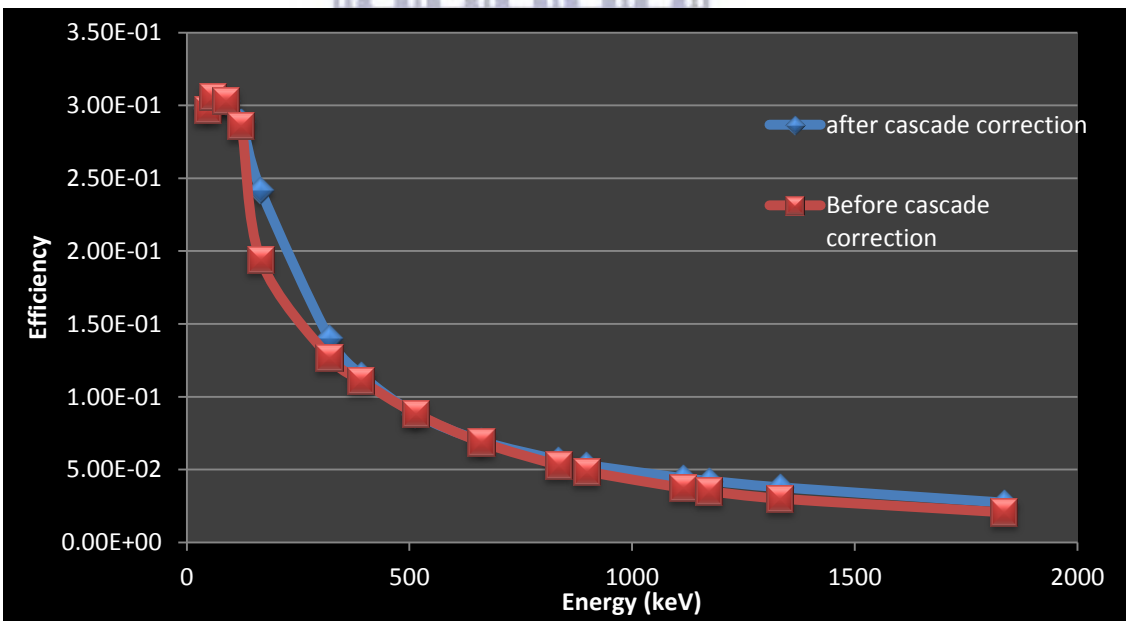

Figure 4.11: Empirical efficiency curves (5th order polynomial) before and after cascade correction (threshold significance: 1.25).

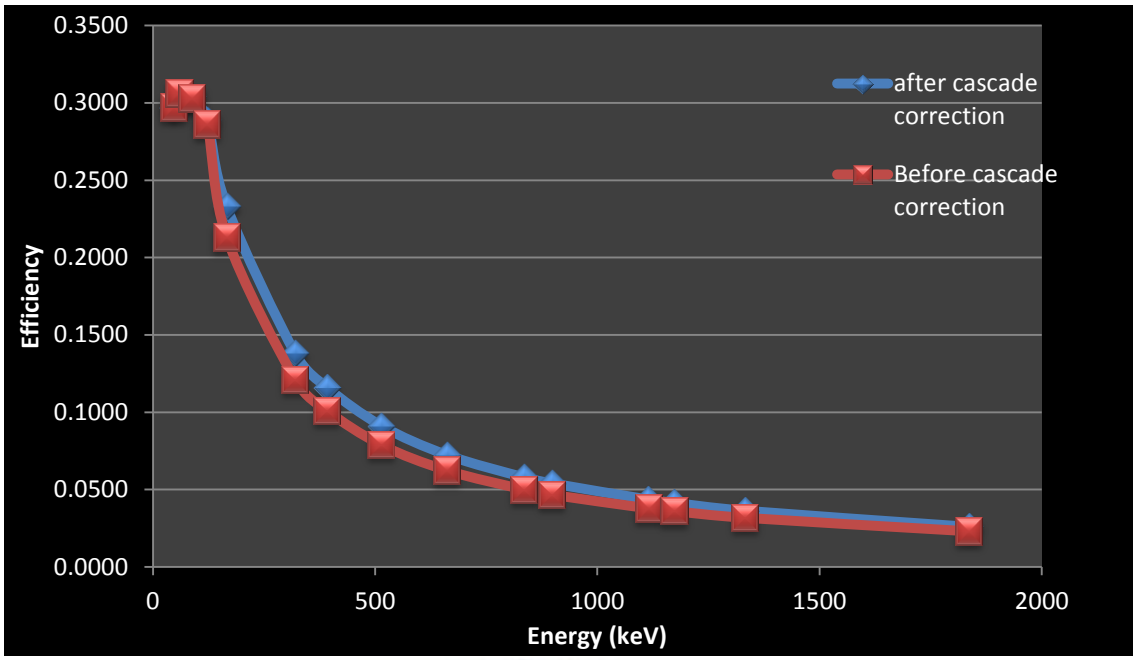

Figure 4.12: Empirical efficiency curves (2nd order polynomial) before and after cascade correction (threshold significance: 3.00).

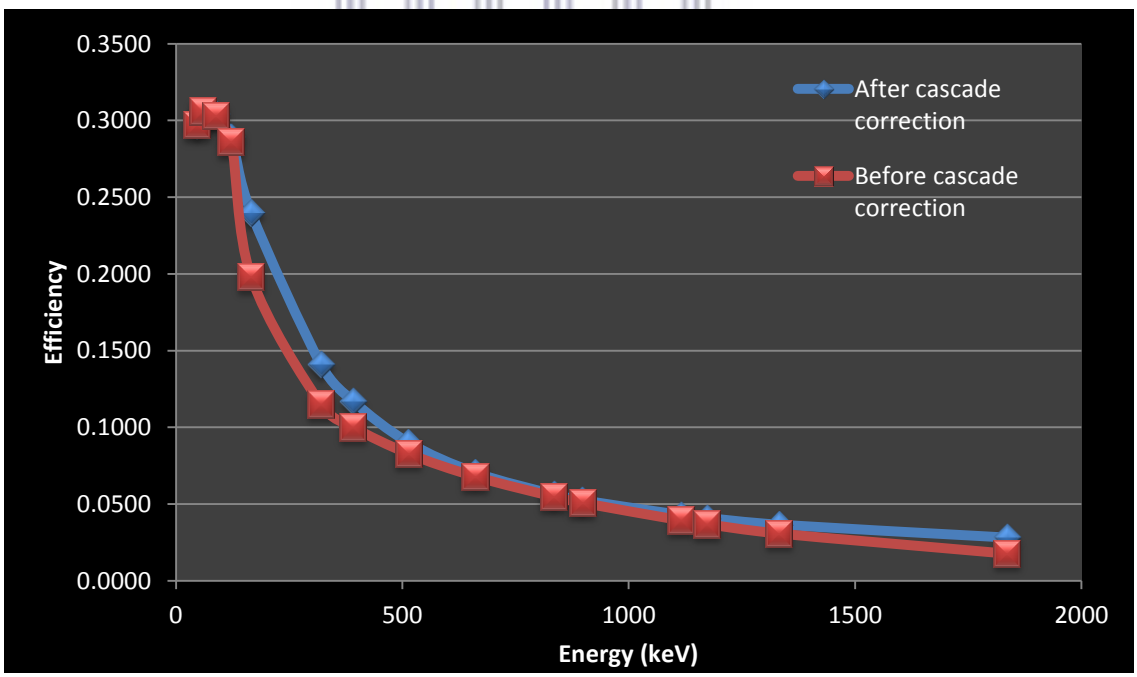

Figure 4.13: Empirical efficiency curves (3rd order polynomial) before and after cascade correction (threshold significance: 3.00).

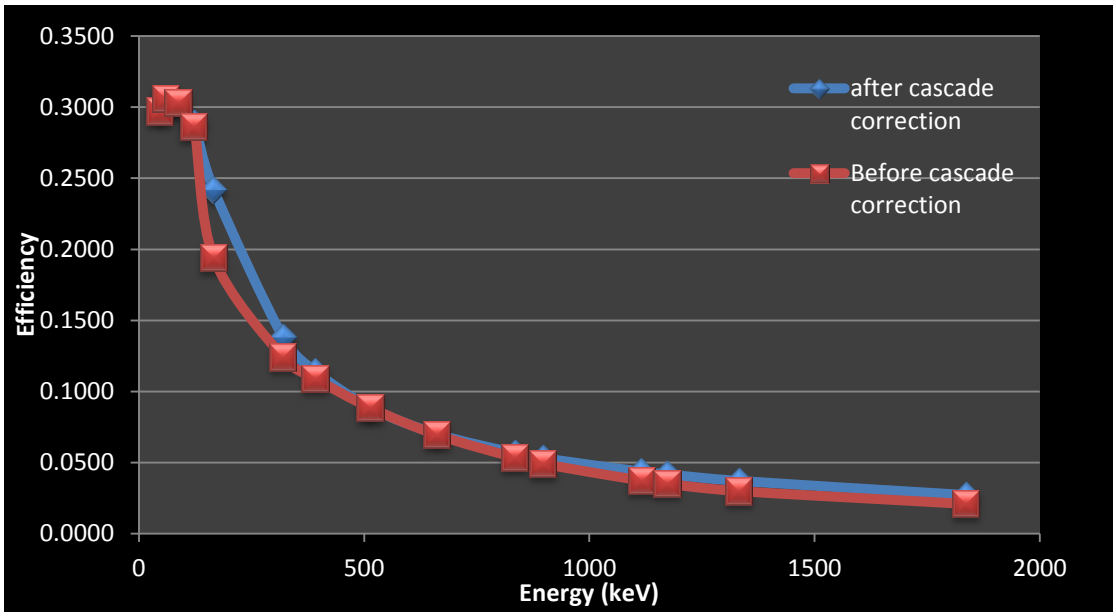

Figure 4.14: Empirical efficiency curves (4th order polynomial) before and after cascade correction (threshold significance: 3.00).

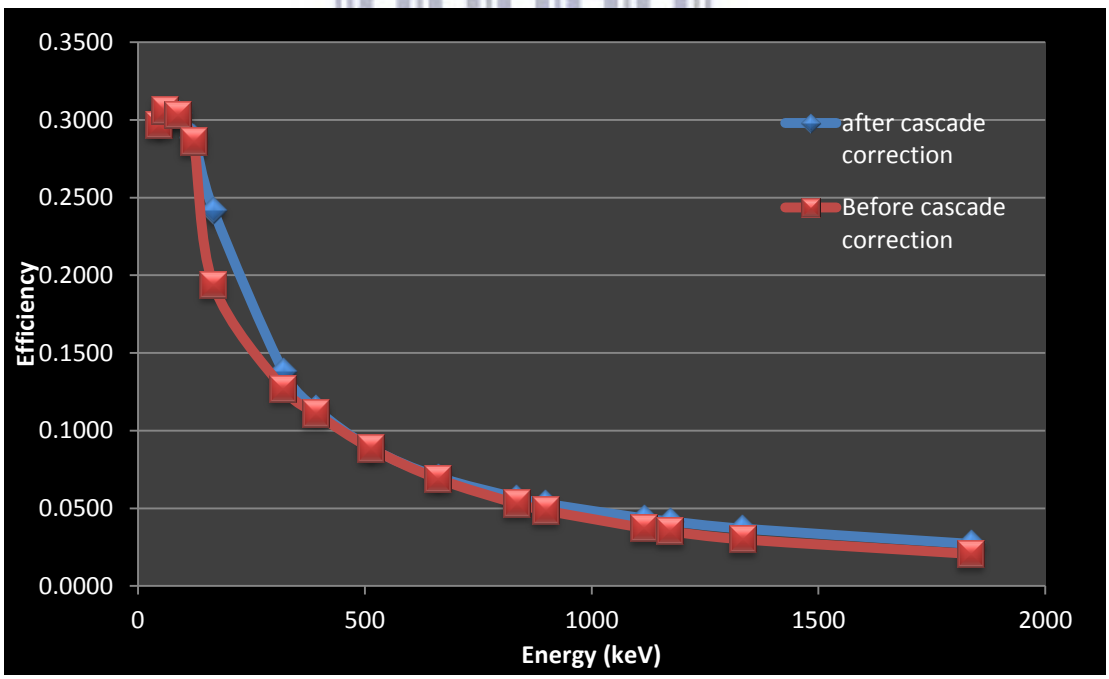

Figure 4.15: Empirical efficiency curves (5th order polynomial) before and after cascade correction (threshold significance: 3.00).

Table 4.11: Sum-coincidence corrections for nuclides in the 2008, 2009 and 2012 PTE.

Nuclide		PTE		
		2008	2009	2012
^{210}Pb	46.54	free	free	free
^{241}Am	59.54	free	free	free
^{109}Cd	88.03	free	free	free
^{57}Co	122.06	1.000	1.000	1.000
^{139}Ce	165.85	0.999	0.999	0.999
^{51}Cr	320.08	free	NA	free
^{113}Sn	391.69	free	free	free
^{85}Sr	513.99	1.000	1.000	1.000
^{137}Cs	661.65	miss	miss	miss
^{54}Mn	834.83	miss	miss	miss
^{88}Y	898.02	0.854	0.853	0.880
^{65}Zn	1115.52	free	free	free
^{60}Co	1173.22	0.838	0.838	0.867
^{60}Co	1332.49	0.832	0.832	0.862
^{88}Y	1836.01	0.827	0.828	0.859

NA Not applied in this PTE

free No coincidence correction required

miss Nuclide energy was not found in the library (Correction is unknown)

4.2.2. LabSOCS Calibration

The LabSOCS calibration software includes several standard geometry templates. The most commonly used templates are the Beaker, Box, Cylinder, Marinelli Beaker and the sphere.

After choosing the most applicable template, which was the cylinder as depicted in Figure 4.16, the necessary physical dimensions of the sample and container were measured and recorded. For a cylinder the following dimensions are necessary; thickness, inside wall height, inside base diameter, material type and the density of the sample and container. The dimensions are defined in mm, where d1.1 is the side wall thickness, d1.2 is the inside diameter of a container or disk diameter, d3.1 is the sample height, d2.1 is

the bottom wall thickness of the container, d4.1 and d5.1 are absorbers and d6.1 is the source- to-detector distance as shown in Table 4.12.

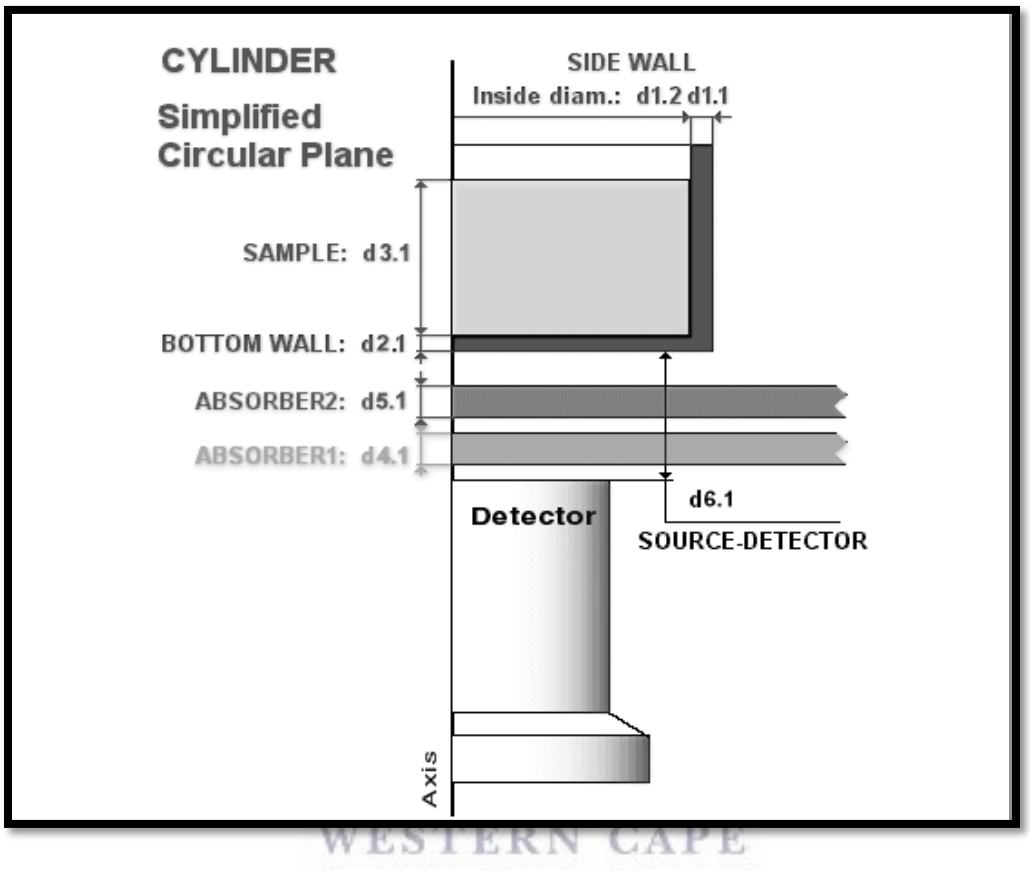

Figure 4.16: Side wall of a Cylinder, Simplified Circular Plane [60].

Table 4.12: LabSOCS MANUAL3M geometry definition in mm.

				Material	Density (g/cm^3)
d1.1/d1.2	Side wall / Diameter	0.3	51	PVC	1.4
d2.1	Bottom Wall	0.4		PVC	1.4
d3.1	Sample	5		3m	0.54
d4.1	Absorber 1	0			
d5.1	Absorber 2	0			
d6.1	Source-to-Detector	0			

4.2.3. VGSL Calibration

The VGSL software includes the four CTBTO sample geometry templates: MANUAL3M, ARAME, Point source and RASA.

The characteristics of the detector under study are to be defined by, crystal type, crystal dimension, dead-layer thickness, crystal-holder dimensions, End Cap Mantle dimensions, End Cap Window dimensions and materials as depicted in Figure 4.17. The characteristics of the detector used in this study are tabulated in Table 4.13 and shown in Figure 4.18.

The parameters of the detector shielding are defined by the inner radius and inner height in mm as shown in Figure 4.19 and Figure 4.20, and the shielding layers depicted in Figure 4.21 with their density in g/cc as shown in Table 4.14. The shielding parameters are further illustrated in Figure 4.22.

The source geometry definition consists of four templates as stated above. The MANUAL3M geometry dimensions are presented in Table 4.15 and illustrated in Figure 4.23. The dimensions are further defined by the height and diameter shown in Figure 4.24 and the sides of the container thickness, which are depicted in Figure 4.25. The sample holder was not defined as the sample in its container is resting directly on the detector end-cap.

Accordingly, all these parameters are to be defined and recorded.

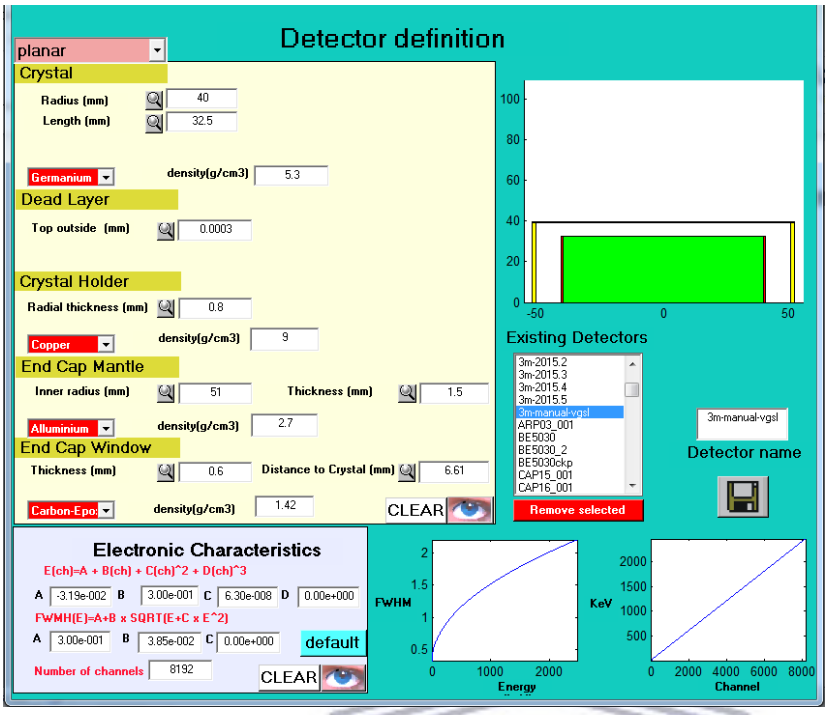

Figure 4.17: VGSL Detector characteristics.

Table 4.13: VGSL characteristics of a BEGe detector.

Detector characteristics	Dimensions (mm)		Material	Density (g/cm^3)
Crystal	Radius	40.000	Germanium	5.3
	Length	32.500		
Dead Layer	Top Outside	0.0003	N/A	N/A
Crystal Holder	Radial Thickness	0.8000	Copper	9.0
End Cap Mantle	Inner Radius	51.000	Aluminum	2.7
	Thickness	1.5000		
End Cap Window	Thickness	0.6000	Carbon Epoxy	1.42
	Distance to Crystal	6.6100		

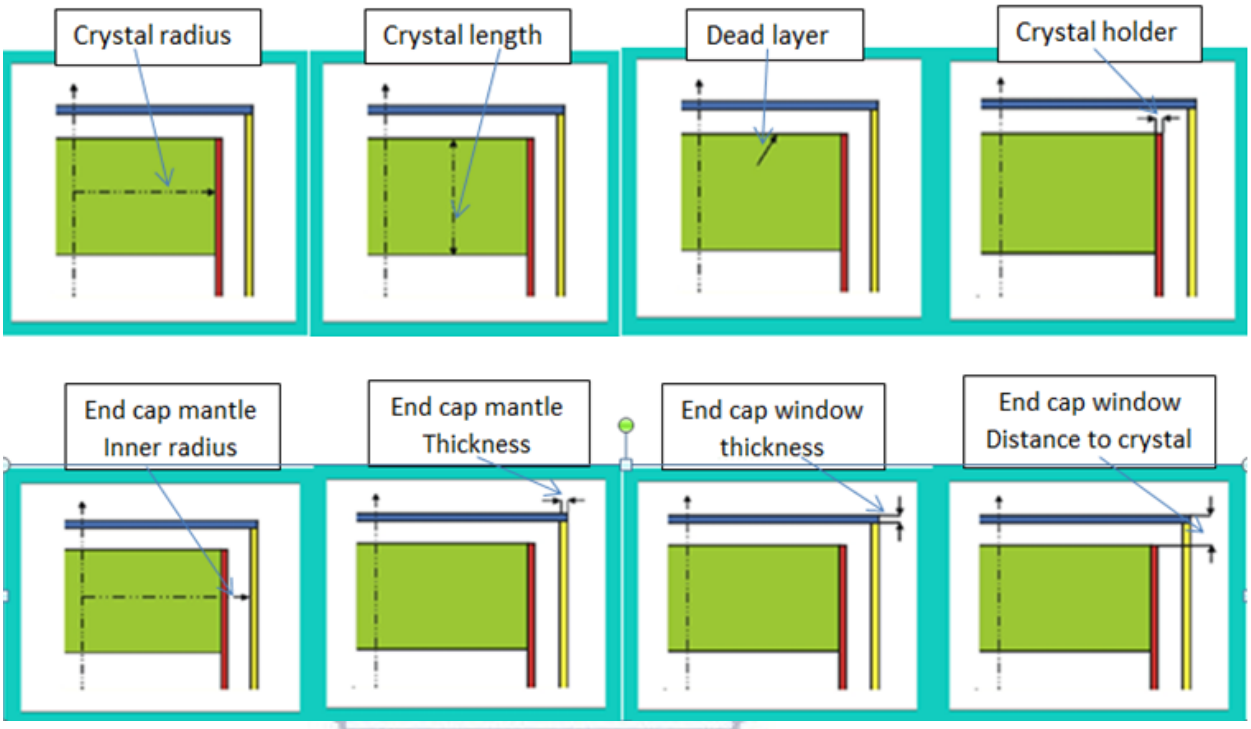

Figure 4.18: VGSL material and dimensional definition of a BEGe detector.

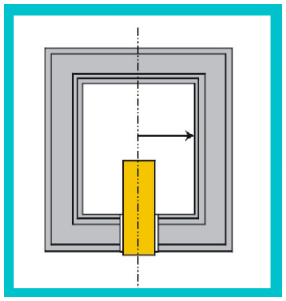

Figure 4.20: Inner radius of lead castle.

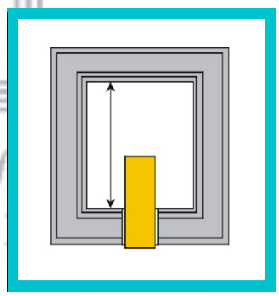

Figure 4.19: Inner height of lead castle.

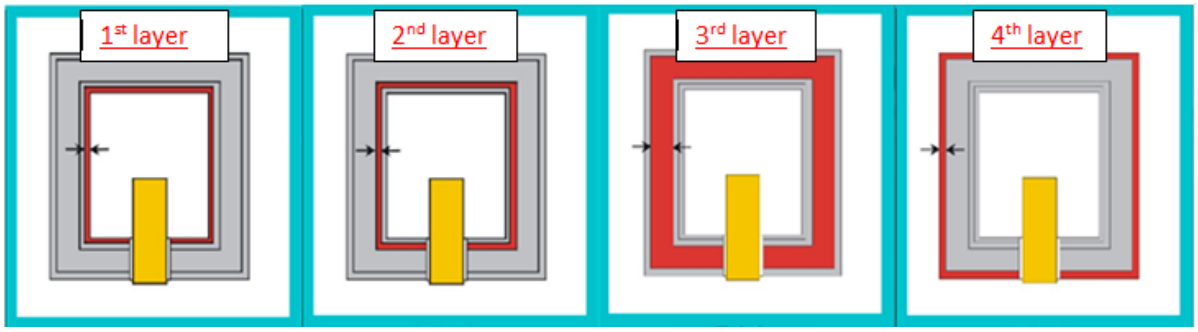

Figure 4.21: Shielding layers of the BEGe detector.

Table 4.14: Properties of the BEGe detector shielding materials used in this work as described in section 3.1.1.

Layers	Material	Density (g/cc)	Thickness (mm)
1	Polypropylene	0.55	4.00
2	Copper	8.96	2.00
3	Tin	7.31	1.00
4	Lead	11.40	150.00

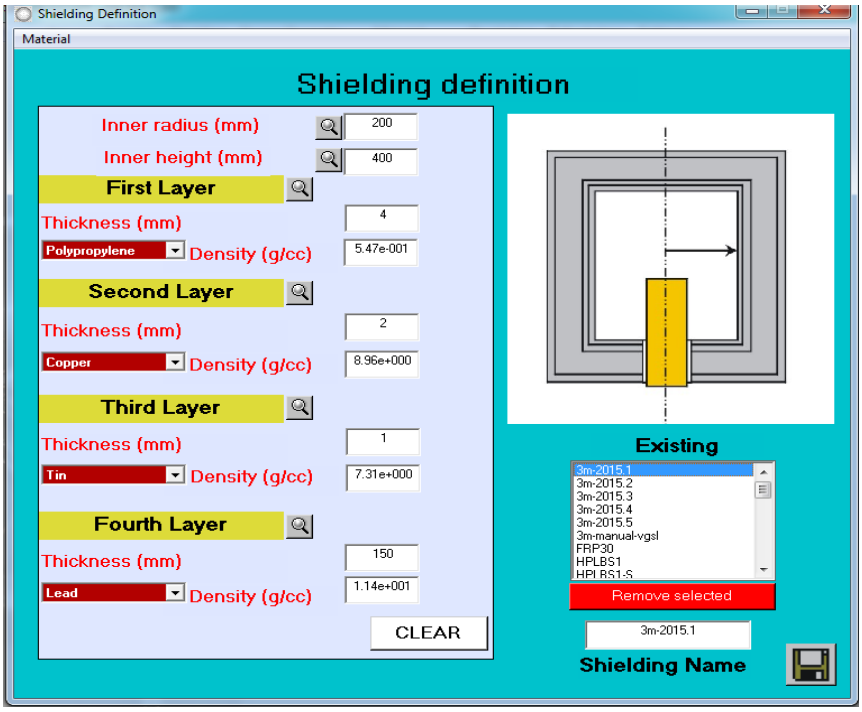

Figure 4.22: VGSL shield layers of a BEGe detector.

Table 4.15: VGSL MANUAL3M geometry definition.

Source Geometry	Dimensions (mm)		Material	Density(g/cm3)
Active Zone	diameter	51.0	Filter	0.54
Container	top	0.4	PVC	1.4
thickness	bottom	0.4		
	side	0.3		

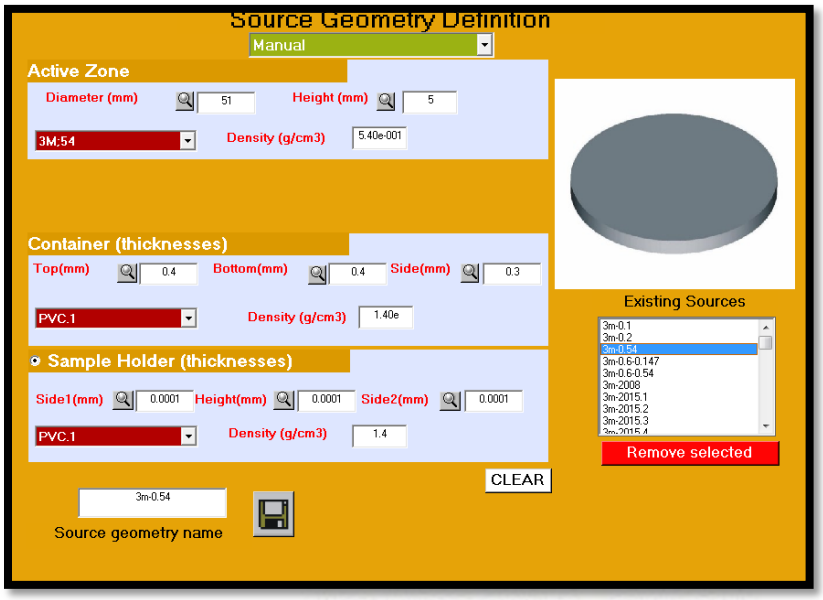

Figure 4.23: The VGSL MANUAL3M geometry definition.

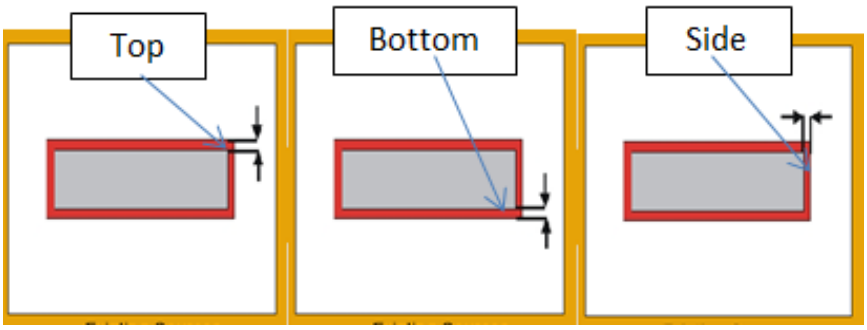

Figure 4.24: Side walls of a MANUAL 3M Container.

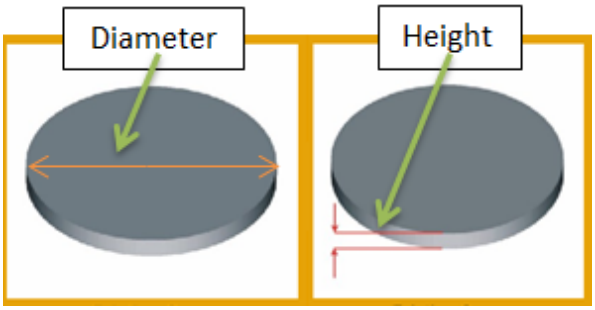

Figure 4.25: Diameter and height of a MANUAL3M sample.

The necessary physical dimensions, detector, shielding and source geometry were defined. Within the source geometry definition, a container and sample material were also defined. For material definition a pre-defined materials list is provided although new materials for samples or containers like carbon-epoxy and PVC (with different density) were added by defining elemental composition, atomic fraction and density and new efficiency curves were simulated and saved.

4.2.4. Evaluation of the MANUAL3M reference sample

Table 4.16 gives the activity values of the MANUAL3M reference sample obtained from the "best" empirical, LabSOCS and VGSL calibration curves. The ratios of the empirical, LabSOCS and VGSL activities over the certified values are presented in Table 4.17. These results were obtained after decay and cascade corrections were applied. The activity ratios are further illustrated in Figure 4.26. From this it can be seen that the empirical and VGSL results compare well with the certified values, while the results of LabSOCS are about 10% higher than the certified activity values more or less over the entire energy region, which comes down to an underestimation of the efficiency by the LabSOCS simulation.

Table 4.16: MANUAL3M reference filter sample activity values after decay and cascade correction compared to the certified values.

Nuclide	Energy (keV)	Activity(Bq)		Activity after decay correction(Bq)					
		Certified		Empirical		LabSOCS		VGSL	
		Value	Unc.	Value	Unc.	Value	Unc.	Value	Unc.
^{57}Co	122.06	0.0078	0.0010	0.0077	0.0010	0.0083	0.0013	0.008	0.0011
^{141}Ce	145.44	1.0600	0.0240	1.0872	0.0147	1.1578	0.1163	1.1141	0.0409
^{139}Ce	165.85	0.0039	0.0001	0.0043	0.0012	0.0046	0.0014	0.0044	0.0012
^{133}Ba	356.01	0.1090	0.0018	0.1128	0.0104	0.1252	0.0150	0.1148	0.0108
^{125}Sb	427.89	0.5520	0.0080	0.5490	0.0148	0.6153	0.0467	0.5609	0.0196
^{58}Co	810.76	1.0600	0.0179	1.0057	0.0166	1.1266	0.0680	1.0240	0.0216
^{54}Mn	834.83	0.1120	0.0014	0.1138	0.0026	0.1273	0.0080	0.1157	0.0030

Table 4.17: MANUAL3M reference filter sample activity ratios after decay and cascade corrections.

Nuclide	Energy (keV)	Ratio							
		Certified		Empirical		LabSOCS		VGSL	
		Value	Unc.	Value	Unc.	Value	Unc.	Value	Unc.
^{57}Co	122.06	1.00	0.18	0.99	0.18	1.06	0.22	1.03	0.20
^{141}Ce	145.44	1.00	0.03	1.03	0.03	1.09	0.11	1.05	0.05
^{139}Ce	165.85	1.00	0.04	1.09	0.31	1.16	0.35	1.11	0.32
^{133}Ba	356.01	1.00	0.02	1.03	0.10	1.15	0.14	1.05	0.10
^{125}Sb	427.89	1.00	0.02	0.99	0.03	1.11	0.09	1.02	0.04
^{58}Co	810.76	1.00	0.02	0.95	0.02	1.06	0.07	0.97	0.03
^{54}Mn	834.83	1.00	0.02	1.02	0.03	1.14	0.07	1.03	0.03
Average				**1.01**		**1.11**		**1.04**	
Standard Deviation				**0.04**		**0.04**		**0.04**	

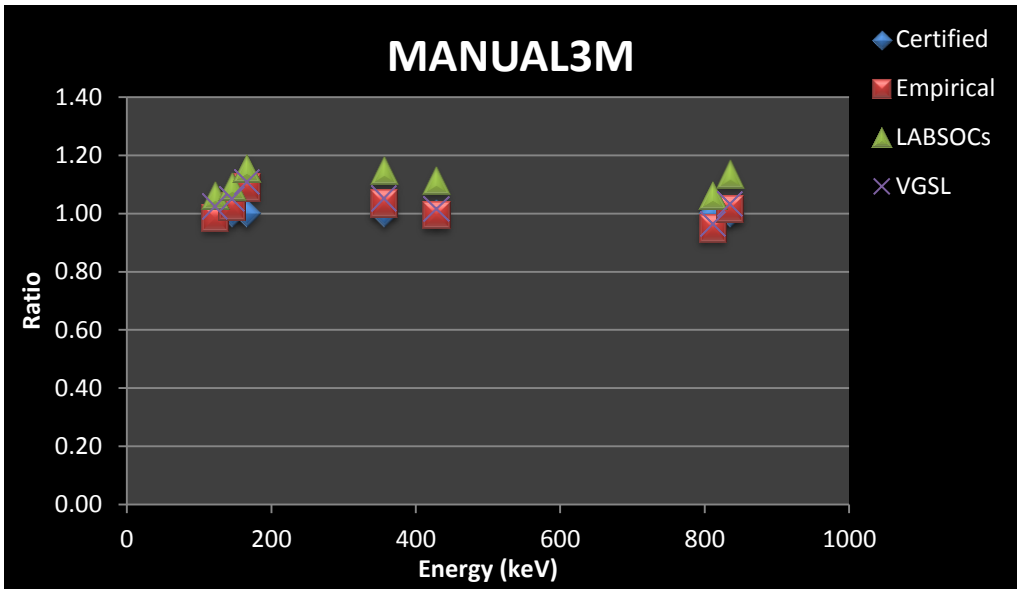

Figure 4.26: Ratios of the MANUAL3M reference filter sample activity after decay and cascade correction.

4.3. HALFMOON Sample Geometry

4.3.1. HALFMOON geometry definition and calibration

The acquisition of the gamma-ray calibration spectra for a HALFMOON sample geometry were carried out in the year 2009 with sufficient counting statistics for the gamma energy lines of interest as shown in Figure 4.27. Figure 4.28 shows the nuclides of interest in the low energy region. The calibration spectrum was acquired with an average dead time below 2%.

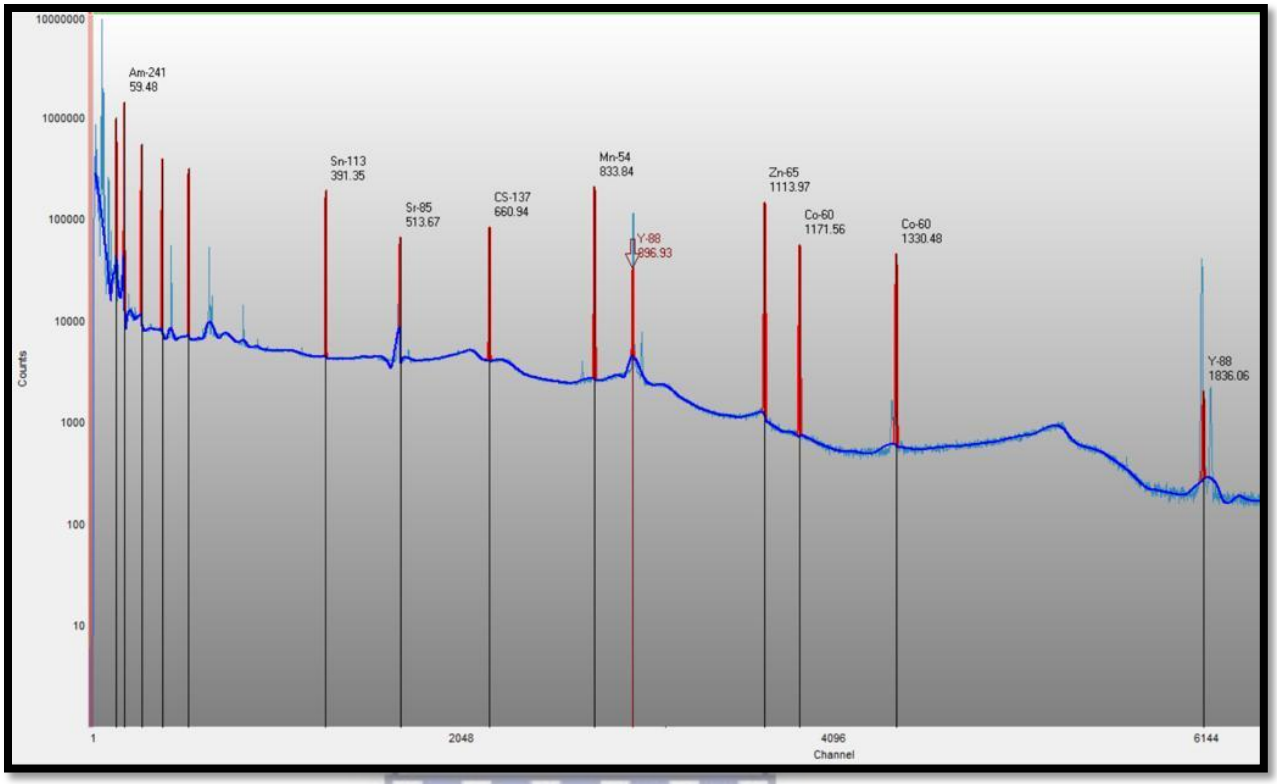

Figure 4.27: Full energy calibration spectrum for a HALFMOON filter sample.

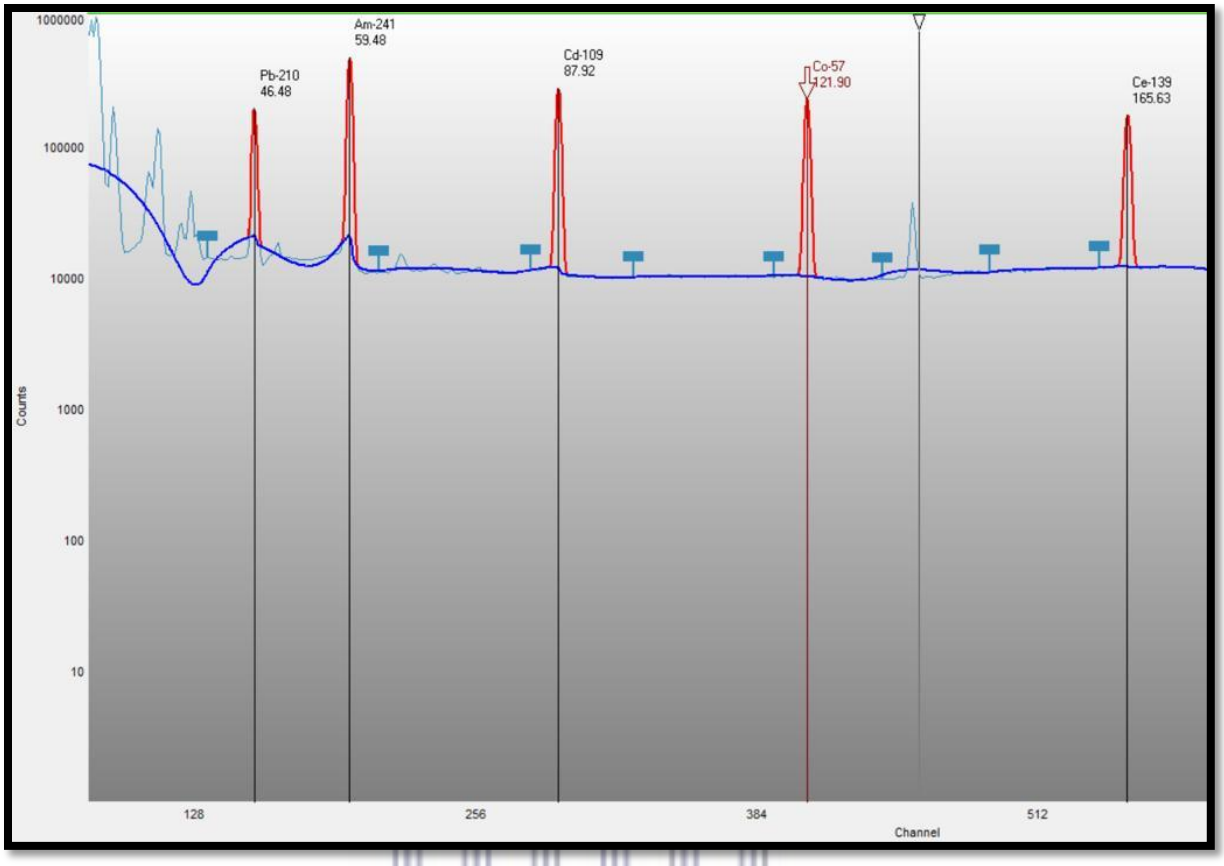

Figure 4.28: Low energy region calibration spectrum for a HALFMOON filter sample.

The source geometry definition used for the year 2009 was the HALFMOON. The geometry dimensions are presented in Table 4.18. The dimensions were further defined by the height and diameter as shown in Figure 4.23, in section 4.2 and the sides of the container thickness which are clearly depicted in Figure 4.25. The sample holder was not defined because it was not used for the study.

Table 4.18: VGSL HALFMOON geometry definition.

Source Geometry	Dimensions (mm)		Material	Density (g/cm^3)
Active Zone	diameter	51.0	Filter	1.67
	height	5.0		
Container thickness	top	0.4	PVC	1.4
	bottom	0.4		
	side	0.3		

The HALFMOON sample material was modeled with a chemical composition of a MANUAL3M used in the year 2008 but with a density of 1.7 g/cc. The density of the HALFMOON was determined taking into account the container geometry.

Tables 4.19 and Table 4.20 give HALFMOON geometry activity values and ratios for the Empirical, LabSOCS and VGSL after coincidence summing correction at a threshold significance of 3.00.

From this it can be seen that the VGSL results are some 6%, while the results of LabSOCS are about 16%, higher than the certified activity values more or less over the entire energy region, which comes down to an underestimation of the efficiency by both the VGSL and LabSOCS simulation.

Figure 4.29 shows the graphical representation of the empirical efficiency and the curves generated from LabSOCS and VGSL.

Table 4.19: HALFMOON calibration activity values after cascade correction compared to the certified values.

Nuclide	Energy (keV)	Activity(Bq)		Activity after cascade correction(Bq)					
		Certified		Empirical		LabSOCS		VGSL	
		Value	Unc.	Value	Unc.	Value	Unc.	Value	Unc.
^{210}Pb	46.54	3546.0	125.2	3576.0	65.8	4116.6	597.4	3819.1	225.3
^{241}Am-	59.54	619.0	11.8	613.4	11.5	694.4	71.4	659.2	40.2
^{109}Cd-	88.03	2622.0	99.1	2685.6	80.8	3041.2	315.6	2911.6	180.5
^{57}Co	122.06	94.7	1.7	94.5	0.9	109.8	11.0	103.9	7.3
^{139}Ce	165.85	145.1	3.7	145.6	2.0	163.5	15.3	155.3	5.8
^{113}Sn	391.69	247.7	4.6	251.0	8.1	297.3	23.0	271.7	13.5
^{85}Sr	513.99	101.5	2.0	106.3	4.7	126.0	9.3	114.3	6.2
^{137}Cs	661.65	118.4	2.2	118.1	0.7	138.9	8.3	125.7	3.0
^{54}Mn	834.83	403.9	5.7	405.4	2.0	472.0	24.1	426.6	8.6
^{88}Y	898.02	418.0	5.9	410.7	2.7	476.6	22.4	430.6	8.7
^{65}Zn	1115.52	840.4	15.6	870.7	5.6	1001.3	40.3	902.5	15.6
^{60}Co	1173.22	194.1	2.4	191.8	0.9	220.1	8.8	198.1	3.1
^{60}Co	1332.49	194.1	2.4	192.8	1.2	220.0	8.8	197.3	2.8
^{88}Y	1836.01	418.0	5.9	420.6	4.3	467.2	18.8	411.1	6.4

Table 4.20: HALFMOON calibration activity ratios after cascade correction.

Nuclide	Energy (keV)	Ratio							
		Certified		Empirical		LabSOCS		VGSL	
		Value	Unc.	Value	Unc.	Value	Unc.	Value	Unc.
^{210}Pb	46.54	1.00	0.05	1.01	0.04	1.16	0.17	1.08	0.07
^{241}Am	59.54	1.00	0.03	0.99	0.03	1.12	0.12	1.06	0.07
^{109}Cd	88.03	1.00	0.05	1.02	0.05	1.16	0.13	1.11	0.08
^{57}Co	122.06	1.00	0.03	1.00	0.02	1.16	0.12	1.10	0.08
^{139}Ce	165.85	1.00	0.04	1.00	0.03	1.13	0.11	1.07	0.05
^{113}Sn	391.69	1.00	0.03	1.01	0.04	1.20	0.10	1.10	0.06
^{85}Sr	513.99	1.00	0.03	1.05	0.05	1.24	0.10	1.13	0.06
^{137}Cs	661.65	1.00	0.03	1.00	0.02	1.17	0.07	1.06	0.03
^{54}Mn	834.83	1.00	0.02	1.00	0.01	1.17	0.06	1.06	0.03
^{88}Y	898.02	1.00	0.02	0.98	0.02	1.14	0.06	1.03	0.03
^{65}Zn	1115.52	1.00	0.03	1.04	0.02	1.19	0.05	1.07	0.03
^{60}Co	1173.22	1.00	0.02	0.99	0.01	1.13	0.05	1.02	0.02
^{60}Co	1332.49	1.00	0.02	0.99	0.01	1.13	0.05	1.02	0.02
^{88}Y	1836.01	1.00	0.02	1.01	0.02	1.12	0.05	0.98	0.02
Average				**1.01**		**1.16**		**1.06**	
Standard Deviation				**0.02**		**0.03**		**0.04**	

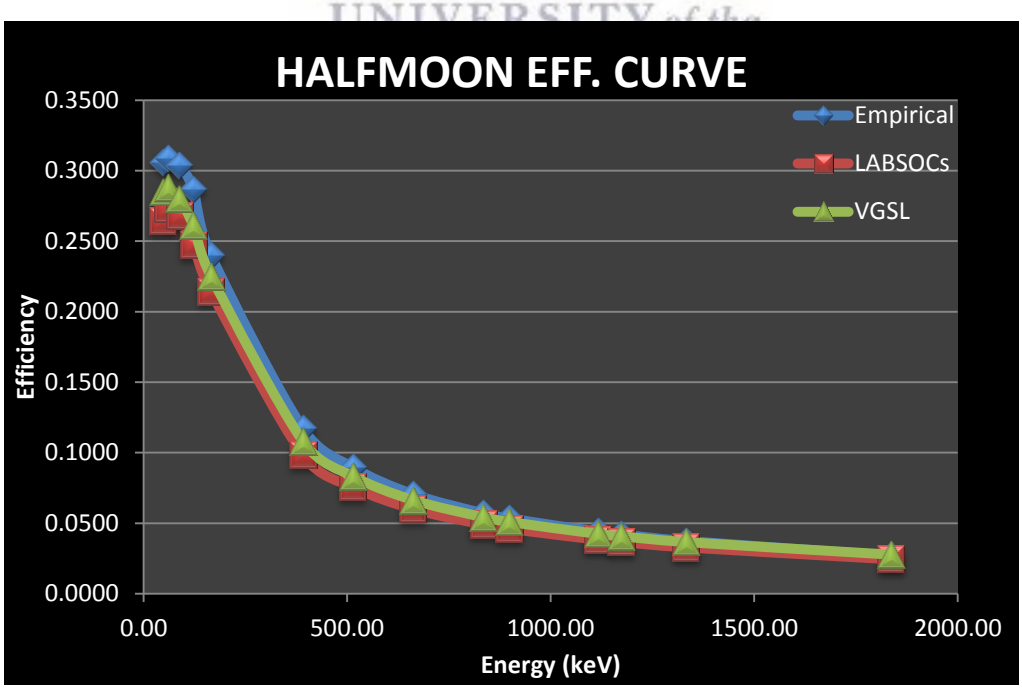

Figure 4.29: HALFMOON efficiency curves after cascade correction

The efficiency curves are represented mathematically by the following equations, of which Equation 4.3.1, 4.3.3 and 4.3.5 are polynomials in the low energy region for the Empirical, LabSOCS and VGSL calibrations respectively. Equation 4.3.2, 4.3.4 and 4.3.6 are the polynomials in the high energy region; where ε is the peak efficiency and E is the peak-energy.

$$Ln\,(\varepsilon) = -4.202 + 1.460 \times \ln(E) - 0.1758 \times \ln(E)^2 \quad (4.3.1)$$

$$Ln\,(\varepsilon) = 94.33 - 88.68 \times \ln(E) + 32.57 \times \ln(E)^2 - 5.870 \times \ln(E)^3 + 0.5172 \times \ln(E)^4 - 0.01790 \times \ln(E)^5 \quad (4.3.2)$$

$$Ln\,(\varepsilon) = -6.290 + 2.379 \times \ln(E) - 0.2832 \times \ln(E)^2 \quad (4.3.3)$$

$$Ln\,(\varepsilon) = 174.3 + 126.7 \times \ln(E) - 36.10 \times \ln(E)^2 + 5.004 \times \ln(E)^3 - 0.3389 \times \ln(E)^4 + 0.008925 \times \ln(E)^5 \quad (4.3.4)$$

$$Ln\,(\varepsilon) = -114.8 + 133.8 \times \ln(E) - 63.43 \times \ln(E)^2 + 15.08 \times \ln(E)^3 - 1.794 \times \ln(E)^4 + 0.08522 \times \ln(E)^5 \quad (4.3.5)$$

$$Ln\,(\varepsilon) = -100.4 + 70.07 \times \ln(E) - 18.92 \times \ln(E)^2 + 2.436 \times \ln(E)^3 - 0.1496 \times \ln(E)^4 + 0.003426 \times \ln(E)^5 \quad (4.3.6)$$

4.3.2. Evaluation of the HALFMOON reference sample

Table 4.21 gives the activity values of the HALFMOON reference sample obtained from the 'best' Empirical, LabSOCS and VGSL calibration curve. The ratios of the Empirical, LabSOCS and VGSL activities over the certified values are presented in Table 4.22 and further illustrated in Figure 4.30. These results were obtained after a cascade correction was applied.

Table 4.21: HALFMOON reference activity values after decay correction compared to the certified values

Nuclide	Energy (keV)	Activity(Bq)		Activity after decay correction (Bq)					
		Certified		Empirical		LabSOCS		VGSL	
		Value	Unc.	Value	Unc.	Value	Unc.	Value	Unc.
^{57}Co	122.06	0.050	0.005	0.048	0.002	0.056	0.006	0.053	0.004
^{141}Ce	145.44	1.533	0.058	1.532	0.024	1.731	0.174	1.643	0.063
^{51}Cr	320.08	22.750	0.776	22.976	0.434	26.978	2.147	24.876	1.075
^{125}Sb	427.89	3.243	0.148	3.055	0.046	3.625	0.248	3.303	0.130
^{103}Ru	497.08	2.667	0.115	2.783	0.158	3.301	0.273	2.996	0.196
^{134}Cs	604.70	3.069	0.105	3.022	0.032	3.567	0.217	3.229	0.090
^{106}Ru	621.84	11.850	0.561	8.213	0.429	9.684	0.769	8.763	0.507
^{137}Cs	661.65	0.766	0.026	0.780	0.007	0.918	0.056	0.830	0.021
^{95}Zr	756.72	1.854	0.079	1.819	0.042	2.128	0.129	1.923	0.060
^{95}Nb	765.79	3.826	0.177	3.678	0.076	4.298	0.410	3.885	0.157
^{58}Co	810.76	2.450	0.084	2.255	0.019	2.629	0.139	2.377	0.051
^{54}Mn	834.83	3.086	0.105	3.075	0.019	3.581	0.183	3.236	0.067
^{65}Zn	1115.52	7.268	0.248	7.278	0.066	8.371	0.342	7.545	0.139
^{60}Co	1173.22	5.536	0.178	5.529	0.038	6.346	0.256	5.713	0.095

Table 4.22: HALFMOON reference activity ratios after decay correction

Nuclide	Energy (keV)	Ratio							
		Certified		Empirical		LabSOCS		VGSL	
		Value	Unc.	Value	Unc.	Value	Unc.	Value	Unc.
^{57}Co	122.06	1.00	0.14	0.96	0.10	1.12	0.16	1.06	0.14
^{141}Ce	145.44	1.00	0.05	1.00	0.04	1.13	0.12	1.07	0.06
^{51}Cr	320.08	1.00	0.05	1.01	0.04	1.19	0.10	1.09	0.06
^{125}Se	427.89	1.00	0.06	0.94	0.05	1.12	0.09	1.02	0.06
^{103}Ru	497.08	1.00	0.06	1.04	0.07	1.24	0.12	1.12	0.09
^{134}Cs	604.70	1.00	0.05	0.98	0.04	1.16	0.08	1.05	0.05
^{106}Ru	621.84	1.00	0.07	0.69	0.05	0.82	0.08	0.74	0.06
^{137}Cs	661.65	1.00	0.05	1.02	0.04	1.20	0.08	1.08	0.05
^{95}Zr	756.72	1.00	0.06	0.98	0.05	1.15	0.08	1.04	0.05
^{95}Nb	765.79	1.00	0.07	0.96	0.05	1.12	0.12	1.02	0.06
^{58}Co	810.76	1.00	0.05	0.92	0.03	1.07	0.07	0.97	0.04
^{54}Mn	834.83	1.00	0.05	1.00	0.03	1.16	0.07	1.05	0.04
^{65}Zn	1115.52	1.00	0.05	1.00	0.04	1.15	0.06	1.04	0.04
^{60}Co	1173.22	1.00	0.05	1.00	0.03	1.15	0.06	1.03	0.04
Average				**0.97**		**1.13**		**1.03**	
Standard Deviation				**0.08**		**0.10**		**0.09**	

The average activity ratio for the Empirical, LabSOCS and VGSL to the certified activity values is 0.97 ± 0.08, 1.13 ± 0.10 and 1.03 ± 0.09 respectively. It is noted that ^{106}Ru is a possible outlier in all instances, for reasons unknown at this stage, and may be discarded from the results if necessary.

From this it can be seen that the Empirical and VGSL results are in good agreement with the certified values while the results of LabSOCS are some 13% higher than the certified activity values more or less over the entire energy region, which comes down to an underestimation of the efficiency by the LabSOCS simulation.

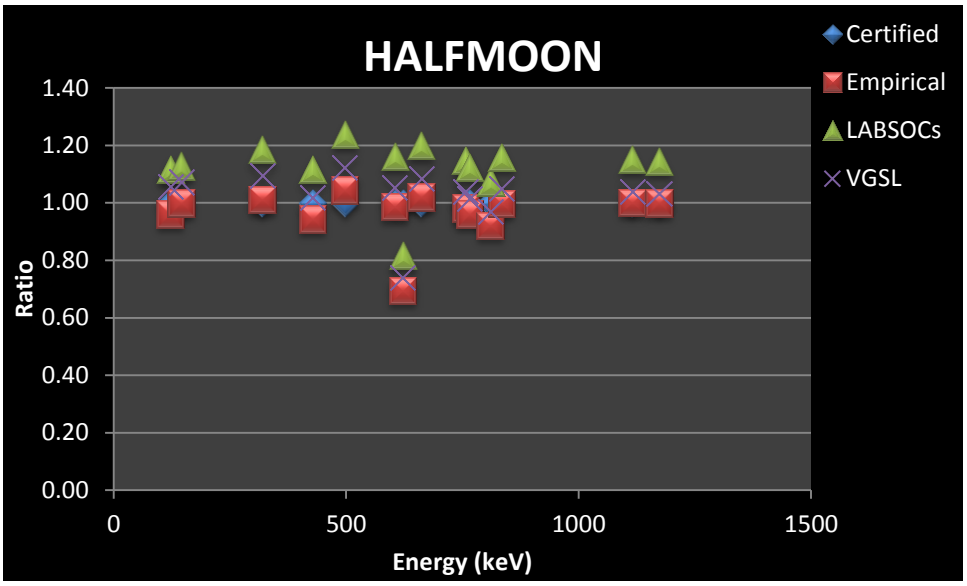

Figure 4.30: Ratios of the HALFMOON reference activity after decay correction.

4.4. ARAME Sample Geometry

4.4.1. ARAME geometry definition and calibration

The acquisition of the gamma-ray calibration spectra for an ARAME sample geometry were carried out in the year 2012 with sufficient counting statistics for the gamma energy lines of interest as shown in Figure 4.31. Figure 4.32 shows the nuclides of interest in the low energy region. The calibration spectrum was acquired with an average dead time below 2%.

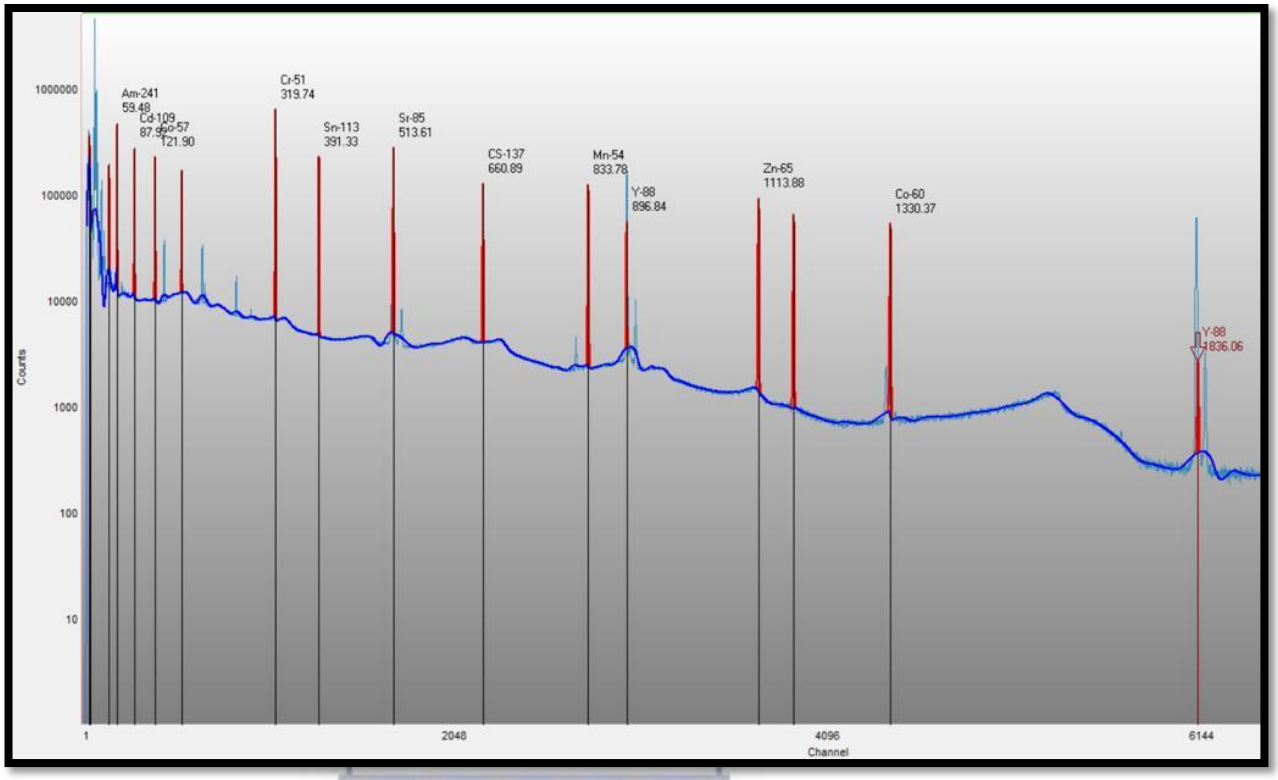

Figure 4.31: Full energy calibration spectrum for ARAME filter sample.

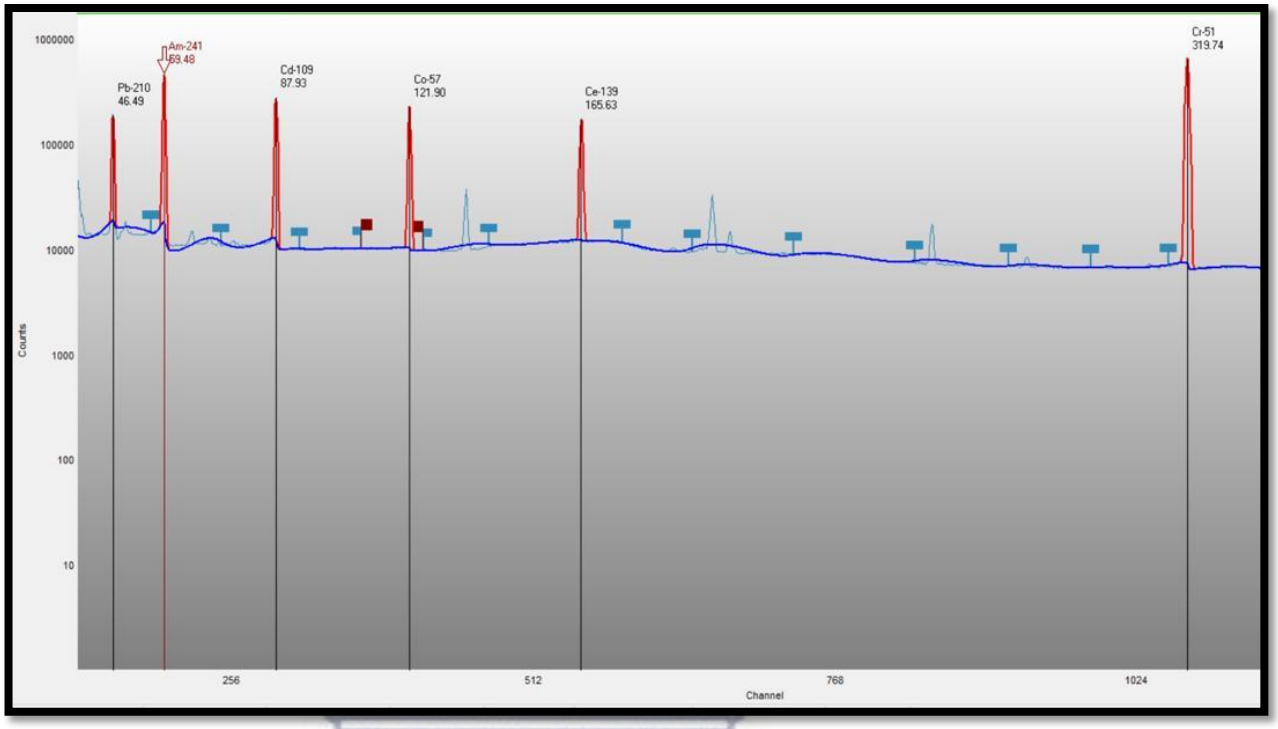

Figure 4.32: Low energy region calibration spectrum for ARAME filter sample.

The ARAME geometry dimensions are presented in Table 4. The dimensions are defined by the height, diameter and the sides of the container thickness which are clearly depicted in Figure 4.33. The sample holder was not defined because it was not used for the study. The VGSL source geometry definition is illustrated in Figure 4.34.

Table 4.23: VGSL ARAME geometry definition for the year 2012.

Source Geometry	Dimensions (mm)		Material	Density (g/cm3)
Active Zone	diameter	82.0	Filter	0.54
Inactive Zone	Side 1	90.0	PVC	1.4
Container thickness	top	1.0	PVC	1.4

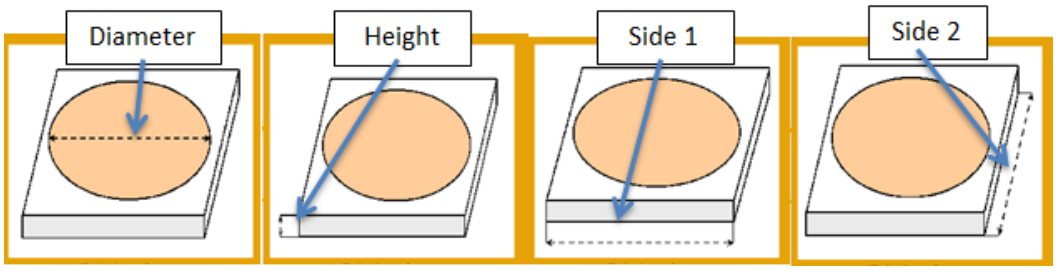

Figure 4.33: Sample and container definition of ARAME geometry.

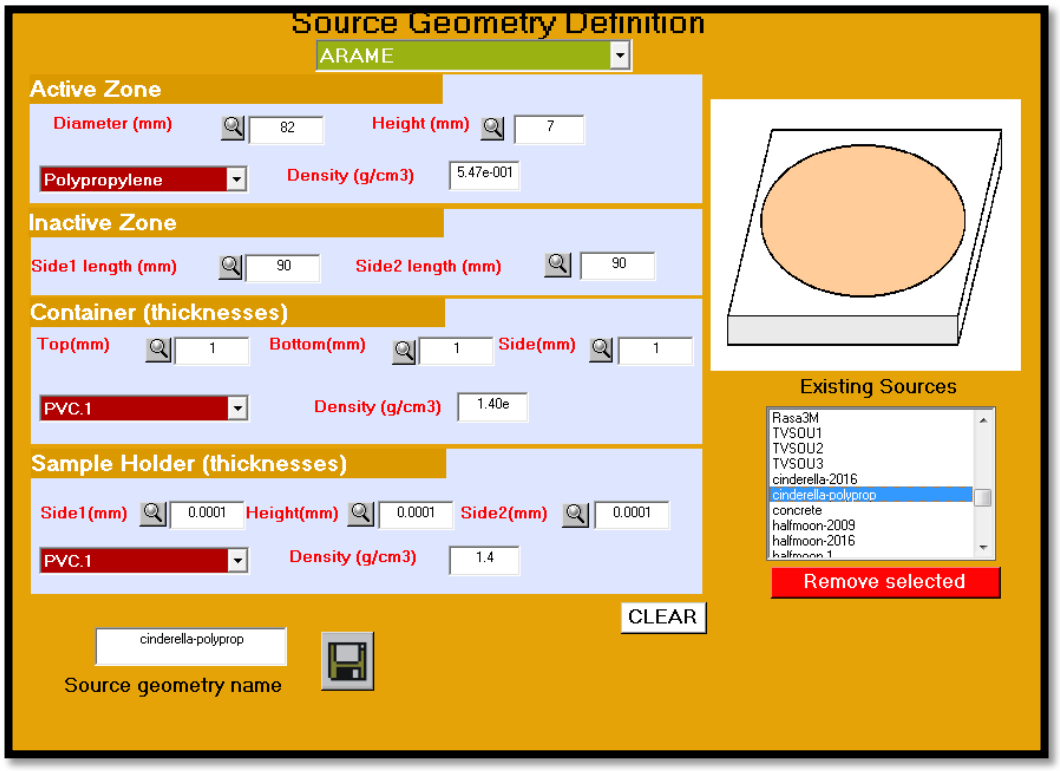

Figure 4.34: The VGSL ARAME geometry definition for the year 2012.

The necessary physical dimensions, detector, shielding and source geometry including the container and sample material are defined. A pre-defined materials list is provided although new materials for samples or containers can be added by defining the elemental composition, atomic fraction and density. The ARAME sample material was modeled as polypropylene; chemically composed of H and C with a density of 0.55 g/cm^3 obtained from the weighed ARAME filter (31.75 g) and the calculated volume (57.73 cm^3). The

material's elemental composition and the corresponding atomic fraction were pre-defined within the VGSL software and added as a new material into the LabSOCS software.

Table 4.24 and Table 4.25 represent ARAME (or Cinderella) geometry activity values and ratios for the Empirical, LabSOCS and VGSL after coincidence summing correction at a threshold significance of 3.00. Figure 4.35 is the graphical representation of the efficiency curves generated with LabSOCS and VGSL.

Table 4.24: ARAME calibration activity values after cascade correction compared to the certified values.

Nuclide	Energy (keV)	Activity(Bq)		Activity after cascade correction(Bq)					
		Certified		**Empirical**		**LabSOCS**		**VGSL**	
		Value	**Unc.**	**Value**	**Unc.**	**Value**	**Unc.**	**Value**	**Unc.**
^{210}Pb	46.54	1603.0	48.0	1610.7	39.7	1733.2	251.7	1519.0	89.9
^{241}Am	59.54	255.0	6.0	250.3	3.4	278.5	28.3	250.7	14.7
^{109}Cd	88.03	1319.0	36.0	1289.4	42.4	1457.6	152.2	1340.2	84.6
^{57}Co	122.06	55.0	1.4	54.9	0.8	60.8	6.1	55.4	3.5
^{139}Ce	165.85	56.7	1.6	56.8	0.9	61.5	5.8	56.8	1.9
^{51}Cr	320.08	1034.0	26.0	1033.2	23.7	1122.6	89.2	1014.8	38.6
^{113}Sn	391.69	166.6	4.0	165.8	3.7	181.0	13.0	162.3	5.4
^{85}Sr	513.99	196.0	4.8	202.8	4.2	222.6	13.4	198.0	5.4
^{137}Cs	661.65	247.0	6.0	245.4	6.1	269.2	16.2	238.6	5.8
^{54}Mn	834.83	254.0	6.0	253.8	7.5	276.8	14.2	245.2	4.9
^{88}Y	898.02	418.0	10.0	404.3	12.8	439.5	21.0	389.5	8.0
^{65}Zn	1115.52	530.0	14.0	519.3	16.5	557.1	22.6	493.5	7.7
^{60}Co	1173.22	288.0	6.0	288.1	9.2	307.9	12.5	272.6	4.1
^{60}Co	1332.49	288.0	6.0	288.2	10.0	304.4	12.3	268.9	4.0
^{88}Y	1836.01	418.0	10.0	420.3	37.6	426.9	17.3	371.0	5.3

Table 4.25: ARAME calibration activity ratios after cascade correction.

Nuclide	Energy (keV)	Ratio							
		Certified		**Empirical**		**LabSOCS**		**VGSL**	
		Value	**Unc.**	**Value**	**Unc.**	**Value**	**Unc.**	**Value**	**Unc.**
^{210}Pb	46.54	1.00	0.04	1.00	0.04	1.08	0.16	0.95	0.06
^{241}Am	59.54	1.00	0.03	0.98	0.03	1.09	0.11	0.98	0.06
^{109}Cd	88.03	1.00	0.04	0.98	0.04	1.11	0.12	1.02	0.07
^{57}Co	122.06	1.00	0.04	1.00	0.03	1.11	0.11	1.01	0.07
^{139}Ce	165.85	1.00	0.04	1.00	0.03	1.08	0.11	1.00	0.04
^{51}Cr	320.08	1.00	0.04	1.00	0.03	1.09	0.09	0.98	0.04
^{113}Sn	391.69	1.00	0.03	1.00	0.03	1.09	0.08	0.97	0.04
^{85}Sr	513.99	1.00	0.03	1.03	0.03	1.14	0.07	1.01	0.04
^{137}Cs	661.65	1.00	0.03	0.99	0.03	1.09	0.07	0.97	0.03
^{54}Mn	834.83	1.00	0.03	1.00	0.04	1.09	0.06	0.97	0.03
^{88}Y	898.02	1.00	0.03	0.97	0.04	1.05	0.06	0.93	0.03
^{65}Zn	1115.52	1.00	0.04	0.98	0.04	1.05	0.05	0.93	0.03
^{60}Co	1173.22	1.00	0.03	1.00	0.04	1.07	0.05	0.95	0.02
^{60}Co	1332.49	1.00	0.03	1.00	0.04	1.06	0.05	0.93	0.02
^{88}Y	1836.01	1.00	0.03	1.01	0.09	1.02	0.05	0.89	0.02
AVERAGE				**1.00**		**1.08**		**0.97**	
Standard Deviation				**0.02**		**0.03**		**0.04**	

From this it can be seen that the Empirical and VGSL results are in good agreement with the certified values while the results of LabSOCS are some 8% higher than the certified activity values more or less over the entire energy region, which comes down to an underestimation of the efficiency by the LabSOCS simulation.

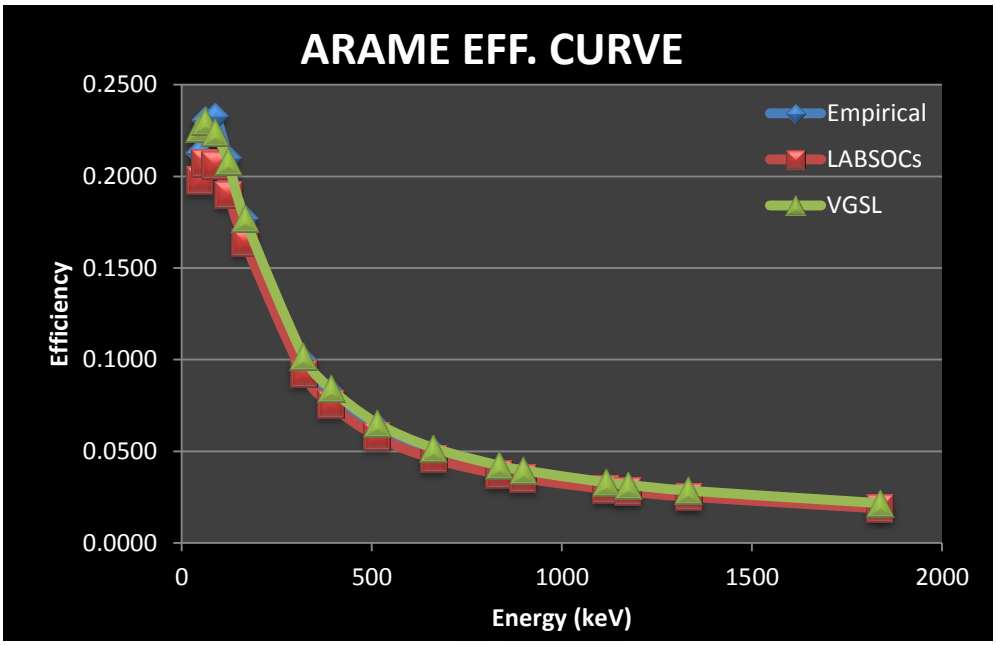

Figure 4.35: ARAME efficiency curves after cascade correction.

The efficiency curves are represented mathematically by the following equations. Equations 4.4.1, 4.4.3 and 4.4.5 are the low energy polynomials for the Empirical, LabSOCS and VGSL, respectively, and Equations 4.4.2, 4.4.4 and 4.4.6 are their respective high energy polynomials; where ε is the peak efficiency and E is the peak-energy

$$Ln\ (\varepsilon) = -10.22 + 4.072 \times \ln(E) - 0.4727 \times \ln(E)^2 \quad (4.4.1)$$

$$Ln\ (\varepsilon) = -74.54 + 48.72 \times \ln(E) - 11.85 \times \ln(E)^2 + 1.252 \times \ln(E)^3 - 0.04935 \times \ln(E)^4 \quad (4.4.2)$$

$$Ln\ (\varepsilon) = -7.440 + 2.761 \times \ln(E) - 0.3243 \times \ln(E)^2 \quad (4.4.3)$$

$$Ln\ (\varepsilon) = -88.10 + 56.93 \times \ln(E) - 13.68 \times \ln(E)^2 + 1.428 \times \ln(E)^3 - 0.05548 \times \ln(E)^4 \quad (4.4.4)$$

$$Ln\,(\varepsilon) = -181.9 + 214.6 \times \ln(E) - 102.7 \times \ln(E)^2 + 24.63 \times \ln(E)^3 - 2.959 \times \ln(E)^4 + 0.1420 \times \ln(E)^5 \quad (4.4.5)$$

$$Ln\,(\varepsilon) = -63.97 + 41.03 \times \ln(E) + 9.786 \times \ln(E)^2 + 1.007 \times \ln(E)^3 - 0.03857 \times \ln(E)^4 \quad (4.4.6)$$

4.4.2. Evaluation of the ARAME reference sample

Table 4.26 depicts the activity values of the ARAME reference sample obtained from the 'best' Empirical, LabSOCS and VGSL calibration curves. The ratios of the Empirical, LabSOCS and VGSL activities over the certified values are presented in Table 4.27. These results were obtained after cascade correction was applied. The average activity ratio for the Empirical evaluation is 0.97 ± 0.08, while the LabSOCS ratio to the certified activity values is 1.06 ± 0.10 and for VGSL this is 0.95 ± 0.10.

The assigned activities of ^{95}Nb and ^{140}La at the reference time were calculated taking into account the ingrowth from their respective parent radionuclides ^{95}Zr and ^{140}Ba.

Taking the uncertainties into consideration all three approaches resulted in acceptable results.

Table 4.26: ARAME reference activity values after decay correction compared to the certified values.

Nuclide	Energy (keV)	Activity(Bq)		Activity after decay correction(Bq)					
		Certified		Empirical		LabSOCS		VGSL	
		Value	Unc.	Value	Unc.	Value	Unc.	Value	Unc.
^{147}Nd	91.11	23.56	0.95	22.88	0.96	25.85	2.78	23.78	1.65
^{144}Ce	133.54	6.04	0.18	6.90	0.46	7.59	0.91	6.94	0.56
^{141}Ce-	145.44	41.40	1.11	41.72	0.61	45.52	4.57	41.88	1.53
^{132}Te	228.16	15.35	0.44	14.45	1.03	15.59	1.65	14.31	1.14
^{103}Ru	497.08	10.05	0.27	10.07	0.60	11.05	0.91	9.83	0.61
^{140}Ba	537.32	73.19	1.97	71.67	11.93	78.66	13.82	69.91	11.69
^{134}Cs	604.7	16.69	0.45	16.30	0.38	17.89	1.08	15.88	0.40
^{137}Cs	661.65	0.27	0.01	0.26	0.01	0.28	0.02	0.25	0.01
^{95}Zr	756.72	31.25	0.83	30.71	1.04	33.60	2.01	29.77	0.87
^{95}Nb	765.79	11.56	0.56	9.19	0.43	10.05	0.93	8.90	0.33
^{140}La	1596.49	60.19	1.69	55.65	7.02	55.66	7.00	48.46	5.19

Table 4.27: ARAME reference activity ratios after decay correction.

Nuclide	Energy (keV)	Ratio							
		Certified		Empirical		LabSOCS		VGSL	
		Value	Unc.	Value	Unc.	Value	Unc.	Value	Unc.
^{147}Nd	91.11	1.00	0.06	0.97	0.06	1.10	0.13	1.01	0.08
^{144}Ce	133.54	1.00	0.04	1.14	0.08	1.26	0.16	1.15	0.10
^{141}Ce	145.44	1.00	0.04	1.01	0.03	1.10	0.11	1.01	0.05
^{132}Te-	228.16	1.00	0.04	0.94	0.07	1.02	0.11	0.93	0.08
^{103}Ru	497.08	1.00	0.04	1.00	0.07	1.10	0.10	0.98	0.07
^{140}Ba	537.32	1.00	0.04	0.98	0.17	1.07	0.19	0.96	0.16
^{134}Cs	604.7	1.00	0.04	0.98	0.03	1.07	0.07	0.95	0.04
^{137}Cs-	661.65	1.00	0.04	0.96	0.05	1.05	0.08	0.93	0.05
^{95}Zr	756.72	1.00	0.04	0.98	0.04	1.08	0.07	0.95	0.04
^{95}Nb	765.79	1.00	0.07	0.79	0.05	0.87	0.09	0.77	0.05
^{140}La	1596.49	1.00	0.04	0.92	0.12	0.92	0.12	0.81	0.09
Average				**0.97**		**1.06**		**0.95**	
Standard Deviation				**0.08**		**0.10**		**0.10**	

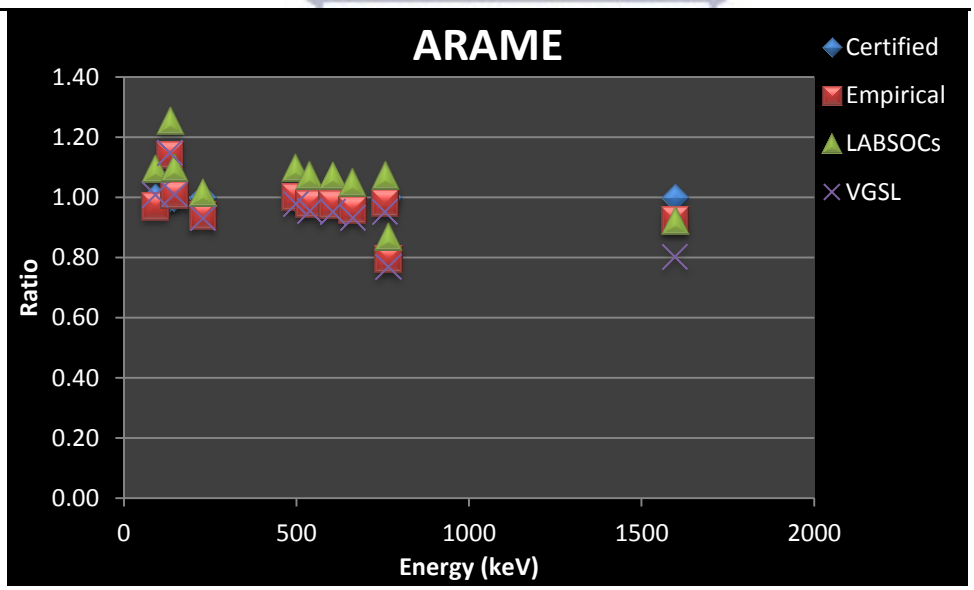

Figure 4.36: Ratios of the ARAME reference activity after decay correction.

4.5. Overall evaluation of the Empirical, LabSOCS and VGSL performance

From the results it is clear that an Empirical efficiency calibration is the better option compared to the two simulated efficiencies from LabSOCS and VGSL software packages evaluated in this study. However, as indicated earlier, in general one does not

have access to these calibration standards for each and every sample delivered to a laboratory. If highly accurate results are mandatory one can prepare such calibration standards. Alternatively, for day-to-day use both LabSOCS and VGSL are viable options.

The use of VGSL requires the knowledge of specific detector parameters and sample matrix and sample holder information, but has the advantage to be extendable to different detectors. Conversely, a LabSOCS calculation requires only information about the positioning, dimensions and nature of the source, but its use is limited to a "characterized" detector by the manufacturer, although the specifications of their "generic" detectors also perform well. The activity bias of the MANUAL3M geometry for LabSOCS and VGSL was 11% and 4% respectively. For the HALFMOON geometry the bias was 15% for LabSOCS and 5% for VGSL. The activity bias of the ARAME geometry for LabSOCS and VGSL was 6% and 5% respectively.

The results obtained are promising. Further improvement may be expected with the development of the parameter settings for the coincidence summing correction factor estimation for PTE analysis. From the obtained results it is clear that the VGSL performs better than LabSOCS in PTEs analysis, but both VGSL and LabSOCS software can be considered reliable for gamma-ray efficiency calibration for the CTBTO sample analysis.

CHAPTER 5

5. APPLICABILITY OF THE LabSOCS and VGSL SOFTWARE FOR NORM-NUCLIDE ANALYSIS IN ENVIROMENTAL SAMPLES

5.1. Introduction

The study of natural radioactivity in environmental samples is important to determine the natural radioactivity in the environment and foodstuffs, to evaluate the possible effects on humans [62]. Measurements of the background activity are also important to quantify the change as a result of an accidental radioactive release.

In the present study soil (IAEA-375), stream sediment (IAEA-314) and the milk powder (IAEA-152) samples have been prepared from IAEA reference materials. These samples were analyzed using an ultra-low background gamma spectrometry system. The activity concentrations were determined for the gamma-emitting nuclides in the ^{238}U and ^{232}Th decay series as well as ^{40}K and ^{137}Cs. The first three are primordial nuclides present since the origin of the earth and present in the soil and stream sediment samples. The occurrence of the radionuclide ^{137}Cs is caused by nuclear weapons testing and nuclear accidents like Chernobyl (1986) and Fukushima (2011). The ^{137}Cs deposited in soil still exists today due to its relatively long half-life of about 30 years [62].

The three IAEA reference materials were measured and analyzed using the LabSOCS and VGSL software and the results of analyses were compared to the certified nuclide concentrations in the respective materials.

5.2. Geometry definition and chemical composition

The geometry used was discussed in chapter 3. The dimensions of the soil, sediment and milk powder samples are given in Tables 5.1, 5.2 and 5.3 together with their calculated density of 1.43 g/cm^3, 0.85 g/cm^3 and 0.54 g/cm^3, respectively. Figure 5.1 shows the geometry definition as displayed in VGSL using the same dimensions used in LabSOCS. The IAEA standard reference materials were modeled according to the best estimated chemical composition given by the IAEA.

- The soil reference material was composed of K (0.59%), Ca (0.51%), Mg (0.57%), Si (46.37%), Al (24.26%), Fe (15.81%), Ti (1.88%), C (3.23%), H (6.41%) and O (0.37%).
- The stream sediment was composed of K (0.53%), Ca (0.41%), Mg (0.51%), Si (41.16%), Al (21.54%), Fe (14.03%), Ti (1.67%), C (6.45%), H (13.05%) and O (0.65%).
- The milk powder reference material was composed of Ca (0.83%), P (0.53%), Na (0.40%), Fe (0.13%), Zn (0.10%), I (0.01%), C (31.61%), H (63.23%) and O (3.16%).

Table 5.1: LabSOCS geometry definition of a soil sample in mm.

No.	Description	d.1	d.2	Material	Density(g/cm^3)
1	Side walls	0.3	70	PVC	1.4
2	Bottom Wall	0.4		PVC	1.4
3	Sample	15		soil	1.43
4	Absorber 1	0			
5	Absorber 2	0			
6	Source - Detector	0			

Table 5.2: LabSOCS geometry definition of a stream sediment sample in mm.

No.	Description	d.1	d.2	Material	Density(g/cm^3)
1	Side walls	0.3	51	PVC	1.4
2	Bottom Wall	0.4		PVC	1.4
3	Sample	10		sediment	0.85
4	Absorber 1	0			
5	Absorber 2	0			
6	Source - Detector	0			

Table 5.3: LabSOCS geometry definition of milk powder sample in mm.

No.	Description	d.1	d.2	Material	Density(g/cm^3)
1	Side walls	0.3	70	PVC	1.4
2	Bottom Wall	0.4		PVC	1.4
3	Sample	15		m.powder	0.54
4	Absorber 1	0			
5	Absorber 2	0			
6	Source - Detector	0			

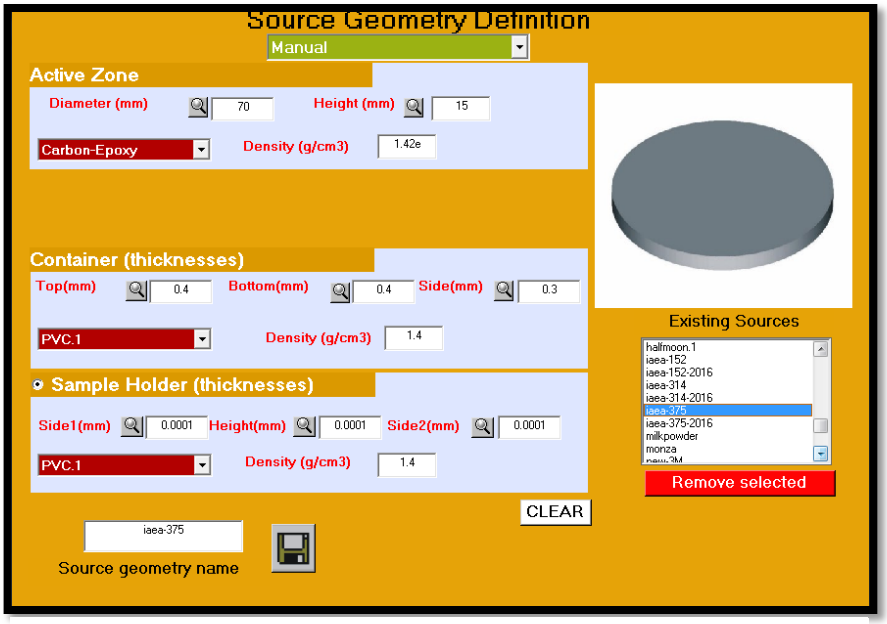

Figure 5.1: The soil sample geometry definition by VGSL.

5.3. Efficiency calibration

The fitted efficiency curves from LabSOCS and VGSL are established using algorithms entrenched in the software. The values are then transferred to Genie 2000 to calculate the activity of the nuclides in the reference samples. Efficiency data points were generated after entering the required parameter values. The values were defined by side walls, bottom wall, sample, absorbers and source to detector distance as shown in Table 5.1, 5.2 and 5.3. For the computation of the efficiency values, the set of energy values ranging from 45 keV up to 2000 keV has been used in the study. The settings used, including the detector choice were taken from chapter 4, listed in chapter 3 and Appendix A.

The LabSOCS efficiency values were generated for milk powder, stream sediment and soil. The low order polynomials are given in Equation 5.2.1, 5.2.2 and 5.2.3, and the high order polynomial are given in Equation 5.2.4, 5.2.5 and 5.2.6 for milk powder, stream sediment and soil, respectively; where ε is the peak efficiency and E is the peak-energy.

$$Ln\,(\varepsilon) = -18.50 + 15.18 \times ln\,(E) - 5.317 \times ln\,(E)^2 + 0.8611 \times ln\,(E)^3 - 0.05427 \times ln\,(E)^4 \quad (5.2.1)$$

$$Ln\,(\varepsilon) = -124.0 + 104.9 \times ln\,(E) - 34.03 \times ln\,(E)^2 + 4.965 \times ln\,(E)^3 - 0.2752 \times ln\,(E)^4 \quad (5.2.2)$$

$$Ln\,(\varepsilon) = -133.4 + 104.7 \times ln\,(E) - 31.62 \times ln\,(E)^2 + 4.304 \times ln\,(E)^3 - 0.2235 \times ln\,(E)^4 \quad (5.2.3)$$

$$Ln\,(\varepsilon) = -100.9 + 68.08 \times ln\,(E) - 17.51 \times ln\,(E)^2 + 2.072 \times ln\,(E)^3 - 0.1088 \times ln\,(E)^4 + 0.001738 \times ln\,(E)^5 \quad (5.2.4)$$

$$ln\,(\varepsilon) = -117.1 + 80.99 \times ln\,(E) - 21.54 \times ln\,(E)^2 + 2.699 \times ln\,(E)^3 - 0.1572 \times ln\,(E)^4 + 0.003228 \times ln\,(E)^5 \quad (5.2.5)$$

$$Ln\,(\varepsilon) = -126.5 + 87.49 \times ln\,(E) - 23.43 \times ln\,(E)^2 + 2.973 \times ln\,(E)^3 - 0.1771 \times ln\,(E)^4 + 0.003807 \times ln\,(E)^5 \quad (5.2.6)$$

The VGSL efficiency values were also generated for milk powder, stream sediment and soil. The polynomial fits for the low energy part of the spectrum are given in Equation 5.2.7, 5.2.8 and 5.2.9, and the high energy polynomials fits are given in Equation 5.2.10, 5.2.11 and 5.2.12 for milk powder, stream sediment and soil, respectively.

$$Ln\,(\varepsilon) = -42.06 + 21.15 * ln\,(E) + 1.650 * ln\,(E)^2 - 2.960 * ln\,(E)^3 + 0.6383 * ln\,(E)^4 - 0.04337 * ln\,(E)^5 \quad (5.2.7)$$

$$Ln\,(\varepsilon) = -595.5 - 26.21 * ln\,(E) + 18.84 * ln\,(E)^2 - 5.037 * ln\,(E)^3 + 0.5823 * ln\,(E)^4 - 0.02418 * ln\,(E)^5 \quad (5.2.8)$$

$$Ln\,(\varepsilon) = -157.0 + 201.9 * ln\,(E) - 111.6 * ln\,(E)^2 + 31.37 * ln\,(E)^3 - 4.388 * ln\,(E)^4 + 0.2418 * ln\,(E)^5 \quad (5.2.9)$$

$$Ln\,(\varepsilon) = -130.7 + 93.93 * ln\,(E) - 26.44 * ln\,(E)^2 + 3.610 * ln\,(E)^3 - 0.2405 * ln\,(E)^4 + 0.006220 * ln\,(E)^5 \quad (5.2.10)$$

$$Ln\,(\varepsilon) = -128.3 + 91.67 * ln\,(E) - 25.59 * ln\,(E)^2 + 3.460 * ln\,(E)^3 - 0.2278 * ln\,(E)^4 + 0.005808 * ln\,(E)^5 \quad (5.2.11)$$

$$Ln\,(\varepsilon) = -114.8 + 78.56 * ln\,(E) - 20.80 * ln\,(E)^2 + 2.610 * ln\,(E)^3 - 0.1540 * ln\,(E)^4 + 0.003287 * ln\,(E)^5 \quad (5.2.12)$$

5.4. Activity results and evaluation

As the stream sediment and soil materials are certified to be in (near) secular equilibrium with all their respective daughters, the activity of ^{238}U can be determined through the daughters ^{214}Pb and ^{214}Bi, although care should be taken with a potential loss of ^{222}Rn upon sample preparation and therefore a 3-week period is allowed between sample preparation and measurement. For ^{232}Th the daughters ^{212}Pb, ^{208}Tl and ^{228}Ac are suitable. Activity calculation for ^{137}Cs and ^{40}K is based on their own specific emission lines.

The IAEA soil material has certified radionuclides activities for ^{232}Th, ^{238}U, ^{40}K, ^{226}Ra and ^{137}Cs at the 95% confidence interval. The activities obtained are shown in Table 5.4 and the activity ratios in Table 5.5 together with the certified values.

The IAEA stream sediment material has certified activity values for ^{232}Th, ^{238}U and ^{226}Ra at the 95% confidence interval. The sediment was analyzed and the activities obtained are shown in Table 5.6 and the activity ratios in Table 5.7.

The IAEA milk powder material has certified activity values for ^{40}K and ^{137}Cs at the 95% confidence interval. The milk powder was analyzed and the activities and ratios obtained are shown at Table 5.8 and Table 5.9, respectively, together with the recommended values.

The ratios of the soil, sediment and milk powder activities compared to the IAEA recommended values are shown in Figure 5.2, Figure 5.3 and Figure 5.4 respectively.

Specific knowledge of NORM measurements have to be applied to reduce the number of candidate nuclides that may interfere with other nuclides during identification (e.g. the ^{235}U-^{226}Ra interference on the 186 keV gamma-peak). Some nuclide activities in the soil and sediment material had to be corrected by applying the appropriate branching ratios. For example, ^{212}Bi undergoes beta decay to ^{212}Po with a 64.06% probability and undergoes alpha decay to ^{208}Tl with a 35.94% probability as shown in Appendix B [63, 65].

Table 5.4: Intercomparison of activities obtained from simulated efficiencies of LabSOCS and VGSL for the IAEA soil reference material.

Nuclide	Energy	Activity(Bq)					
	(keV)	Certified		LabSOCS		VGSL	
		Value	Unc.	Value	Unc.	Value	Unc.
^{235}U	143.76	0.00110	0.00010	MDA	MDA	MDA	MDA
^{235}U	163.33	0.00110	0.00010	MDA	MDA	MDA	MDA
^{235}U	185.71	0.00110	0.00010	0.00110	0.00050	0.0009	0.000
^{226}Ra	186.21	0.02000	0.00100	0.02220	0.00130	0.0200	0.000
^{235}U	205.31	0.00110	0.00010	MDA	MDA	MDA	MDA
^{212}Pb	238.63	0.02050	0.00140	0.01910	0.00160	0.0176	0.000
^{214}Pb	241.98	0.02000	0.00100	0.02670	0.00270	0.0247	0.001
^{214}Pb	295.21	0.02000	0.00100	0.02000	0.00250	0.0182	0.001
^{214}Pb	351.92	0.02000	0.00100	0.02350	0.00220	0.0213	0.001
^{208}Tl	583.19	0.02050	0.00140	0.01860	0.00190	0.0166	0.001
^{214}Bi	609.31	0.02000	0.00100	0.02080	0.00150	0.0186	0.000
^{137}Cs	661.65	5.28000	0.08000	5.02950	0.30220	4.5013	0.112
^{212}Bi	727.17	0.02050	0.00140	0.01790	0.00220	0.0160	0.001
^{228}Ac	911.60	0.02050	0.00140	0.01900	0.00120	0.0169	0.000
^{234m}Pa	1001.00	0.02310	0.00240	0.02290	0.01090	0.0204	0.009
^{214}Bi	1120.29	0.02000	0.00100	0.02470	0.00220	0.0220	0.001
^{40}K	1460.81	0.42400	0.00750	0.39030	0.01690	0.3436	0.007
^{214}Bi	1764.49	0.02000	0.00100	0.02260	0.00160	0.0197	0.001
^{208}Tl	2614.53	0.02050	0.00140	0.02340	0.00150	0.0194	0.001

MDA: Below the Minimum Detectable Activity

Table 5.5: Ratio of the LabSOCS and VGSL activities with their respective uncertainties for the soil reference material.

Nuclide	Energy	Ratio					
	(keV)	Certified		LabSOCS		VGSL	
		Value	Unc.	Value	Unc.	Value	Unc.
^{235}U	143.76	1.00	0.15	-	-	-	-
^{235}U	163.33	1.00	0.15	-	-	-	-
^{235}U	185.71	1.00	0.15	1.02	0.50	0.91	0.10
^{226}Ra	186.21	1.00	0.07	1.11	0.09	1.00	0.07
^{235}U	205.31	1.00	0.15	-	-	-	-
^{212}Pb	238.63	1.00	0.09	0.93	0.10	0.86	0.06
^{214}Pb	241.98	1.00	0.07	1.34	0.15	1.23	0.11
^{214}Pb	295.21	1.00	0.07	1.00	0.13	0.91	0.10
^{214}Pb	351.92	1.00	0.07	1.18	0.12	1.07	0.09
^{208}Tl	583.19	1.00	0.09	0.91	0.11	0.81	0.09
^{214}Bi	609.31	1.00	0.07	1.04	0.09	0.93	0.07
^{137}Cs	661.65	1.00	0.02	0.95	0.06	0.85	0.02
^{212}Bi	727.17	1.00	0.09	0.87	0.12	0.78	0.10
^{228}Ac	911.6	1.00	0.09	0.93	0.08	0.83	0.07
^{234m}Pa	1001.00	1.00	0.15	0.99	0.48	0.88	0.43
^{214}Bi	1120.29	1.00	0.07	1.23	0.12	1.10	0.10
^{40}K	1460.81	1.00	0.03	0.92	0.04	0.81	0.02
^{214}Bi	1764.49	1.00	0.07	1.13	0.10	0.98	0.08
^{208}Tl	2614.53	1.00	0.09	1.14	0.10	0.95	0.09
	Average	**1.00**		**1.04**		**0.93**	
Standard Deviation		**0.00**		**0.13**		**0.12**	

Table 5.6: Intercomparison of activities obtained from simulated efficiencies of LabSOCS and VGSL for the IAEA stream sediment reference material.

Nuclide	Energy	Activity(Bq)					
	(keV)	Certified		LabSOCS		VGSL	
		Value	Unc.	Value	Unc.	Value	Unc.
^{235}U	143.76	0.033	0.002	0.051	0.006	0.047	0.004
^{235}U	163.33	0.033	0.002	0.036	0.009	0.034	0.008
^{235}U	185.71	0.033	0.002	0.034	0.008	0.033	0.003
^{226}Ra	186.21	0.732	0.055	0.742	0.038	0.661	0.016
^{235}U	205.31	0.033	0.002	0.029	0.004	0.027	0.003
^{212}Pb	238.63	0.072	0.004	0.072	0.006	0.065	0.002
^{214}Pb	241.98	0.732	0.055	0.779	0.065	0.711	0.026
^{214}Pb	295.21	0.732	0.055	0.740	0.060	0.669	0.024
^{214}Pb	351.92	0.732	0.055	0.744	0.060	0.668	0.026
^{208}Tl	583.19	0.072	0.004	0.068	0.008	0.060	0.006
^{214}Bi	609.31	0.732	0.055	0.739	0.046	0.655	0.020
^{212}Bi	727.17	0.072	0.004	0.076	0.021	0.067	0.018
^{228}Ac	911.6	0.072	0.004	0.069	0.005	0.061	0.004
^{234m}Pa	1001.03	0.706	0.048	0.577	0.115	0.509	0.100
^{214}Bi	1120.29	0.732	0.055	0.775	0.036	0.684	0.020
^{214}Bi	1764.49	0.732	0.055	0.768	0.035	0.664	0.017
^{208}Tl	2614.53	0.072	0.004	0.071	0.005	0.058	0.004

Table 5.7: Ratio of the LabSOCS and VGSL activities with their respective uncertainties for the stream sediment reference material.

Nuclide	Energy	Ratio					
	(keV)	Certified		LabSOCS		VGSL	
		Value	Unc.	Value	Unc.	Value	Unc.
^{235}U	143.76	1.00	0.08	1.55	0.21	1.45	0.14
^{235}U	163.33	1.00	0.08	1.11	0.29	1.03	0.25
^{235}U	185.71	1.00	0.08	1.03	0.25	1.00	0.11
^{226}Ra	186.21	1.00	0.11	1.01	0.09	0.90	0.07
^{235}U	205.31	1.00	0.08	0.90	0.14	0.82	0.11
^{212}Pb	238.63	1.00	0.08	0.99	0.10	0.90	0.06
^{214}Pb	241.98	1.00	0.11	1.06	0.12	0.97	0.08
^{214}Pb	295.21	1.00	0.11	1.01	0.11	0.91	0.08
^{214}Pb	351.92	1.00	0.11	1.02	0.11	0.91	0.08
^{208}Tl	583.19	1.00	0.08	0.94	0.12	0.83	0.10
^{214}Bi	609.31	1.00	0.11	1.01	0.10	0.89	0.07
^{212}Bi	727.17	1.00	0.08	1.05	0.29	0.92	0.25
^{228}Ac	911.6	1.00	0.08	0.95	0.09	0.84	0.07
^{234m}Pa	1001.03	1.00	0.1	0.82	0.17	0.72	0.15
^{214}Bi	1120.29	1.00	0.11	1.06	0.09	0.93	0.07
^{214}Bi	1764.49	1.00	0.11	1.05	0.09	0.91	0.07
^{208}Tl	2614.53	1.00	0.08	0.99	0.09	0.80	0.07
	Average	**1.00**		**1.03**		**0.93**	
Standard Deviation		**0.00**		**0.15**		**0.15**	

Table 5.8: Intercomparison of activities obtained from simulated efficiencies of LabSOCS and VGSL for the IAEA milk powder reference material.

Nuclide	Energy	Activity (Bq)					
	(keV)	Certified		LabSOCS		VGSL	
		Value	Unc.	Value	Unc.	Value	Unc.
^{137}Cs	661.65	2.129	0.078	2.060	0.126	1.789	0.048
^{40}K	1460.81	0.539	0.032	0.501	0.039	0.431	0.029

Table 5.9: Ratio of the LabSOCS and VGSL activities with their respective uncertainties for the milk powder reference material.

Nuclide	Energy	Ratio					
	(keV)	Certified		LabSOCS		VGSL	
		Value	Unc.	Value	Unc.	Value	Unc.
^{137}Cs	661.65	1	0.03	0.97	0.07	0.84	0.07
^{40}K	1460.81	1	0.16	0.93	0.09	0.80	0.09
Average		1		**0.95**		**0.82**	
Standard Deviation		0		**0.03**		**0.03**	

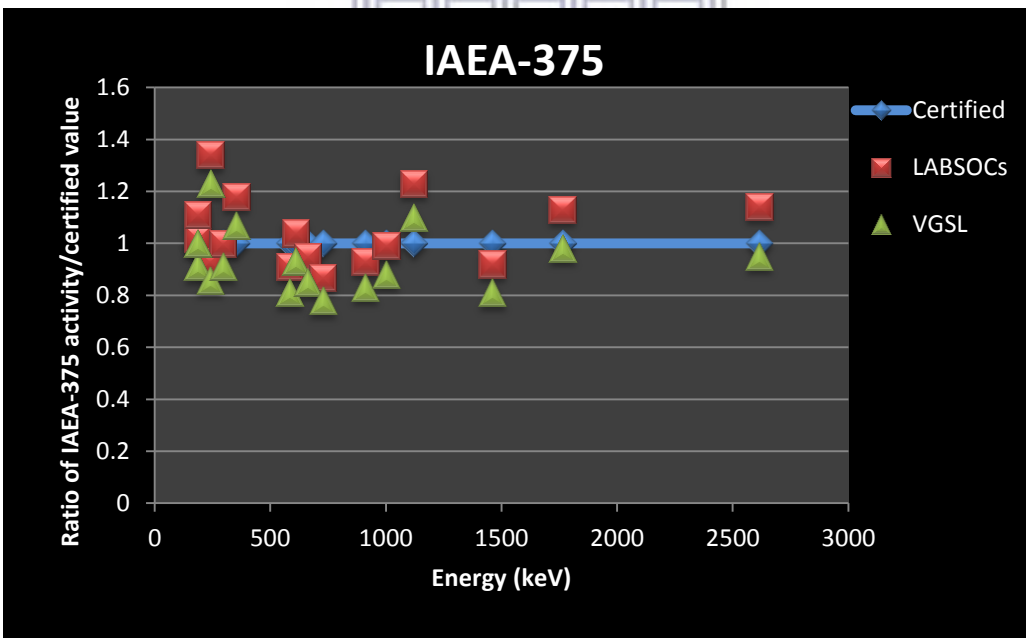

Figure 5.2: Ratio of the LabSOCS and VGSL activities to the reference activities in the IAEA-375 soil reference material.

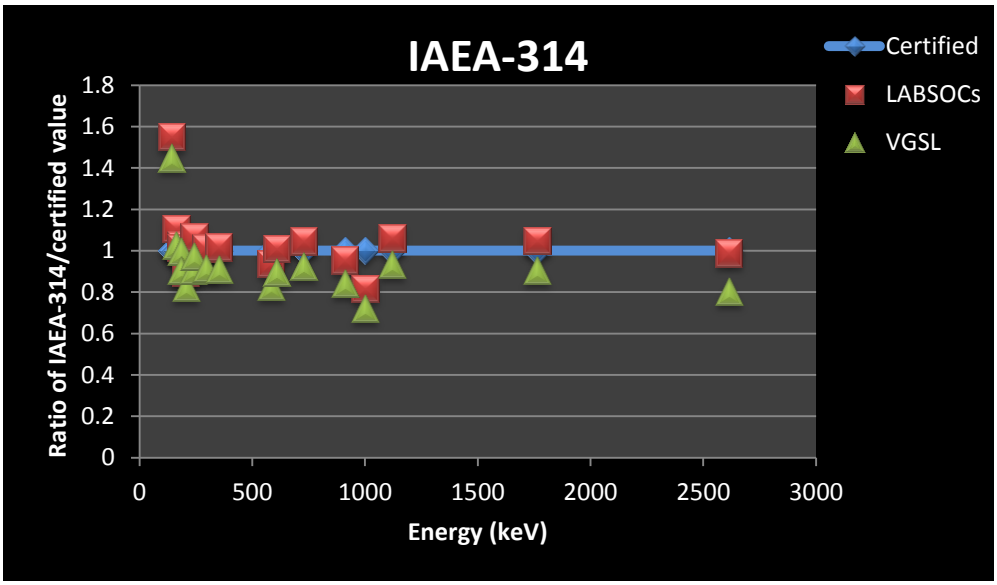

Figure 5.3: Ratio of the LabSOCS and VGSL activities to the reference activities in the IAEA-314 stream sediment reference material.

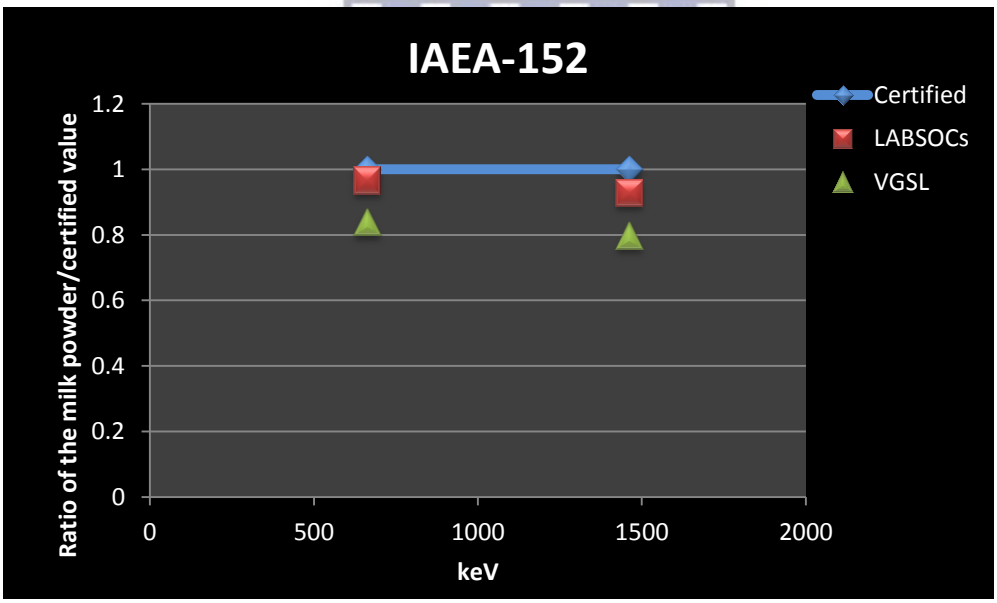

Figure 5.4: Ratio of the LabSOCS and VGSL activities to the reference activities in the IAEA-152 milk powder reference material.

5.4.1. Evaluation of the soil data

The average activity ratio of 1.04 ± 0.13 for LabSOCS and 0.93 ± 0.12 for VGSL indicate that there is a good correlation between the two modeled efficiencies and both can be used in the analysis of NORM nuclides.

5.4.2. Evaluation of the sediment data

The average activity ratio of 1.03 ± 0.15 for LabSOCS and 0.93 ± 0.15 for VGSL indicate that there is a good correlation between the LabSOCS modeled efficiency and the VGSL modeled efficiency. The modeled efficiencies are underestimated especially in the lower energy region.

5.4.3. Evaluation of the milk data

The average activity ratio of 0.95 ± 0.03 for LabSOCS and 0.82 ± 0.03 for VGSL indicate that the VGSL modeled efficiency is overestimated, which may be due to the major element composition of the milk matrix.

CHAPTER 6

6. CONCLUSION

6.1. Summary

Gamma-ray spectrometry requires certified radionuclide reference standards to establish an experimental efficiency calibration for a wide variety of sample geometries and materials. In general these standards are expensive and one has to prepare the calibration sources oneself, which requires a stringent quality control system and highly skilled personnel. Efficiency calibration software is now commercially available to overcome these disadvantages. In this study, the commercially available Canberra software (Genie 2000 in combination with LABSOCs) was compared to specifically developed software, VGSL. The empirically generated efficiency calibration to identify the nuclides present in reference sources available from a number of PTEs provided by the CTBTO during the last decade were used to test the two packages. Subsequently, heir applicability and accuracy in the analysis of environmental samples for NORM- nuclides were evaluated.

The first experiments compared the efficiency calibrations obtained from simulations using LABSOCs, VGSL, and empirical calibrations from measurement of the PTE certified radionuclides sources using a well characterized BEGe detector.

Several parameter settings were varied to find the optimal values. The polynomial orders for the fit to the efficiency curve were investigated as well as the significance threshold parameter. From the observed results, the empirical efficiency calibration curve of the fifth and fourth order polynomial with the threshold of 3.00 yielded accurate results, which were in agreement with the certified values and were used as standard parameters to perform efficiency calibration for the three geometries, MANUAL3M, HALFMOON and ARAME\CINDERELLA.

The average activity ratio for the MANUAL3M sample geometry of LABSOCs to the certified activity values was 1.11 ± 0.04 and for VGSL was 1.04 ± 0.04. The average activity ratio for the HALFMOON sample geometry to the certified activity values was 1.13 ± 0.10 and for VGSL was 1.03 ± 0.09. For the ARAME geometry the LABSOCs ratio to the

certified activity values was 1.06 ± 0.10 and for VGSL was 0.95 ± 0.10. The results indicate that VGSL and LabSOCS software can be considered reliable for gamma-ray efficiency calibration for CTBTO sample analysis.

In the second part of the thesis, IAEA standards for NORM-nuclides were analyzed with optimized parameters and settings (including coincidence summing and the significance threshold parameter) which were found for the analysis of the CTBTO PTEs samples for the software packages. The IAEA-314 stream sediment sample was collected from the Kalan area of the west Kalimantan, Borneo, Indonesia. The IAEA-375 material (top soil to a depth of 20 cm) was obtained from the Staryi Viskov collective farm in Novozybkov, Brjansk, Russia and the IAEA-152 material was produced from cow's milk obtained from animals that had grazed on land contaminated with radioactive fallout resulting from the Chernobyl incident.

The average activity ratio for the soil sample of LABSOCs to the certified activity values was 1.04 ± 0.13 and for VGSL was 0.93 ± 0.12. The average activity ratio for the stream sediment sample to the certified activity values was 1.03 ± 0.15 and for VGSL was 0.93 ± 0.15. For the milk powder ~ Cs-137, the LABSOCs ratio to the certified activity values is 0.95 ± 0.03 and for VGSL was 0.82 ± 0.03.

From the PTE reference samples and IAEA standard for NORM-nuclides analysis, LabSOCS generally performs better than VGSL in NORM analysis. This is in contrast to the PTE analysis. This might be due to the fact that VGSL was developed specifically for PTE sample analysis hence the geometries entrenched within the software are CTBTO related.

The use of VGSL requires the knowledge of specific detector parameters, but has the advantage of being extendable to different detectors. Conversely, LABSOCs efficiency calculation requires only information about the positioning, dimensions and nature of the source, but its use is limited to a previously "characterized'' detector.

LabSOCS software in general can be considered reliable for gamma-ray efficiency calibration for NORM analysis, while VGSL is a reasonable alternative where uncertainties up to 10% are acceptable. For more accurate results an empirical efficiency calibration is the

preferred option, although not for routine analysis of environmental samples as this option is not cost effective.

6.2. Outlook

Further improvements on the results obtained may be expected with the development of the parameter settings.

Future work should focus on the influence of:

- the elemental composition on the LabSOCS and VGSL efficiency calibration,
- the possible inhomogeneity of the sample due to sample preparation,
- further passive and active background shielding of the BEGe-detector on the quality of the gamma-spectra, and
- interactive peak fitting on the peak content, especially where large discrepancies in the activity were observed.

Appendix A The detector characterization parameters

```
# Genie 2000 V3.2 Generic Detector Characterizations V1.0


# PO 76240 BIO-TEKNIK BE5030 S/N 4832
4832,78.08,31.50,82.55,101.60,133.40,10.5,10.5,26,4832.par,4, #
Ge,0.001,5.35, #
C,0.5,2.7, #
AL,1.6,2.7, #
Ge,0.34,5.35, #
CU,1.279,8.96,#
AL,1.6,2.7, #
Ge,0.617,5.35,#
CU,2.907,8.96, #
AL,5,2.7
```

These detector parameters include detector dimensions, (scintillator, dead layer etc. as well as the density for each material.

Appendix B Decay schemes of ^{212}Pb, ^{212}Bi and ^{214}Pb [64]

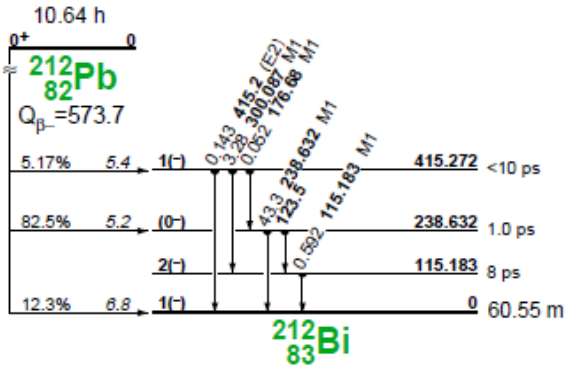

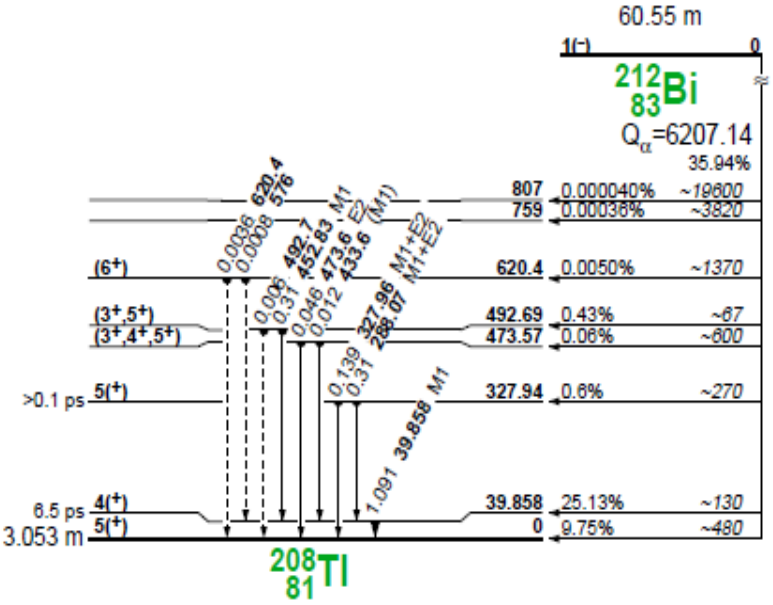

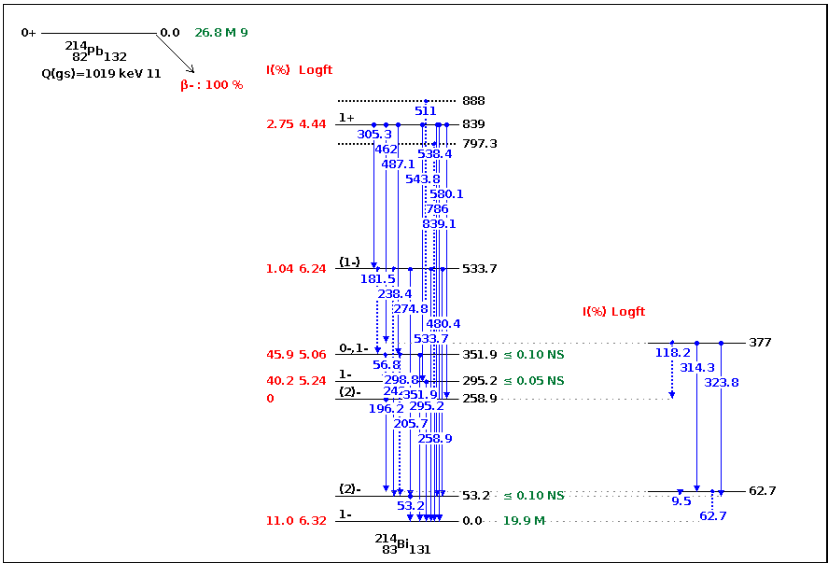

Appendix C Decay schemes of ^{60}Co, ^{139}Ce and ^{88}Y [64]

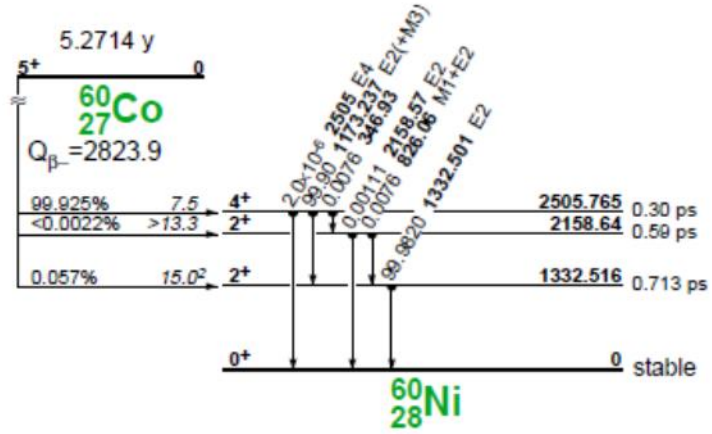

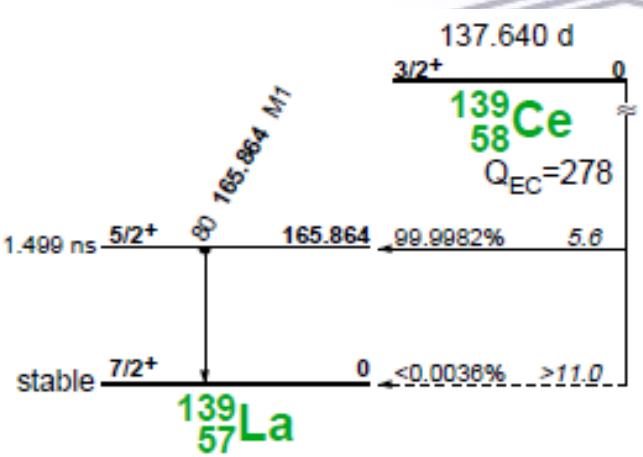

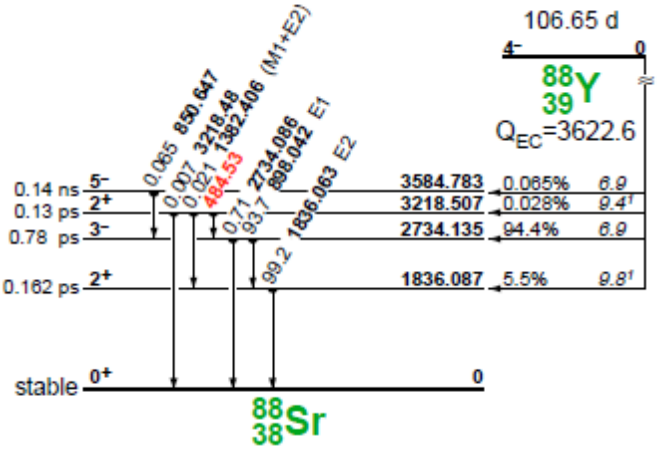

Appendix D Genie 2000 Peak Area and continuum calculation

Note that the material in this appendix is mostly taken directly from the Canberra Manual [9] and is included for completeness.

Peak locate

The Genie 2000 architecture provides five algorithms for locating peaks of interest in a spectrum. The chosen algorithm for this MSc study is the 'Second Difference Method', which is a slightly modified version of their previous SAMPO80 software version.

The peak centroid is defined as:

$$centroid = \frac{\sum_i i.ss_i}{\sum_i ss_i} \quad (1)$$

where i is the channel number, and

$$ss_i = \frac{dd_i}{sd_i} \quad (2)$$

The terms on the right side of equation (2.10) are defined as the generalized second difference

$$dd_i = \sum_{j=-k}^{j=+k} c_j^2 (y_{i+j}) \quad (3)$$

and its standard deviation

$$sd_i = \sqrt{\sum_{j=-k}^{j=+k} c_j^2 (y_{i+j})} \quad (4)$$

The counts per channel are denoted by y and the summation is done over 2k+1 channels where the number k depends on the coefficients c defined as:

$$c_j = \frac{100(j^2-(cw)^2)}{(cw)^2} . e - \frac{j^2}{2(cw)^2} \quad (5)$$

where cw is the calibrated expected Gaussian width (cw = FWHM/2.355 in units of channels).

The first coefficient c_0 is always -100, and the set of coefficients is terminated at k, where the absolute value of the next coefficient would

be less than one. The second coefficient is then adjusted so that the sum of the coefficients is zero.

The expected peak-width value is automatically determined by the program based on the shape calibration data for the spectrum to be analyzed. Furthermore, the coefficients are recalculated every 100 channels to make sure that the peak locate algorithm is appropriate for the types of peaks expected. The peak locate algorithm also contains a test for the peak shape. Regions where the sign of the second difference remains unchanged for too long are classified as Compton edges or other continuum features, which are rejected as real peaks.

Peak Area

Genie 2000 provides two different algorithms for calculating peak areas in a spectrum, i.e. the Library (Gamma-M) and the Sum/Non-Linear LSQ fit. The Library (Gamma-M) is used where only specific nuclides are of interest, and for NaI-crystal analysis. The Sum/ Non-Linear LSQ fit is best suited for Ge-crystal analysis, but can also be used for NaI-crystal analysis. The Sum/Non-Linear Least Square fit peak area algorithm calculates peak areas of multiplets and singlets [9].

The Sum/Non-Linear Least Square fit peak Area algorithm

Peak areas for multiplets and fitted singlets are calculated using the non-linear square method in Genie 2000. Assuming that a peak region has a set of data points (x_i, y_i), a mathematical model through these data points has to be fitted, where x_i is the channel number and y_i are the number of counts at channel x_i. It is assumed that there exists a function F as shown in the following equation:

$$F = (x_i, \alpha_1, \alpha_2, \ldots, \alpha_m) = y_i \qquad (6)$$

where the α is a free parameter of the model to be determined from the best fit through the data points. To determine these free parameters the method of least squares is used, which requires that the quantity χ^2 be a minimum

$$\chi^2 = \sum_i w_i . [y_i - F(x_i, \alpha)]^2 \qquad (7)$$

where w_i is the weight associated with the i^{th} data point.

In this formalism, if the uncertainties of the data points are not equal, each point should be weighted by $1/\sigma_i^2$, where σ_i is the standard deviation of the i^{th} data point.

For Poisson distribution data, $\sigma_i^2 = y_i$, and

$$w_i = \frac{1}{y_i} \tag{8}$$

where y_i are the counts in channel i.

In gamma spectrometry, the continuum is subtracted from the data points before the fit, $\sigma_i^2 \neq y_i$.

In the case of a linear continuum subtraction, the modified channel content is given by

$$y_i' = y_i - \frac{1}{n}.B_1 - \frac{i.(B_2 - B_1)}{n.(N+1)} \tag{9}$$

and the weighting factor by

$$w_i' = \frac{1}{y_i + \frac{B_1.(N+1-i)^2 + B_2 i^2}{[n(N+1)]^2}} \tag{10}$$

where

N is the number of channels in the peak region of interest (ROI),

n is the number of continuum channels on each side of the peak (currently always the same number on both sides of the peak),

B_1 is the sum of counts in the continuum region to the left of the peak (Figure 1), and

B_2 is the sum of counts in the continuum region to the right of the peak (Figure 1).

In the case of a step-continuum subtraction, the modified channel contents is written as

$$y_i' = y_i - \frac{1}{n}.B_1 - \frac{(B_2-B_1)}{nG}\sum_{j=1}^{i} y_j \quad (11)$$

and the weighting factor is modified to become

$$w_i' = \frac{1}{y_i + \frac{B_1.(G-P_i)^2 + B_2.P_i^2 + (B_2-B_1)^2.P_i}{(nG)^2}} \quad (12)$$

where,

G is the total sum of gross count in the peak ROI,

N is the number of channels in the peak ROI,

n is the number of continuum channels on each side,

B_I is the sum of counts in the continuum region to the left of the peak (Figure 2), and

B_2 is the sum of counts in the continuum region to the right of the peak (Figure 2).

For peaks having very poor statistics, equations (10) and (12), tend to overweight channels having lower counts. Phillips [42] showed that the use of straight statistical weighting causes an underestimation of the areas of such peaks. A better approach is to use a weighting factor that is based on an average of the number of counts in several adjacent channels. Therefore, y_i in equations (10) and (11) is replaced with

$$y_i = \frac{y_{i-1}+2y_i+y_{i+1}}{4} \quad (13)$$

whenever $y_i < 100$.

The quantity χ^2 defined in Equation (2.15) is minimized when

$$\frac{\partial \chi^2}{\partial \alpha_j} = 0 \quad (14)$$

for all α_j.

This minimization requirement yields a set of simultaneous equations that may be solved for the α, provided that the function $F(x_i, \alpha)$ is linear with respect to the α. If the function is not linear with respect to α, as is the case with both of the Gaussian models for a photopeak shape

(with or without the tail parameter), it may be linearized by expanding it in a Taylor's series ∞

$$F(X,\alpha) = F_0 + \sum_{j=i}^{m} \frac{\partial F_0}{\partial \alpha_j}\delta\alpha_j + \frac{1}{2}\sum_j \sum_k \left[\frac{\partial^2 F_0}{\partial \alpha_j \partial \alpha_k}\delta\alpha_j \delta\alpha_k\right] + \cdots \quad (15)$$

Substituting the Taylor's series expansion in Equation (15) into Equation (7) and keeping only the first order terms, the equation for χ^2 becomes

$$\chi^2 = \sum_i w_i \left[y_i - F_0 - \sum_j \frac{\partial F_0}{\partial \alpha_j}\delta\alpha_j\right]^2 \quad (16)$$

This is now linear in terms of $\delta\alpha_j$ and may be minimized with respect to them as

$$\frac{\partial \chi^2}{\partial(\delta\alpha_k)} = -2\sum_i w_i \frac{\partial F_0}{\partial \alpha_j}\left[y_i - F_0 - \sum_j \frac{\partial F_0}{\partial \alpha_j}\delta\alpha_j\right] = 0 \quad (17)$$

In matrix notation, a system of linear equations is represented by

$$\bar{b} = M.(\overline{\delta\alpha}) \quad (18)$$

where

$$M_{ij} = \sum_i . w_i . \frac{\partial F_0}{\partial \alpha_j} . \frac{\partial F_0}{\partial \alpha_k} \quad (19)$$

and

$$b_k = \sum_i . w_i . (y_i - F_0) . \frac{\partial F_0}{\partial \alpha_K} \quad (20)$$

This gives rise to an iterative procedure, generally referred to as the method of non-linear least squares. There are many different ways of iterating towards the final solution. One way used in the study is the method developed by Marquardt D.W. [43]. The Marquardt algorithm improves the convergence process and reduces the divergence with the help of damping process. The algorithm proceeds by testing the convergences. The iteration is assumed to have converged if:

- change in the peak position is less than 0.01 channels,
- change in the peak width parameter, W, is less than 0.005W,

- change in the height parameter is less than two counts, or less than one-half of the standard deviation in the peak height, whichever is greater, and
- change in the tailing parameter is less than 0.5W.

If the four conditions are not met, the iteration is terminated.

Peak Area for Multiplets and Fitted Singlets

During the peak area calculations, the number of peaks can be larger than one, and the FWHM and tailing parameter values are either fixed or variable depending on the selected options.

Matrix equation in the case of peak fitting may not always be solvable. A test is included in the algorithm to make sure that the matrix from the fit is not singular. A technique that assumes that the matrix is symmetric has been chosen, since least-squares method always results in a symmetric matrix. The QL method and algorithm is used to obtain a diagonal matrix and the QL algorithm is defined by,

$$A_T^{(i+1)} = Q^{(i)T} A_T^{(i)} Q^{(i)}, \; for\, i = 1 \ldots . n \tag{21}$$

where $A_{T\,(i)}$ is the tridiagonal matrix and iteration i and $Q^{(i)}$ is the orthogonal matrix at iteration i.

The orthogonal matrix, $Q^{(i)}$ and tridiagonal matrix, $A_T(i)$, for iteration $i = 1$ are obtained by the householder method. The iteration is continued until iteration n where a diagonal matrix is obtained at which time the eigenvalues of A are along the diagonal of $A_T(n)$. If the iteration counter reaches $n = 30$ without producing a diagonal matrix, the L_∞ method to determine the properties of the fit are used instead when eigenvalues can be calculated; they are used to calculate the following condition number [44].

$$k(A) = \frac{\max_{1 \le i \le n} |\lambda_i|}{\min_{1 \le i \le n} |\lambda_i|} \tag{22}$$

if $log_{10}(k(A)) > 16.0$

The matrix may be badly scaled, or nearly singular. The algorithm then deletes the smallest peak from a multiplet (in terms of peak height) and re-computes the fit until the matrix is no longer singular. If the last or only peak in the ROI still produces a singular matrix, it is deleted from the peak records and the calculations moves to the next region.

If the eigenvalues of the matrix cannot be computed, the algorithm calculated the L_∞ norm for both A and A^{-1}. The L_∞ norm [45] of A is defined as

$$\|A_\infty\| = max_{\substack{\sum_{j=1}^{n}|a_{ij}| \\ 1\le i\le n}} \tag{23}$$

and the L_∞ Norm of A^{-1} as

$$\|A^{-1}\|_\infty = max_{\substack{\sum_{j=1}^{n}|b_{ij}| \\ 1\le i\le n}} \tag{24}$$

where b_{ij} are the individual values of matrix A^{-1}.

In this case, the condition number is defined as

$$k(A) = \|A\|_\infty \|A^{-1}\|_\infty \tag{25}$$

Again if $\log_{10}\big(k(A)\big) > 16.0$

If the last or only peak in the ROI still produces a singular matrix, it is deleted from the peak records and the calculation moves to the next region. In the Sum/Non –Linear LSQ Fit algorithm, peaks that are already within the energy tolerance after the peak locate, and peaks that would be moved inside the energy tolerance by the interactive multiplet fit are deleted from the results. For the best results, the multiplet is refit with the remaining peaks, or treated as singlets if only one peak remains.

After the multiplets (or singlets) envelope has been fitted with the best fit, the areas of the individual peaks within the multiplets (or the singular peak) are determined by numerical integration over the ROI using the fit function and the fit parameters for the individual peak in the fitted multiplet. In each case, the peak area may be expressed by

$$P_a = A_g + A_\tau \tag{26}$$

where A_g is the area under the Gaussian portion, which is defined by

$$A_g = \int_{cp-\tau}^{Re} He^{\frac{-(x-C_p)^2}{2\sigma^2}} dx \tag{27}$$

and A_t is the area under the tail portion, which is defined by equation

$$A_\tau = \int_{R_s}^{C_p-\tau} He^{\frac{2x-2C_p+\tau}{2\sigma^2}} dx \tag{28}$$

The area under the tail portion can be calculated by solving the integral of equation (31) in closed form. The area under the Gaussian portion A_G is calculated using the Gauss-Quadratic integration method.

After the multiplet or singlet envelope has been fitted with the best fit, the algorithm checks to see if the fitted peak area (or the sum of the fitted peak area is a multiplet) is very different from the simple sum area of the peak (or peaks) if the fitted peak area is more than 150% or less than 50% of the sum area, the area of the singlet is automatically calculated as a simple sum. In the case of a multiplet, the areas of the individual peaks within the multiplet are determined by apportioning the total multiplet area based on the peak height and width of each component. In the case of a two-component multiplet, for example, the areas A_1 and A_2 of the two components are given by

$$A_1 = \frac{P_1\sigma_1 A_t}{P_1\sigma_1 + P_2 P_2} \tag{29}$$

$$A_2 = A_t - A_1 \tag{30}$$

where

A_t is the total multiplet area,
P_1 is the height of peak one,
σ_1 is the Gaussian width of peak one,
P_2 is the height of peak two, and
σ_2 the Gaussian width of peak two.

In general, the area of the i^{th} component of multiplet is given by

$$A_i = \frac{P_i\sigma_i A_t}{\sum_K^N P_K\sigma_K} \tag{31}$$

where N is the number of peaks in the multiplet.

Continuum function

The continuum of a spectrum can be established by selecting either a linear function or a step function. The linear function is tolerable when the spectrum's continuum is relatively flat; it is a simple straight forward equation that estimates the continuum under the peaks as a trapezoid. The step function is chosen if there are any regions in the spectrum where the continuum is significantly higher on the left side of a peak region than on the right side; this function automatically reduces to a flat line if the continuum is flat. The "none" function is normally used only with Alpha spectra.

The linear continuum, B, shown in Figure 1 is calculated from the sample spectrum using

$$B = \left(\frac{N}{2n}\right)(B_1 + B_2) \tag{32}$$

where,

N is the number of channels in the peak ROI,

n is the number of continuum channels on each side,

B_1 is the sum of counts in the continuum region to the left of the peak, and

B_2 is the sum of counts in the continuum region to the right of the peak.

A step continuum, B, shown in Figure 2 is calculated from the sample spectrum using

$$B = \sum_{I=1}^{N}\left(\frac{B_1}{n}\right) + \frac{(B_2 - B_1)}{nG}\sum_{j=1}^{i} y_j \tag{33}$$

where,

y_j is the counts per channel in channel j,

G is the total sum of counts (gross) in the peak ROI,

N is the number of channels in the peak ROI,

n is the number of continuum channels on each side,

B_1 is the sum of counts in the continuum region to the left of the peak, and

B_2 is the sum of counts in the continuum region to the right of the peak.

Having two peaks that are close together, reducing the number of continuum channels may give better results. Increasing the number of continuum channels reduces the number of peaks thus close lying peaks will be considered as a multiplet instead of as a singlet.

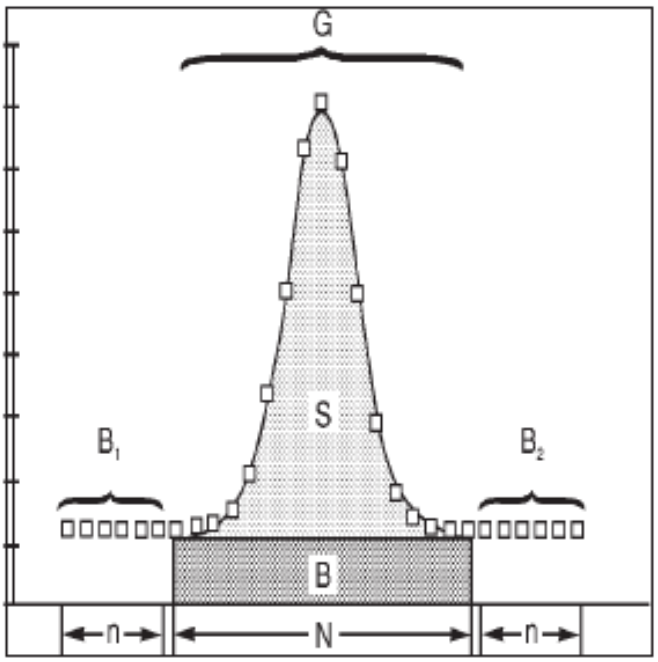

Figure 1: Linear Continuum Calculation Parameters [9]

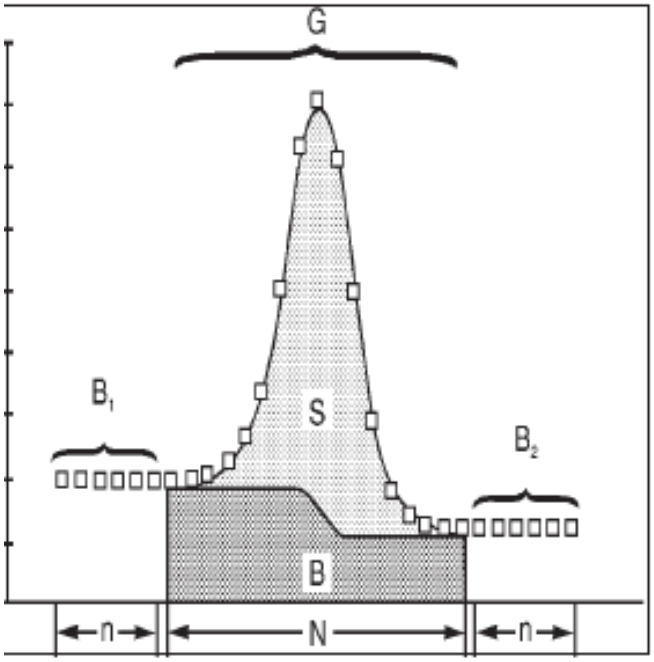

Figure 2: Step Continuum Calculation Parameters [9]

References

[1] Dias, M.S., Takeda, M.N. and Koskinas, M.F., (2002). *Cascade summing corrections for HPGe spectrometers by the Monte Carlo method.* Appl. Radiat. Isot., 56(1-2), 105-109.

[2] Plenteda, R., (2002). *A Monte Carlo Based Virtual Gamma Spectroscopy Laboratory. Ph.D. Thesis*. Universitaetsbibliothek der Technischen Universitat Wien, Resselgasse 4, A-1040, Vienna, Austria. Wien, Technische Universitat Wien 118 pp.

[3] http://www.ctbto.org/specials/who-we-are/ (17 September 2013).

[4] http://hlabsoft.com/web/hl2009/productinfo.php (27 March 2012)

[5] IAEA, (1998). *Intercomparison of gamma-ray analysis software packages*. IAEA-TECDOC-1011, International Atomic Energy Authority, Vienna, Austria.

[6] Aarnio, P.A., Nikkinen, M.T. and Routti , J.T., (2001). *UNISAMPO, comprehensive software for gamma-spectrum processing*. J. Radioanal. Nucl. Chem., 248(2), 371-375.

[7] De Lucia, S.R., Maihara, V.A., and De Menezes, M.O., (2009). *Development of gamma ray spectrometry software for neutron activation analysis using the open source concept*. Proceedings of the International Nuclear Atlantic Conference held on 27 September to 2nd October, Brazil.

[8] Zahn, G.S., Genezini, F.A. and Moralles, M., (2009). *Evaluation of peak-fitting software for gamma spectrum analysis*. Proceedings of the International Nuclear Atlantic Conference held on 27 September to 2nd October, Brazil.

[9] Canberra Industries Inc., (2006). *Genie 2000 3.1 Operations Manual*, Meriden, CT.

[10] Abbas, K., Simonelli, F., D'Alberti, F., Forte, M. and Stroosnijder, M.F., (2002). *Reliability of two calculation codes for efficiency calibration of HPGe detectors*. Appl. Radiat. Isot., 56, 703-709.

[11] VGSL, (2004). User Manual, Version 3.66, 12 August 2004.

[12] http://www.nucleide.org/ICRM_GSWG/Presentation/Presentation_VGSL.pdf (28 January 2014).

[13] Canberra Industries Inc., (1999). *LabSOCS calibration software Manual*, Meriden, CT.

[14] http://www.canberra.com/products/radiochemistry_lab/pdf/LabSOCS-ss-C40167.pdf (28 November2013).

[15] http://www.canberra.com/literature/isocs/application_notes/ISOCS-LabSOCS-App-Note-C39530.pdf (28 November 2013).

[16] Lepy, M. C. et al., (2010). *Intercomparison of methods for coincidence summing corrections in gamma-ray spectrometry*. Appl. Radiat. Isot., 68,1407-1412.

[17] Nelson, G. and Reilly, D., (1991*). Gamma-Ray Interactions with matter, in Passive Non-destructive Analysis of Nuclear Materials*, Los Alamos National Laboratory, NUREG/CR-5550, LA-UR-90-732, pp.27.

[18] Gilmore, G. and Hemingway, J., (1995). *Practical Gamma-ray spectrometry*, John Wiley & Sons Ltd, Chichester, England, pp.24-27.

[19] http://www.physics.hku.hk/~phys0607/lectures/chap06.html (1st April 2014).

[20] Smith, B., (1998). *Radiometric Techniques Part 3: Gamma-Spectrometry, Measurement of Radioactivity*, RA-TRM-112, Pretoria, South Africa.

[21] http://ffden-2.phys.uaf.edu/211_fall2010.web.dir/John_Netardus/Physics.htm (2nd April 2014).

[22] http://www.hardhack.org.au/book/export/html/14 (2nd April 2014)

[23] Montgomery, D.M. and Montgomery, G.A., (1995). *A method for assessing and correcting coincidence summing effects for germanium detector efficiency calibrations*. J. Radioanal. Nucl. Chem., 193(1), 71-79.

[24] Semkow, T. M. et al., (1990). *Coincidence summing in gamma-ray spectroscopy*. Nucl. Instr. Meth. Phys. Res., A, 290, 437-444.

[25] Coote, G.E. and McCallum, G.J., (1975). *Influence of source-detector distance on relative intensity and angular correlation measurements with Ge (Li) spectrometers.* Nucl. Instr. Meth. Phys. Res., A, 130, 189-197.

[26] Debertin, K. and Schotzig, U., (1979). *Coincidence summing correction in Ge (Li)-spectrometry at low source-to-detector distances*. Nucl. Instr. Meth. Phys. Res., A, 158, 471-477.

[27] Andreev, D.S., Erokhina, K.I., Zvonov, V.S. and Lemberg, I.Kh., (1972). *Consideration of cascade transition in determining the absolute yield of gamma rays*, Instr. Expt. Techn., 25, 1358.

[28] Andreev, D.S., Erokhina, K.I., Zvonov, V.S. and Lemberg, I.Kh., (1973). *Determination of the γ-detection efficiency in energy peaks by means of nuclides having a complicated decay scheme in close-geometry conditions*, Izv. Akad. Nauk. SSR, Ser. Fiz., 37(8), 1609-1612.

[29]Morel, J., Chauvenet, B. and Kadachi, A., (1983). *Coincidence-summing correction in gamma-ray spectrometry for normalized geometries*. Appl. Radiat. Isot., 34, 1115-1122.

[30] Korun, M. and Martini, R., (1993). *Coincidence summing in gamma and X-ray spectrometry*. Nucl. Instr. Meth. Phys. Res., A, 325, 478-484.

[31] Haase, G., Tait, D. and Wiechen, A., (1993). *Monte Carlo of several gamma-emitting source and detector arrangements for determining corrections of self-attenuation and coincidence summation in gamma-spectrometry*. Nucl. Instr. Meth. Phys. Res., A, 329, 483-492.

[32] Wang, T.K. et al., (1996). *HPGe detector true-coincidence correction for extended cylinder and Marinelli-beaker sources*. Nucl. Instr. Meth. Phys. Res., A, 376, 192-202.

[33] De Felice, P., Angelini, P., Fazio, A. and Biaqini, R., (2000). *Fast procedures for coincidence-summing correction in gamma-ray spectrometry.* Appl. Radiat. Isot., 52, 745-752.

[34] Nielsen, S.P., & Palsson, S.E., (1998). *An Intercomparison of software for processing Ge gamma-ray spectra*. Nucl. Instr. Meth. Phys. Res., A, 416, 415-424.

[35] Arnold, D., Menno Blaauw, M., Fazinic, S. and Kolotov, V.P., (2005). *The 2002 IAEA Intercomparison of software for low level gamma-ray spectrometry*, Nucl. Instr. Meth. Phys. Res., A, 536, 196-210.

[36] Karhu, P., De Geer, L.E., McWilliams, E., Plenteda, R. and Werzi, R., (2006). *Proficiency test for gamma spectroscopic analysis with a simulated fission product reference spectrum*. Appl. Radiat. Isot., 64, 1334-1339.

[37] Pibida, L., Hsieh, E., Fuentes-Figueroa, A., Hammond, M.M., Karam, L., (2006). *Software studies for germanium detectors data analysis*. Appl. Radiat. Isot., 64(10-11), 1313-1318.

[38] Innocent, A.J., Onimisi, M.Y., and Jonah, S.A., (2013). *Evaluation of Naturally Occurring Radionuclide Materials in soil sample collected from some Mining sites in Zamfara State, Nigeria*. Br. J. Appl. Sci. Technol., 3, 684-692.

[39] Hussain, H. H. and Hussain, R. O., (2011). *Natural Occurring Radionuclides Material In: Radioisotopes-Application in Physical Science,* ed. By Singh, N. InTech, Rijeka, Croatia, pp.3.

[40] http://www.world-nuclear.org/info/Safety-and-Security/Radiation-and-Health/Naturally-Occurring-Radioactive-Materials-NORM/ (15 April 2014)

[41] http://www.canberra.com/literature/fundamental-principles/pdf/Spectrum-Analysis.pdf-----this (10 April 2014)

[42] Philips, G.W., (1978). *Fitting peaks with very low statistics*. Nucl. Instr. and Meth., 153, 449.

[43] Marquardt, D.W., (1963). *An algorithm for least squares estimation of non-linear parameters*. J. Soc. Ind. Appl. Math. B. Numer. Anal., 11, 431-441.

[44] Bar-Shalom, Y., Rong Li, X., Kirubarajan, T., (2001). *Estimation with Application to tracking and navigation: theory algorithms and software.* John Wiley & Sons , New York, USA.

[45] Burden, R.L., and Faires J.D., (1989). *Numerical Analysis*. PWS-KENT Publishing Company, 4th Edition.

[46] http://www.pharmacopeia.cn/v29240/usp29nf24s0c821s13.html (10 April 2014)

[47] Canberra Industries Inc., (2003). *Germanium detectors user's manual*, Meriden, CT.

[48] Jeong Hee Han, Jeong-Heon Choi, (2010). *Broad Energy HPGe Gamma Spectrometry for Dose Rate Estimation for Trapped Charge Dating*. J. Anal. Sci.Technol., 1(2), 98-108.

[49] http://www.canberra.com/products/detectors/germanium-detectors.asp (08 January 2013)

[50] Nadalut, Duran, E.B. and Barbara, (2007). *2007 Proficiency Test Exercise for Radionuclide Laboratories Supporting the Network of IMS Radionuclide Stations*, CTBT/PTS/TR, Vienna, Austria.

[51] Nadalut, Duran, E.B. and Barbara, (2011). *Interlaboratory Comparison Exercise 2011 for Radionuclide Laboratories Supporting the Network of IMS Radionuclide Stations*, Vienna, Austria.

[52] Dean, J. et al., (2013). *Proficiency Test Exercise 2012 for the CTBT Radionuclide Laboratories Supporting the Radionuclide Station Network*, NPL Report AIR (RES) DRAFT v8.2, Vienna, Austria.

[53] http://www.technet.pnnl.gov/sensors/nuclear/proects/ARSA_RASA.stm (11 June 2014)

[54] Harms A., Gilligan C., Gasparro, J. and Pearce, A., (2011). *Proficiency \Test Exercise 2010 for the CTBT Radionuclide Laboratories Supporting the Radionuclide Station Network*, NPL Report AIR (RES) 042, Vienna, Austria.

[55] IAEA, (2000). *^{226}Ra, Th and U in stream sediment.* Analytical Quality Control Services, Reference Sheet, Reference Material IAEA-314, Vienna, Austria.

[56] IAEA, (2000). *Radionuclides and trace elements in soil*. Analytical Quality Control Services,Reference Sheet, Reference Material IAEA-375, Vienna, Austria.

[57] IAEA, (2000). *Radionuclides in milk powder.* Analytical Quality Control Services, Reference Sheet, Reference Material IAEA-152, Vienna, Austria.

[58] Willemse, M.L., (2012). *Method for radon tight sealing of samples with applicable alluminium foil*, RA-WIN-233 Pretoria, South Africa.

[59] Abbas, K., Simonelli, F., D'Alberti, F., Forte, M. and Stroosnijder, M.F., (2002). *Reliability of two calculation codes for efficiency calibration of HPGe detectors*. Appl. Radiat. Isot., 56, 703-709.

[60] 2012 report Canberra Industries Inc., (2006). *Genie 2000 3.1 Customization Tools Manual*, Meriden, CT.*Genie 2000 3.1 Customization Tools Manual*, Meriden, CT.

[61] Bruggeman, M., Vidmar, F., Amouriq, F., Verheyen, L., (2014). *Efficiency calibration of BEGe and extended range detectors*. Appl. Radiat. Isot., 87, 356-360.

[62] Malain, D., (2007). *Measurement of NORM in Environmental Samples*. Master's Thesis. Department of Physics, School of Electronics & Physical Sciences, University of Surrey.

[63] Nichols, A.L., (2010). *^{212}Bi – Comments on evaluation of decay data*. http://www.nucleide.org/DDEP_WG/Nuclides/Bi-212_com.pdf (28 October 2014)

[64] http://www.nndc.bnl.gov (National Nuclear Data Base at Brookhaven National Lab.)

[65] T. Airton Almeida Junior, M.S. Nogueira, V. Vivolo, M.P.A. Potiens and , L.L. Campos , *Mass Attenuation coefficients of X-rays in different Barite concrete used in radiation protection as shielding against ionizing radiation*., Radiation Physics and Chemistry 140 (2017) 349–354

[66] Chedade, W., (2007). *True Coincidence Summing Correction in Gamma Spectroscopy*. Master's Thesis, Faculty of Environmental Physics, Universität Bremen.